Università degli studi di Roma "Sapienza"

Facoltà di Scienze Matematiche Fisiche e Naturali

Dottorato in Scienza dei Materiali

XXVI ciclo

Glycosylated cationic liposomes for specific drug delivery

Relatori:

Ruggero Caminiti

Giovanna Mancini

Candidato:

Antonio Martino

Summary

Chapter I

Introduction

Nano-particles for therapeutic applications

Currently, the efficiency of existing and newly-developed therapeutics is often hampered by the absence of a proper biodistribution because they rely on non-targeted compounds.

Packaging of drugs into targeted nanoparticles seems an obvious concept for accomplishing improvement of overall therapeutic efficacy, quality of life (by diminishing undesirable side effects) and reduction of health care costs. Indeed targeting is more easily amenable to nanoparticles than to drugs. Moreover, the use of nanoparticles could solve additional problems of many potent drugs, including: (i) poor aqueous solubility, (ii) optimization of drug combinations, and (iii) unfavorable pharmacokinetic behavior, which may result in severe toxicity due to the need of using relative high concentrations of drugs in order to achieve efficacy.

Over the past two decades, rapid progress has been made in comprehending the recognition processes and molecular interactions that govern and control the assembly of supramolecular systems. This knowledge, in turn, has greatly facilitated the engineering of devices and systems at the nanoscale level with fundamentally new physical, chemical and biological properties, functions and applications, due to their nanoscale size and large surface area. A number of these nanodevices or nanoparticles have been applied in medicine, particularly within the field of oncology[1], to solve the inadequacies of most therapeutic agents to reach the desired targets with marginal or no collateral damage. Nanoparticles should be designed in order to be able to (i) retain their cargo (drugs and/or contrast agents), (ii) evade the immunological surveilling system following systemic administration, (iii) reach selectively the diseased site (targeting), (iv) bypass extra- and intracellular barriers, and (v) release their cargo at the target site.

The first nanoparticles that reached health-care fruition, and are still the object of a wide interest, were liposomes, initially composed of pure phospholipids and more recently also consisting of cationic lipids with or without phospholipids. They are the archetypal, simplest form of nanoparticle for drug delivery. Next to liposome-based nanoparticles,

1 Ferrari M. *et al.* **2005**, *Nature Reviews*, 5,161

other typologies have entered the field of nanomedicine, each with different strengths and weaknesses. The most frequently applied are listed below:

-Polymeric nanoparticles, are prepared from polymers and can be obtained either in the form of vesicular systems (a cavity surrounded by a polymer membrane), or nanospheres (matrix systems where the polymer is homogeneously distributed in a linear or branched fashion). In spite of the development of various synthetic and semi synthetic polymers, natural polymers still benefit from a large popularity in nanomedicine application.

-Dendrimers are perfectly monodisperse polymers with a highly branched three-dimensional architecture that confers them into a spherical shape.

-Gold nanoshells are nanoclusters of gold atoms (1.5-2.0 nm in size) stabilized by a protective layer of organic molecules[2]. These systems are endowed of specific properties either in relation to the gold core or the organic monolayer.

-Magnetic nanoparticles comprise an inorganic magnetic core and a biocompatible surface coating, for example, polymers (e.g. dextran or proteins) or amphiphilic molecules (e.g. fatty acids or phospholipids), that provide stability and functionality under physiological conditions. More complex modifications include specific targeting ligands, dyes or therapeutic agents[3].

-Semiconductor nanoparticles comprise highly luminescent quantum dot cadmium/selenium cores differently coated. Although questions about their potential cytotoxicity has been raised, quantum dots are attractive alternatives to fluorescent dyes for ultrasensitive biological detection when covalently coupled to biomolecules due to their bright fluorescence, narrow emission, broad UV excitation, and high photostability.

-Silica nanoparticles are synthesized by reacting tetraethyl orthosilicate with a template made of micellar rods. The result is a collection of nano-sized spheres or rods that are filled with a regular arrangement of pores whose size and geometry can be tuned by differential doping. The large surface area of the pores allows the particles to be filled with a drug to be delivered to cells via endocytosis. Careful sizing of the silica nanoparticles can be accomplished by osmotic procedures.

-Carbon nanotubes are formed of coaxial graphite sheets rolled up into cylinders. These structures can be obtained either as single- (one graphite sheet) or multi-walled nanotubes (several concentric graphite sheets). Aqueous dispersions of functionalized carbon

2 Daniel C. *et al. Chem. Rev.*, **2004**, 104, 293

3 Pankhurst Q. A. *et al. J. Phys. D: Appl. Phys.*, **2009**, 42, 224001; McCarthy J.R. *et al. Adv. Drug Deliv. Rev.*, **2008**,60, 1241

nanotubes (CNTs) are widely investigated for biomedical applications, such as drug delivery, gene delivery, or cellular/in vivo imaging and tissue-repair scaffolds[4].

The simplest nanoparticles (first generation) target the diseased site by passive mechanisms, such as extravasation through gaps in tumour neovasculature combined with a small size (50-100 nm) and prolonged circulation time provided by a stealth layer (for example, polyethylene glycol) that prevents their premature uptake by phagocytes. Surface charge and morphology are other features that might convey specificity towards certain targets.

In more sophisticated nanoparticles (second generation) additional functionalities allow for molecular recognition of the target tissue or for active or triggered release of nanoparticle cargo. Therefore, antibodies, ligands, aptamers, and small peptides that bind to specific target-cell surface markers, expressed at the diseased or target site, have been used as targeting moieties, thus functionalizing the surface of the nanoparticles.

A recent successful example of targeting functionality concerns magnetic targeting for drug and gene delivery. In this case, targeting is controlled remotely by exploiting a magnetic component of the nanoparticle.

A remote control has also been proposed for triggering drug release by external stimuli such as specific radiation, ultrasound, ac magnetic fields, or heat, that act on a sensitive component, integrated within the nanoparticle. On the other hand, controlled release can be generated by including responsive components such as pH sensitive lipids and/or polymers or molecules, which can be processed and activated by enzymes that localize specifically to the disease site. Although no second generation nanoparticle has yet been approved by the American Food and Drug Administration, numerous current clinical trials involve targeting of nanoparticles.

More recent advancements concern a third generation of nanoparticles[5]. These are multicomponent and multifunctional systems where different nanoparticles are nested into a single construct. In these systems the functions of biorecognition, toxicity and biological barrier avoidance are decoupled, however they act in sequence and in synergy. An example of third generation nanoparticles are the so called nano-shuttles, which are self-assemblies of gold nanoparticles within a bacteriophage matrix[6]. Another example is the "nanocell" that comprises a lipid based nanoparticle, enveloping a polymeric core. A conventional

4 Prato M. *et al. Acc. Chem. Res*, **2008**, 41, 60
5 Riehemann K. *et al. Angew. Chem. Int. Ed.*, **2009**, 48, 872
6 Souza G.R. *et al. Proc. Natl. Acad. Sci. U.S.A.*, **2006**, 103,1215

cancer drug is conjugated to the polymer core and an anti-angiogenic agent is included in the lipid envelope. When nanocells accumulate in tumor cells by a passive mechanism, the sequential release of the antio-angiogenic agent and of the cytotoxic drug causes an initial disruption of tumor vascular growth and traps the drug conjugated nanoparticle core within the tumor to allow eventual delivery of the cytotoxic drug[7]. Silica nanoparticles are another example of third generation nanoparticles. They have been designed for being actual sequential multi-stage systems that should be capable of crossing biological barriers and reaching their target, due to decoupled functions of their single components[8].

Liposomes as drug delivery systems (DDS)

As mentioned above, liposomes, or vesicles, are nanoparticles consisting of closed bilayers (one or more) of amphiphilic molecules that include a part of the aqueous medium in which they are dispersed. (Figure 1.1). Amphiphilic molecules that form liposomes can be lipids of natural origin (phospholipids, glycolipids) and all those surfactants with low solubility in water, with the polar head relatively small and relatively bulky hydrophobic region. Since their first description in 1965, liposomes had a dual role: on the one hand they represent a versatile model of cell membranes[9], on the other hand, are flexible and well characterized drug delivery systems that can be used for the transport of a wide range of compounds (drugs, nucleic acids, enzymes) within cells and tissues. The formation and organization of these systems through non-covalent bonds have several advantages i) ease preparation, ii) complete biocompatibility, if composed of natural phospholipids, iii) possibility of loading hydrophilic and hydrophobic molecules (however, more suitable drugs to be delivered by liposomes are those that have a high oil/water partition coefficient and that do not need to be administered in high doses), iv) protection of the encapsulated substances from the lytic enzyme (such as proteases or nucleases) action, or from denaturing environments; v) facilitating active substances to be internalized by cells, vi) capability, as a function of

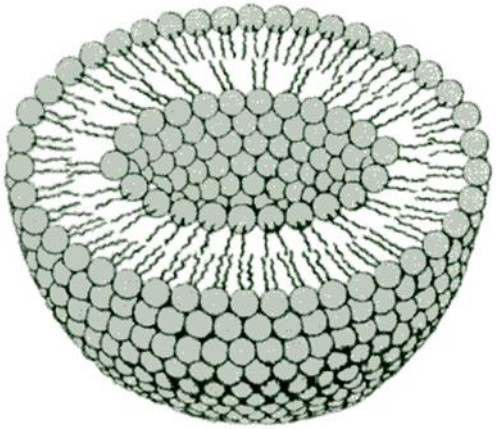

Figure 1.1. Liposome

7 Sengupta S. *et al. Nature*, **2005**, 436,568
8 Tasciotti E. *et al. Nanotechnol.*, **2008**, 3,151
9 Allen M *et al. Advanced Drug Delivery Reviews*, **2013**, 65, 36

composition, size and surface charge, to specifically release drug into cells with phagocytic activity and to localize at the level of specific tissues and organs, vii) ability to decrease the toxicity of certain active principles avoiding, for example, the accumulation in the heart (doxorubicin) or in kidneys (amphotericin B).

On the basis of their size and number of bilayers, liposomes can be classified as i) multilamellar vesicles (MLV), *i.e.* vesicles composed of many lipid bilayers and characterized by a diameter >500 nm; ii) large unilamellar vesicles (LUV) characterized by a single lipid bilayer and by a diameter >100 nm; and iii) small unilamellar vesicles (SUV) characterized by a single lipid bilayer and a diameter of 20-100 nm.

Liposomes can be also classified on the basis of their composition and functions (Figure 1.2) as[10] a) c*onventional:* prepared from neutral phospholipids, lecithin or sphingomyelin as main constituents, using cholesterol, negatively charged phospholipids and synthetic lipids as additives. In vivo, when administered intravenously, they are removed within a few hours by the RES macrophages. Therefore, these liposomes are used as drug carriers when the target organ is RES, where are often localized bacteria, fungi and parasites. b) *inert (Stealth):* they do not interact with biological fluids, and with the RES cells thus being able to remain in the bloodstream for longer times compared to the conventional liposomes. STEALTH ® liposomes belong to this category; they are formulated with specific lipids, such as the ganglioside GM1, phosphatidylinositol hydrogenated HP1, which give the liposomes an average life-time of up to twelve hours, compared to the minutes of conventional formulations. The inert liposomes, escaping the uptake of RES, remain in circulation for longer times with respect to conventional liposomes. Considering the fact that the blood vessels in tumors are fenestrated and therefore accessible to liposomes, a longer life bloodstream promotes the accumulation in tumors and inflamed tissues (passive targeting); so they are the most suitable for systemic administration to tumors and inflamed tissues; c) *reactive:* liposomes with fusogenic properties and/or sensitive to certain external stimuli such as pH or concentration of a particular ion, such as calcium. These liposomes are often defined as polymorphs because they undergo a phase change upon the interaction with the cell environment. An example of reactive liposomes are those formulated with lipids that form vesicles at a pH close to neutrality and give micelles at a lower pH thus triggering the release of the encapsulated content. Because generally tumor tissues feature a pH lower than the physiological one, these liposomes are

10 Lasic D.D. *et al. Science*, **1995**, 217, 1245

particularly interesting in the formulation of drug delivery system for cancer therapy[11]; d) s*pecific or targeted:* these are stabilized liposomes specifically functionalized with antibodies or receptor ligands (for example, folic acid, sugars) (active targeting). In the class of targeted liposomes can be listed also magnetic liposomes, these are obtained by entrapping magnetic material in the core of lipid vesicles. The application of external magnetic field will convey the magnetic liposomes to the target. Several groups have investigated the use of magnetoliposomes for site specific targeting, cell-sorting and as magnetic resonance contrast enhancing agents[12]. For example Babincova *et al.*[13] have used doxorubicin (DOX) carrying magnetoliposomes for site specific chemotherapy in response to externally applied AC magnetic field. The results of this study showed that magnetoliposomes can be specifically heated to 42°C for a few minutes to obtain the massive release of the encapsulated doxorubicin. An *in vivo* study on the administration of adriamycin (ADR) encapsulated in magnetoliposomes showed that the application of an

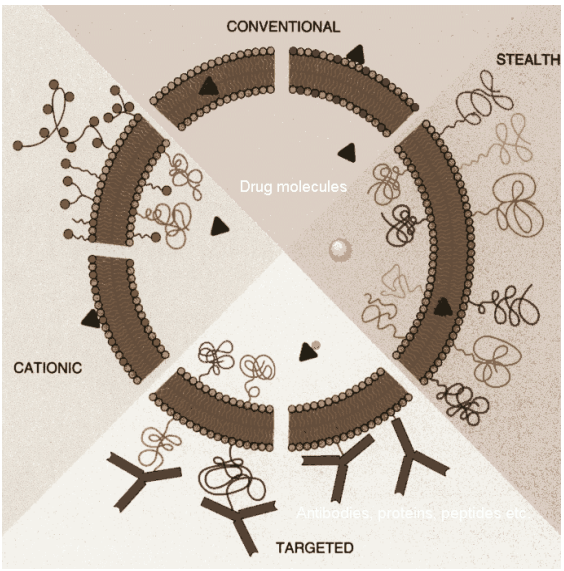

Figure 1.2. Different type of liposomes used as DDS. From Laic D. D. *et al. J. of Controlled Release*, **1997**, 48, 203.

external magnetic field yielded a ~ 4-fold higher ADR concentration in the tumor with respect to free ADR. This result showed that systemic chemotherapy could effectively

11 Wang C.Y. *et al. Biochim. Biophys. Res. Commun.*, **1987**, 147, 980; Immordino M.L. *et al. Int. J. Nanomedicine* **2006,** 1(3), 297
12 Saiyed Z. M. *et al. BioMagnetic Research and Technology*, **2003**, 1:2
13 Babincová M. *et al. Bioelectrochemistry*, **2002**, 55, 17

control the primary tumor without significant side effects, due to the targeting of magnetic ADR liposomes[14].

Other liposomes that can be classified as specific are the cationic liposomes. These are liposomes formulated with cationic synthetic lipids, and the positive charge of their surface ascribe them a specific biological behavior. The first cationic liposomes, formulated with dioleoilfosfatidiletanolammina (DOPE) and chloride of N-[1-(2,3-dioleilossi)propyl]-N,N,N-trimethylammonium (DOTMA), a synthetic cationic lipid, were proposed in 1987 to introduce a plasmid into cell lines. Since then, many other cationic formulations have been used in gene therapy protocols. Over the past ten years there has been a renewed interest in these systems, because they are characterized by an intrinsic selectivity towards certain organs and/or tissues such as the endothelium of tumor vessels, liver, and lungs[15]. Furthermore, it has been demonstrated that cationic liposomes are able to induce apoptosis in macrophages and lymphocytes[16].

Active targeting: glycosylated liposomes

Some of the molecules used to attribute active targeting to liposomes are, as mentioned above, sugars residues[17]. Molecular recognition events involving carbohydrates occur in a wide variety of important biological processes including the functions of the immune system, interaction of viruses and bacteria, and tissue growth. Cell-to-cell communication events, which are driven by highly specific carbohydrate-protein interactions, are included in these recognition phenomena. These specific interactions occur through the interaction of glycolipid, glycoprotein, or polysaccharide found on cell surfaces and lectins, proteins characterized by the presence of carbohydrate-binding sites[18].

The functionalization of liposome surface with sugars moieties is generally obtained by including in the lipid formulations glycosylated amphiphilic molecules. In these molecules the polar sugar residue(s) is(are) linked to a hydrophobic region, constituted by one or more hydrophobic alkyl chains that have the role of anchoring the sugar moiety to the liposome bilayer, through a hydrophilic spacer, which has the role of ensuring a good exposure of the sugar on the surface of the liposome. The architecture of these sugar-

14 Kubo T. *et al. Int. J. Oncol.*, **2001**, 18,121
15 Dass C.R. *et al. J. Control. Rel.*, **2006**, 113, 155
16 Aramaki Y. *et al. FEBS Lett*, **1999**, 460, 472; Aramaki Y. *et al.,Pharm. Res.*, **2000**,17, 515
17 Keerti J. *et al. Biomaterials*, **2012**, 33, 4166; Faivre V. *et al.*, *Expert Opin Drug Deliv*., **2010**,7, 1031
18 Guo C.X. *et al.J. Phys. Chem.*, **2005**,109, 18769

carrier molecules is crucial in determining the chemical and physical stability of liposomes as well as their specificity towards target proteins.

Faivre *et al.*[19] studied the interactions of different proteins - specific receptors of fucose and glucose respectively – with mixed liposomes composed of dimyristoyl-phosphatidylcholine (DMPC) and synthetic glycolipids bearing units of fucose and glucose. Their results showed that the liposome agglutination induced by the proteins increased as a function of the increase, from 40% to 60%, of the amount of glycolipids in the lipid formulation.

In the study of Stimac *et al.*[20] liposomes were formulated including 30% of two different mannosylated amphiphiles in liposomes of egg-phosphatidylcholine/cholesterol/ dicetylphosphate. The results of the investigation showed that the presence of the mannosylated compounds in the formulation affected the size and structural features of the liposomes. The study of the interaction of mannosylated liposomes with *Concanavalin A* (ConA), a plant lectin specific for different type of sugars, showed that the nature of the mannosylated lipid strongly controls the interaction with the protein. In conclusion, the literature reports on the physicochemical characterization of glycosylated liposomes cleary demonstrate that the nature of the glycolipid influences both the organization and stability of the liposomes and their interaction with receptors.

Other reports concern *in vivo* investigation on drug targeting that exploit galactose-receptor interaction on the alveolar macrophages[21] or HIV virus[22] and mannose-receptor interaction on Kupffer cells[23] or various macrophages[24]. In particular Shimada *et al.*[25] reported on the biological behavior (*in vitro* and then *in vivo*) of synthetic glycolipids included in liposomes of dipalmitoylphosphatidylcholine (DPPC). The investigated glycolipids were characterized by the different length of the polyethylene chain (PEG_{10}, PEG_{20} and PEG_{40}) connecting the sugar moiety to the hydrophobic region. The agglutination experiments with the galactose-specific lectin-agarose from *Ricinus Communis* (RCA-120) showed that only in the presence of the PEG_{10} chain (from 9 Å to 35 Å) the galactose moieties were

19 Faivre V. *et al. Chemistry and Physics of Lipids*, **2003**, 125,147
20 Štimac A. *et al*., *Biochimica et Biophysica Acta*, **2012**, 1818, 2252
21Chono S. *et al*. *Drug Dev. Ind. Pharm.*, **2010**, 36,102; Chono S. *et al*. *J. Control Rel.*, **2008**, 127, 50
22 Minakshi G. *et al. Eur. J. Pharm. Sci.*, **2008**, 33, 271
23-25 Shimada k. *et al*. *Biochimica et Biophysica Acta*, **1997**, 1326, 329
24 Jain S. *et al*. *Journal of drug delivery*, **2011**, 2011

properly exposed for an adequate interaction with the lectin. The *in vivo* experiments using liposomes with PEG_{10} showed that the uptake and the recognition in the Kupffer cells was faster compared to control liposomes.

In the work of Garg *et al.* units of galactose, fucose and mannose sugar were esterified with palmlitoyl chloride in dimethylformamide to obtain galactosylated, fucosylated and mannosylated liposomes[26]. The authors investigated the hepatic toxicity, cellular uptake and pharmacokinetics of stavudine[27] and azidothymidine[28] entrapped in two different galactosylated liposomes (Gal-Lip) . They found that stavudine entrapped in galactosylated liposomes did not show the hematological and hepatic toxicity in the presence of a high uptake of galactosylated formulations by liver parenchymal cells from albino rats. Analogously hematological toxicity was not observed for 10 days in the case of azidothymidine loaded in galactosylated vesicles. Cellular uptake of azidothymidine-Gal-Lip was 8.5 and 1.8 folds larger compared to free drug and uncoated liposomes, respectively, and there was a prolonged release with higher accumulation to tissues compared to normal liposomes. Matsui and coworkers[29] developed oligomannose-coated liposomes of dipalmitoylphosphatidylethanolamine (DPPE) as delivery systems for anticancer drugs and found that these carriers were successfully taken up by mouse peritoneal macrophages and the anticancer drugs were carried to metastatic sites in the peritoneal cavity in mice. The clinical application of this system to gastric cancer patients was investigated to verify whether the oligomannose-coated liposomes could be up taken by human peripheral blood monocytes and human peritoneal macrophages to carry them to micrometastatic foci in the mouse omentum and resected omentum from cancer patients in ex vivo studies. Finally the authors suggested that oligomannose-coated liposomes can be successfully explored for the delivery of anticancer drugs to the metastatic sites via selective uptake by peritoneal macrophages through receptor mediated endocytosis.

Kaur *et al*. developed surface engineered liposomes including positively charged, negatively charged and mannose coated liposomes for specific targeting of zidovudine, an

---

26-27 Minakshi G., *Eur. J. Pharm. Biopharm.*, **2007**, 67, 76
28 Minakshi G., *J. Drug Target*, **2006**, 14, 1
29 Matsui M *et al*., *Cancer Science*, **2010**, 101, 1670
30 Chanchal D.K., *J. Drug Target.*, **2008**, 16, 798

antiviral drug, to lymph nodes and spleen[30]. The authors obtained the positively charged, negatively charged and mannose coated vescicles using stearylamine, dicetyl-phosphate and mannose-terminated stearylamine, respectively. In organ distribution studies, reduced concentration of zidovudine in serum with increased amounts in the spleen and lymph nodes was observed by using mannose coated liposomes. Fluorescent microscopic studies showed a high localization of surface engineered liposomes in the lymph nodes and spleen with highest uptake of mannose coated liposomes followed by the negatively charged and then by the positively charged liposomes with minimum uptake of plain liposomes. It was concluded that zidovudine loaded mannose coated liposomes could be exploited as potential carriers for the treatment of viral diseases such as AIDS whose target site is the lymphatic system.

Aim of the work

The aim of this work is the synthesis and the characterization of cationic glycosylated amphiphiles (GA) to be included in liposome formulations to ascribe them both a positive charge and specificity toward sugar receptors. A number of synthetic possibilities will be explored by exploiting glucose as sugar residue (Chart 1.1, glycolipids 1-4). A synthetic procedure explored on glucose will be then extended to lactose because most human lectins are galactose receptors (Chart 1.1, glycolipid **5**). Liposomes composed of phospholipids and defined GA, *i.e.* GA **1** and **4** will be characterized by different physicochemical techniques such as dynamic light scattering, UV and fluorescence spectroscopy. The potentiality of these liposome formulations as targeting drug delivery systems will be ascertained by investigating their interaction with Con A, a plant lectin derived from the Jack Bean (*Canavalia ensiformis*), that provides an optimal model system for the study of multivalent lectin binding. In fact Con A exists as a tetramer, four chains, in basic conditions, each monomer featuring a glucose binding site[31]. The interaction with Con A will be studied by experimental techniques such as dynamic light scattering, UV and fluorescence spectroscopy and by a theoretical approach based on molecular docking, useful to describe the interaction of a single GA with the protein, and molecular dynamic simulations that will give an atomistic description of the interaction between the protein

31 Glen B.T. *et al. J. Am. Chem. Soc.*, **2009**, 131(15), 5471

and the lipid bilayer formed by a phospholipid and one of the GAs. The theoretical approach will allow rationalizing the experimental findings and identifying the role of some structural features of the GA to address a rational design of new GAs.

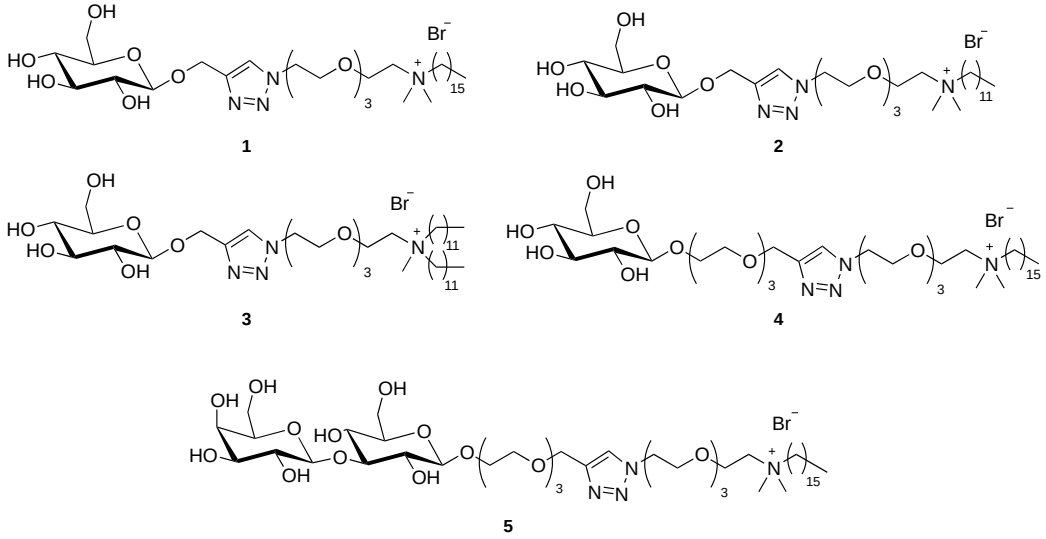

Chart 1.1. Glycosylated cationic amphiphiles.

The theoretical investigation will rely on the study of the binding of glycosylated lipid bilayers with a single monomeric unit of ConA, (PDB code 3D4K[32], Chain A). The protein is composed of 237 aminoacids and the structure of the complex formed by ConA with a trimannoside was elucidated by X-rays[32]. The aminoacid residues of the binding site involved in the binding with the trimannoside are Asparagine 14 (Asn 14), Leucine 99 (Leu 99), Tyrosine 100 (Tyr 100), Aspartic acid 208 (Asp 208), Arginine 228 (Arg 228) as shown in Figure 1.3. The ConA contains two metal binding site, site S1 binds Mn^{2+} ion while site S2 binds Ca^{2+} ion. The manganese ion (Mn 238) is octahedrally coordinated to the following aminoacidic residues: Glutammic acid 9 (Glu 9), Asp 10, Asp 19, Histidine 24 (His 24), and two water molecules. The calcium ion (Ca 239) is seven fold coordinated and interacts with two oxygen atoms from Asp 10 as well as with residues Tyr 12, Asn 14, Asp 19 and two water molecules. The presence of the two metal ions is fundamental for the binding o saccharidic moiety with the protein.

32 Kadirvelraj R *et al. J. Am. Chem. Soc.*, **2008**, 130, 16933

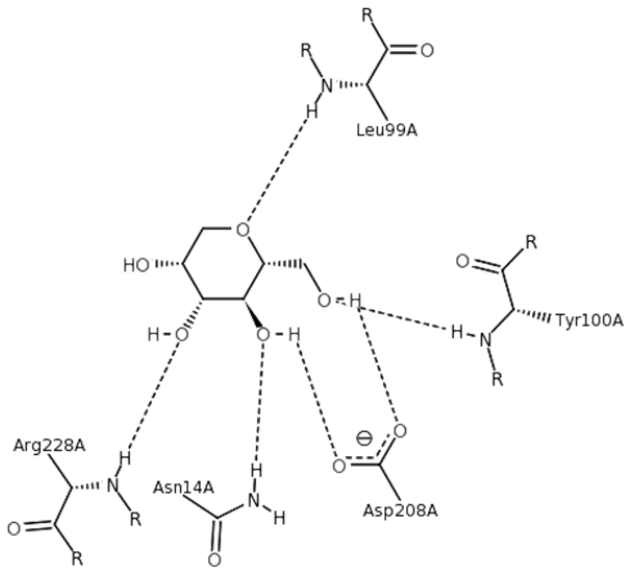

Figure 1.3. Visualization of the aminoacidic residues involved in the binding with ConA. From Kadirvelraj R. *et al. J. Am. Chem. Soc.*, **2008**, 130, 16933.

Chapter 2

Synthesis and characterization of novel glycosylated amphiphiles

This chapter describes the synthesis and characterization of the five novel glycosylated amphiphiles **1, 2, 3, 4** and **5** reported in Chart 2.1.

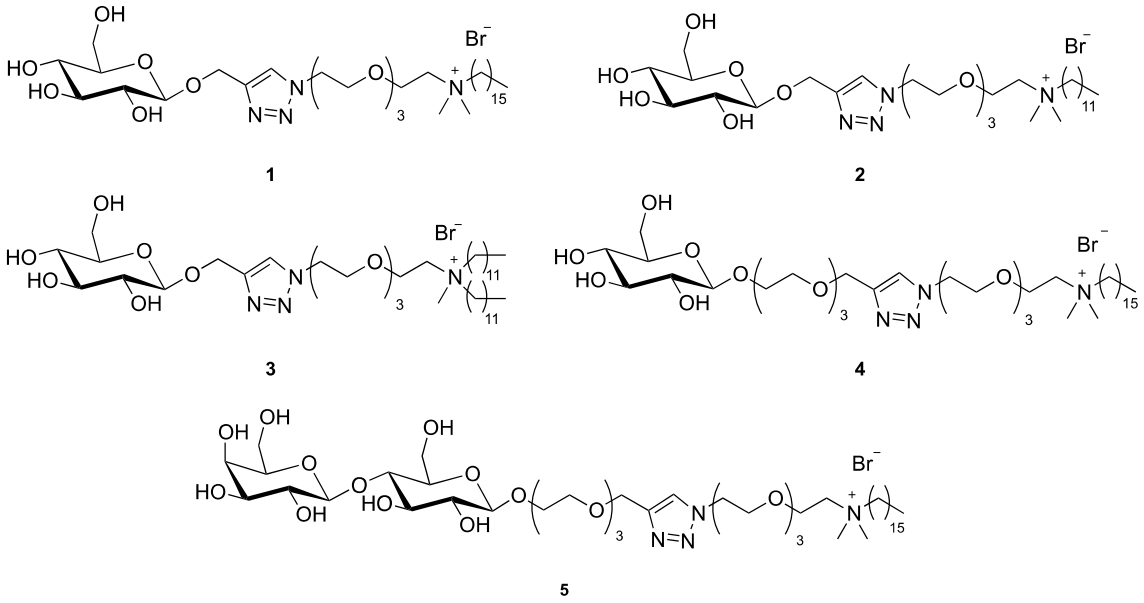

Chart 2.1.

Experimental

Instrumentation

NMR spectra were recorded on a Bruker300 Avance spectrometer (operating at 300.13 for ^{1}H and 75.47 MHz for ^{13}C) and on a Bruker 400 Avance spectrometer (operating at 400 MHz for ^{1}H and 100 MHz for ^{13}C). Deuterated solvents were used as internal standards.

HRMS-ESI spectra were recorded on a LTQ Orbitrap XL instrument.

Steady-state fluorescence experiments were carried out on a Fluoromax-4 Horiba-JobinYvon spectrofluorimeter.

Conductivity measurements were carried out on a Hanna conductimeter, HI-9932, equipped with a thermostating apparatus, in the temperature range 4–60 °C. All measurements were done in a jacketed cell that was maintained at the appropriate temperature (±0.1 °C).

Dynamic laser light scattering (DLS) measurements were performed with a Malvern Nano-ZetaSizer spectrometer, equipped with a 5 mWHeNe laser (wavelength = 632.8 nm) and a digital logarithmic correlator.

Materials

D(+)-Glucose was purchased from Merck. Fluoresceinisothiocyanate labeled Concanavalin A (FITC-ConA) was purchased from Invitrogen. Phosphate buffer saline (PBS) tablet (0.01 M phosphate buffer, 0.0027 M KCl, 0.137 M NaCl, pH 7.4 at 25° C) and all the starting materials for the synthesis were purchased from Sigma-Aldrich.

Synthesis of amphiphiles 1, 2, 3, 4, 5

*Preparation of 2-(2-(2-(2-hydroxyethoxy)ethoxy)ethoxy)ethyl-4methylbenzensulphonate **9***

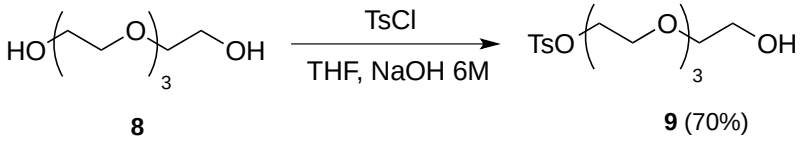

8 **9** (70%)

10 mL of NaOH 6 M and 45 mL of tetraethyleneglycol **8** (0.26 mol) were added to 10 mL of THF at 0°C. A solution of 5.0 g of tosyl chloride (TsCl) (26.2 mmol) in 30 mL of THF was added dropwise and the reaction mixture was stirred until complete addition of TsCl. The mixture was then diluted with 200 mL of THF and 800 mL of water and NaCl was added until complete phases separation. The organic layer was separated, the solvent was removed under reduced pressure and the residual dissolved in CH_2Cl_2. The organic phase was extracted with water (10 x 150 mL) and dried over anhydrous Na_2SO_4. The solvent was removed under reduced pressure to afford 6.4 g of **9** (yield 70%) as a pale yellow oil.

^{1}H-NMR (δ $CDCl_3$, 300 MHz) ppm: 2.43 (s, 3H, CH_3); 2.65 (s, 1H, OH);3.59-3.68 (m, 14H, CH_2OCH_2, C$\underline{H}_2$OH); 4.15 (t, $^3J_{HH}$ =6.50 Hz, 2H, CH_2OTs); 7.32-7.75 (m, 4H, aromatic).
^{13}C-NMR (δ $CDCl_3$, 75 MHz) ppm: 22.33 (CH_3); 61.74, 68.76, 69.27, 70.35, 70.45, 70.69, 70.76, 72.45 ($\underline{C}H_2O\underline{C}H_2$, $\underline{C}H_2OH$); 128.02, 129.86, 138.21, 140.83 (aromatic).

*Preparation of 2-(2-(2-(2-azidoethoxy)ethoxy)ethoxy)ethanol **10***

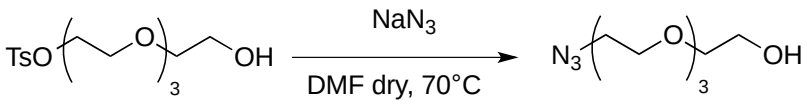

9 **10** (77%)

1.98 g of **9** (5.7 mmol) and 0.5 g of NaN_3 (7.6 mmol) were suspended in 10 mL of dry DMF under nitrogen. The mixture was stirred and heated at 70°C for 14 hours. The solvent was removed under high vacuum and the oily residue was washed with CH_2Cl_2. After filtration the solvent was removed under reduced pressure to afford 0.96 g of **10** (yield 77%) as a yellow oil.

^{1}H-NMR (δ $CDCl_3$, 300 MHz) ppm: 2.81 (s,1H, OH); 3.38 (t, $^3J_{HH}$ =6.02 Hz, 2H, CH_2N_3); 3.61-3.70 (m, 14H, CH_2OCH_2, $C\underline{H}_2OH$).

^{13}C-NMR (δ $CDCl_3$, 75 MHz) ppm: 50.67; 61.70; 70.05; 70.35; 70.60; 70.66; 70.70; 72.48.

*Preparation of 2-(2-(2-(2-bromoethoxy)ethoxy)ethoxy)ethanol **11***

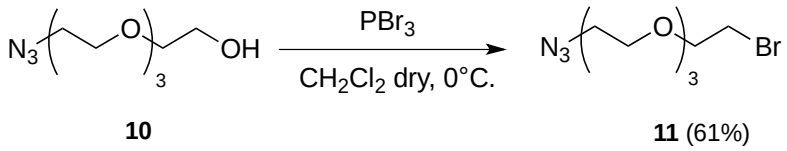

10 **11** (61%)

0.96 g of **10** (4.4 mmol) were dissolved in 15 mL of dry CH_2Cl_2 under nitrogen. The mixture was cooled to 0°C and a solution of 0.13 mL of PBr_3 (1.46 mmol) in 10 mL of dry $CH_2Cl_2$was added dropwise. The reaction was then neutralized by aqueous $NaHCO_3$ saturated solution. The aqueous phase was extracted with CH_2Cl_2 (2 x 20 mL), the combined organic layers were dried over anhydrous Na_2SO_4 and, after filtration and the solvent was removed under reduced pressure. The oily residue was purified by silica gel cromatography (eluent $CHCl_3$) to afford 0.75 g of **11**(yield 61%).

^{1}H-NMR (δ $CDCl_3$, 300 MHz) ppm: 3.37 (t, $^3J_{HH}$ =6.04 Hz, 2H, CH_2N_3); 3.47 (t, $^3J_{HH}$ =6.65 Hz, 2H, CH_2Br); 3.65-3.70 (m, 10H, OCH_2CH_2O, $C\underline{H}_2CH_2N_3$); 3.82 (t, $^3J_{HH}$=6.65 Hz, 2H, $C\underline{H}_2CH_2Br$).

^{13}C-NMR (δ $CDCl_3$, 75 MHz) ppm: 50.67; 61.70; 70.05; 70.35; 70.60; 70.66; 70.70; 72.48.

*Preparation of propargil-β-D-glucopiranoside **7***

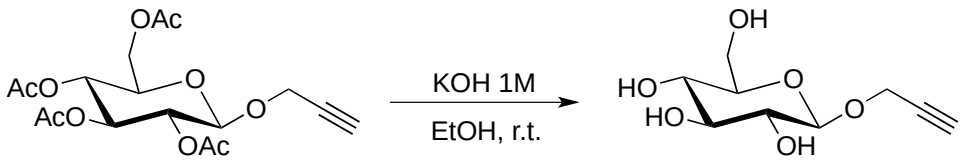

6 **7** (58%)

20mL of aqueous KOH 1M were added to a solution of 1.01 g of 2-propinil-tetra-O-acetil-*β*–D-glucopiranoside **6** (2.6 mmol) in 60 mL of EtOH. The mixture was stirred at room temperature for 1.5 hours and then neutralized by the addition of Amberlite IR-120. After filtration the solvent was removed under reduced pressure and the residue was purified by silica gel cromatography (eluent CH_2Cl_2/MeOH=8/2) to give 0.34 g (1.5 mmol) of **7** (yield 58%) as pale yellow oil.

^{1}H-NMR (δ CD_3OD, 300 MHz) ppm: 2.86 (t, $^4J_{HH}$ =2.88 Hz, 1H, H9); 3.20 (t, $^3J_{HH}$ =8.33 Hz,1H, H2); 3.26-3.41 (m, 3H, H3 ,H4 ,H5); 3.63-3.69 (m, 1H, H6); 3.84-3.89 (m, 1H, H6); 4.41-4.45 (m, 2H, H7); 4.45 (d, $^3J_{HH}$ =8.33 Hz,1H, H1).

^{13}C-NMR (δ CD_3OD, 75 MHz) ppm: 55.20; 61.25; 70.03; 72.89; 74.18; 76.45; 76.50; 79.46; 100.65 (C1).

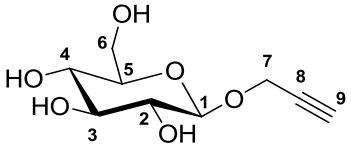

*Preparation of triazolic adduct **12***

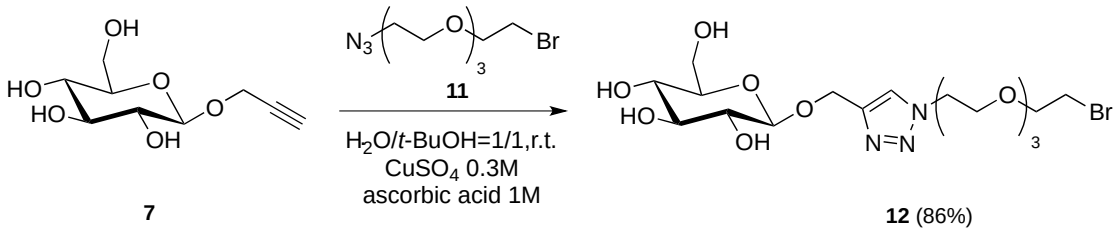

0.42 g of **11** (1.5 mmol) and 0.32 g of **7** (1.5mmol) were suspended in 6 mL of H_2O/*t*-BuOH (1:1). 150 μl of a freshly prepared aqueous solution of ascorbic acid 1 M and 50 μl of an aqueous solution of $CuSO_4 \cdot 5H_2O$ 0.3 M were then added to the mixture. The reaction was stirred at room temperature for 1 day. The mixture was then cooled to 0°C, neutralized by $NaHCO_3$ and the solvent was removed under reduced pressure. The residue was washed with MeOH, filtered to remove salts and the solvent was removed under reduced pressure. The crude product was purified by silica gel cromatography (eluent $CHCl_3$/MeOH=85/15) to give 0.65 g (1.3 mmol) of **12** (yield 86%) as a pale yellow oil.

^{1}H-NMR (δ CD_3OD, 300 MHz) ppm: 3.20 (t, $^3J_{HH}$ =8.69 Hz, 1H, H2); 3.29-3.35 (m, 3H, H3, H4, H5); 3.51 (t, $^3J_{HH}$ =6.52 Hz, 2H, H17); 3.58-3.70 (m, 9H, H12, H13, H14, H15, H6(1H)); 3.79 (t, $^3J_{HH}$ =6.52 Hz, 1H, H16); 3.90 (m, 2H, H11, H6(1H)); 4.39 (d, $^3J_{HH}$ =8.69 Hz, 1H, H1); 4.53 (t, $^3J_{HH}$ =6.25 Hz,2H, H10); 4.76-5.02 (m, 2H, H7); 8.15 (s, 1H, H9).

^{13}C-NMR (δ CD_3OD, 75 MHz) ppm: 30.15 (C17); 49.85 (C10); 61.45 (C6); 61.66 (C7); 69.01 (C11); 70.04, 70.11, 70.16, 70.26 (C5, C12, C13, C14, C15); 70.96 (C16); 73.66 (C2); 76.61 (C3); 76.67 (C4); 102.15 (C1); 124.32 (C9); 144.11 (C8).

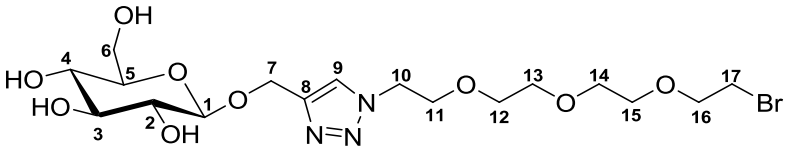

Preparation of N-didodecyl-N-methylamine

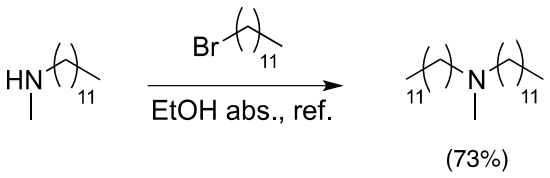

A solution of 1.0 mL (3.9 mmol)of N-methyldodecylamine and 1.1 mL (3.6mmol) of 1-bromododecane in 2 mL of absolute EtOH was heated at reflux for one day. Upon cooling the solid residue was filtered, washed with *n*-hexane and crystallized from EtOH to afford 0.96 g (yield 73%) of the pure product as a pale yellow powder.

^{1}H-NMR (δ $CDCl_3$, 300 MHz) ppm: 0.88 (t, $^{3}J_{HH}$ =7.54 Hz, 6H, $CH_2C\underline{H}_3$); 1.26-1.38 (m, 40H, $NCH_2(C\underline{H}_2)_{10}CH_3$); 2.26 (s, 3H, $NC\underline{H}_3$); 2.46 (t, $^{3}J_{HH}$ =7.08 Hz , $NC\underline{H}_2$).

^{13}C-NMR (δ $CDCl_3$, 75 MHz) ppm: 14.10 ($CH_2\underline{C}H_3$); 22.65; 27.33; 28.13; 29.55; 29.36; 32.05; 60.68.

*Preparation of glucosylated amphiphile, GA **1***

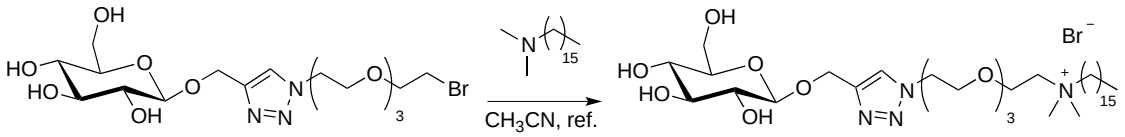

12 **1** (55%)

0.65 mL of N,N-dimethyl-N-hexadecylamine (1.95mmol) and 0.65 g of **12** (1.3mmol) were suspended in 10 mL of CH_3CN. The mixture was heated at reflux for one week. The solvent was removed under reduced pressure and the residue was washed several times with Et_2O to give 0.55 g (0.71 mmol) of the product **1** (yield 55%).

^{1}H-NMR (δ CD_3OD, 400 MHz) ppm: 0.81 (t, $^3J_{HH}$ =7.66 Hz, 3H, H35); 1.22-1.42 (m, 26H, H22, H23, H24, H25, H26, H27, H28, H29, H30, H31, H32, H33, H34); 1.79 (m, 2H, H21); 3.18 (s, 6H, H18, H19); 3.21 (t, $^3J_{HH}$ =7.96 Hz, 1H, H2); 3.29-3.47 (m, 4H, H3, H4, H5, H20); 3.56-3.79 (m, 11H, H6(1H), H12, H13, H14, H15, H17); 3.83-3.92 (m, 5H, H6(1H), H11); 4.41 (d, $^3J_{HH}$ =7.96 Hz, 1H, H1); 4.59 (t, $^3J_{HH}$ =6.38 Hz, 1H, H10); 4.76-5.00 (m, 2H, H7); 8.11 (s, 1H, H9).

^{13}C-NMR (δ CD_3OD, 100 MHz) ppm: 13.15 (C35); 21.74, 22.36, 22.53, 26.06, 28.92, 29.09, 29.23, 29.30, 29.38, 29.42, 31.69 (C21, C22, C23, C24, C25, C26, C27, C28, C29, C30, C31, C32, C33, C34); 50.09 (C10); 51.00 (C18, C19); 61.34 (C6); 61.68 (C7); 63.08 (C17); 64.43 (C16); 65.62 (C20); 68.98 (C11); 70.01, 70.15, 70.25 (C5, C12, C13, C14, C15); 74.01 (C2); 76.60 (C3); 76.64 (C4); 102.22 (C1); 124.72 (C9); 144.11 (C8).
HRMS: calculated for $C_{35}H_{69}N_4O_9$ $[M\text{-}Br^-]^+$: 689.5065;found: 689.5086.
$[\alpha]_D$ (CH_3OH, C=0.81) $= -10.35°$

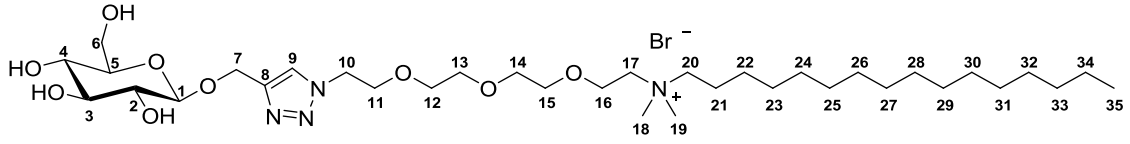

*Preparation of GA **2***

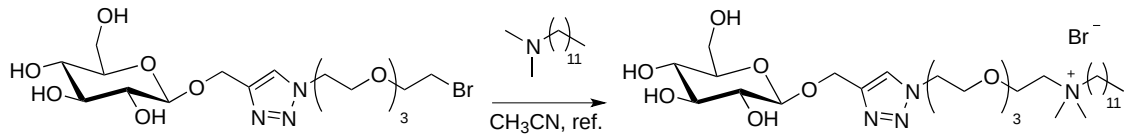

12 **2** (56%)

GA **2** was prepared with a 56% yield by alkylation of N-dimethyl-N-dodecylamine with compound **12** according to the procedure described above for the preparation of GA**1**.

^{1}H-NMR (δ CD_3OD, 400 MHz) ppm: 0.81 (t, $^{3}J_{HH}$ =7.66 Hz, 3H, H31); 1.22-1.42 (m, 18H, H22, H23, H24, H25, H26, H27, H28, H29, H30); 1.79 (m, 2H, H21); 3.18 (s, 6H, H18, H19); 3.21 (t, $^{3}J_{HH}$ =7.96 Hz, 1H, H2); 3.29-3.47 (m, 4H, H3, H4, H5, H20); 3.56-3.79 (m, 11H, H6(1H), H12, H13, H14, H15, H17); 3.83-3.92 (m, 5H, H6(1H), H11); 4.41 (d, $^{3}J_{HH}$ =7.96 Hz, 1H, H1); 4.59 (t, $^{3}J_{HH}$ =6.38 Hz, 1H, H10); 4.76-5.00 (m, 2H, H7); 8.11 (s, 1H, H9).

^{13}C-NMR (δ CD_3OD, 100 MHz) ppm: 13.10 (C31); 21.72, 22.29, 22.3, 26.10, 28.92, 29.23, 29.30, 29.42, 29.48, 31.69 (C21, C22, C23, C24, C25, C26, C27, C28, C29, C30); 50.15 (C10); 51.09 (C18, C19); 61.30 (C6); 61.62 (C7); 63.09 (C17); 64.53 (C16); 65.70 (C20); 68.85 (C11); 70.00, 70.10, 70.22 (C5, C12, C13, C14, C15); 74.10 (C2); 76.65 (C3); 76.67 (C4); 102.20 (C1); 124.70 (C9); 144.21 (C8).

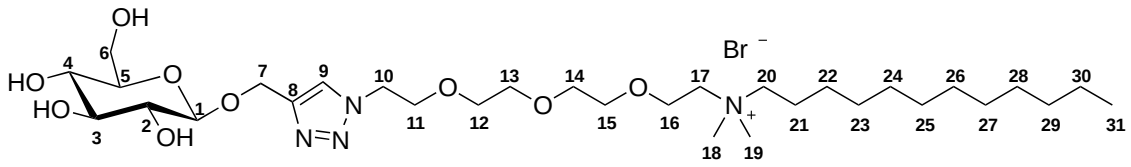

*Preparation of GA **3***

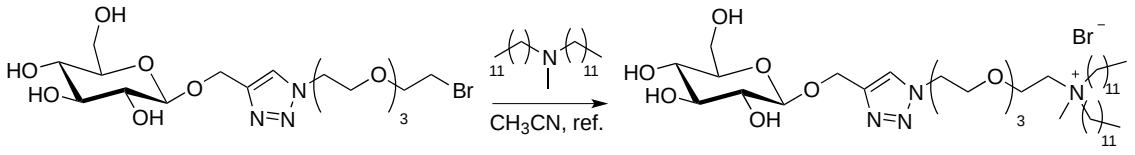

12 **3** (48%)

GA **3** was prepared with a 48% yield by alkylation of N-didodecyl-N-methylamine with compound **12** according to the procedure described above for the preparation of GA**1**.

^{1}H-NMR (δ CD_3OD, 400 MHz) ppm: 0.81 (t, $^{3}J_{HH}$ =7.64 Hz, 6H, H30); 1.22-1.42 (m, 36H, H21, H22, H23, H24, H25, H26, H27, H28, H29); 1.78 (m, 4H, H20); 3.18 (s, 3H, H18); 3.21 (t, $^{3}J_{HH}$ =7.96 Hz, 1H, H2); 3.29-3.47 (m, 7H, H3, H4, H5, H19); 3.56-3.79 (m, 11H, H6(1H), H12, H13, H14, H15, H17); 3.81-3.92 (m, 5H, H6(1H), H11); 4.41 (d, $^{3}J_{HH}$ =7.96 Hz, 1H, H1); 4.58 (t, $^{3}J_{HH}$ =6.38 Hz, 1H, H10); 4.76-5.00 (m, 2H, H7); 8.15 (s, 1H, H9).

^{13}C-NMR (δ CD_3OD, 100 MHz) ppm: 13.10 (C30); 21.72, 22.28, 22.32, 26.15, 28.92, 29.25, 29.41, 29.42, 29.48, 31.69 (C20, C21, C22, C23, C24, C25, C26, C27, C28, C29); 50.15 (C10); 51.22 (C18); 61.29 (C6); 61.62 (C7); 63.15 (C17); 64.52 (C16); 65.85 (C20); 68.85 (C11); 69.89, 69.97, 70.15 (C5, C12, C13, C14, C15); 74.10 (C2); 76.65 (C3); 76.67 (C4); 102.20 (C1); 124.81 (C9); 144.25 (C8).

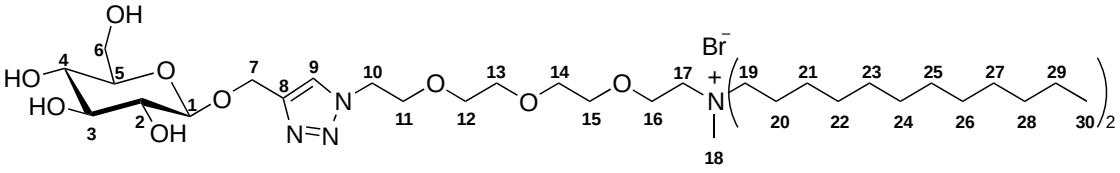

*Preparation of penta-O-acetyl-β-D-glucopyranoside **14***

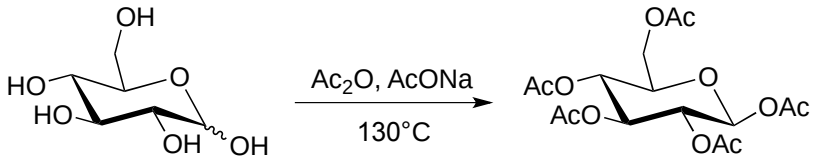

13 **14**(67%)

16.1 g of AcONa (0.2 mol) were suspended in 68 mL of acetic anhydride and the mixture was heated to 130 °C. 5.0 g of glucopyranose **13** (0.027 mol) were added and the reaction was stirred for 16 hours. 350 mL of ice and water were then added to the cooled mixture and the suspension was stirred overnight. After filtration a pale brown solid was obtained that was purified by crystallization from EtOH to give 7.1 g of **14** (yield 67%) as a white solid.

^{1}H-NMR (δ $CDCl_3$, 300 MHz) ppm: 1.98-2.14 (m, 15H, 5OAc); 3.79-3.86 (m, 1H, H5); 4.07-4.15 (m, 1H, H6); 4.24-4.32 (m, 1H, H6); 5.08-5.17 (m, 2H, H2, H3, H4); 5.23 (t, $^{3}J_{HH}$ =8.55 Hz, 1H, H3); 5.72 (d, $^{3}J_{HH}$ =8.52 Hz, H1).

^{13}C-NMR (δ $CDCl_3$, 75 MHz) ppm: 20.58, 20.72, 20.83 (CH_3, OAc); 61.44, 67.73, 70.22, 72.73,72.80 (C2, C3, C4, C5, C6); 91.70 (C1); 168.98, 169.26, 169.40,170.12, 170.62 (CO, OAc).

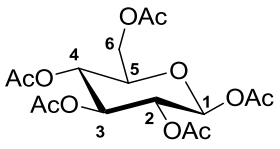

*Preparation of 2-(2-(2-propargyloxyethoxy)ethoxy)ethanol **16***

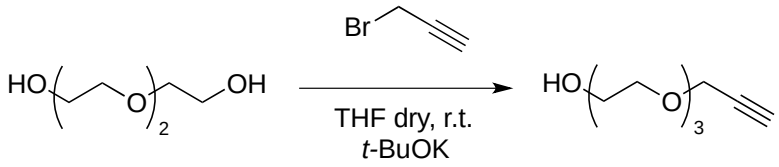

15 **16** (51%)

3.5 mL of triethylene glycol **15** (26 mmol) were dissolved in 150 mL of dry THF under nitrogen. Molecular sieves (4Å) and 2.9 g of *t*-BuOK (26 mmol) were added and the mixture was stirred for 1 hour. 2.9 mL of propargyl bromide (26 mmol) were then added dropwise and the reaction was stirred at room temperature overnight. The mixture was filtered over celite washing with CH_2Cl_2, and the solvent was removed under reduced pressure. The oily residue was purified by silica gel cromatography (eluent AcOEt) to give 2.53 g of **16** (13.4 mmol, yield 51%) as pale yellow oil.

^{1}H-NMR (δ $CDCl_3$, 300 MHz) ppm: 2.36 (t, $^{4}J_{HH}$ =2.35 Hz, 1H, CH); 3.15 (s, 1H, OH); 3.35-3.61 (m, 12H, CH_2OCH_2, $C\underline{H}_2OH$); 4.04 (d, $^{4}J_{HH}$ =2.35 Hz, 2H, $C\underline{H}_2CCH$).

^{13}C-NMR (δ $CDCl_3$, 75 MHz) ppm: 58.33, 61.60, 68.85, 70.11, 70.14, 70.41, 72.41 ($\underline{C}H_2O\underline{C}H_2$, $\underline{C}H_2OH$); 74.69, 79.45(sp carbons).

*Preparation of compound **21***

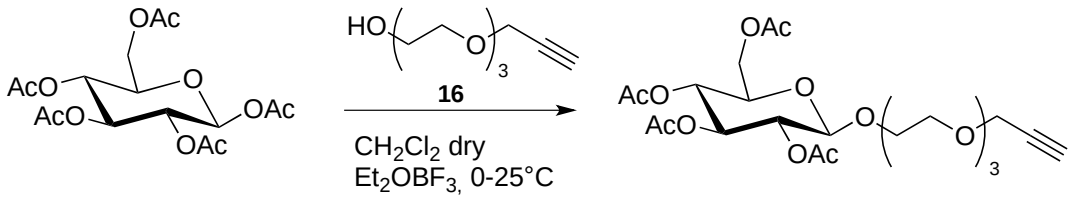

14 **21** (44%)

4.60 g of penta-*O*-acetylglucopyranoside **14** (11.8 mmol) and 1.85 g of **16** (9.8 mmol) were dissolved in 35 mL of dry CH_2Cl_2 under nitrogen. The solution was cooled to 0°C and 7.5 mL of $Et_2O{\cdot}BF_3$ (59 mmol) were added dropwise. The reaction mixture was heated to room temperature and stirred overnight. The mixture was then neutralized by an aqueous $NaHCO_3$satured solution, the aqueous phase was extracted with CH_2Cl_2 (2 x 20 mL) and the combined organic layers were dried over anhydrous Na_2SO_4. After filtration, the solvent was removed under reduced pressure. The oily residue was purified by silica gel cromatography (eluent CH_2Cl_2/AcOEt=7/3) to give 2.23 g of **21** (yield 44%) as a brown oil.

^{1}H-NMR (δ $CDCl_3$, 300 MHz) ppm: 1.94-2.15 (m, 12H, OAc); 2.38 (t, $^4J_{HH}$ =2.35 Hz, 1H, H15); 3.52-3.64 (m, 12H, H5, H7(1H), H8, H9, H10, H11, H12); 3.81-3.94 (m, 1H, H7); 4.03-4.11 (m, 1H, H6); 4.13 (d, $^4J_{HH}$ =2.35 Hz, 2H, H13); 4.14-4.23 (m, 1H, H6); 4.56 (d, $^3J_{HH}$ =7.98 Hz,1H, H1, β anomer); 4.92 (t, $^3J_{HH}$ =7.98 Hz,1H, H2); 4.96-5.08 (m, 1H, H4); 5.14 (t, $^3J_{HH}$ =8.02 Hz, 1H, H3).

^{13}C-NMR (δ $CDCl_3$, 75 MHz) ppm: 20.57, 20.59, 20.65, 20.72 (CH_3, OAc); 58.35; 61.91; 68.37; 69.01; 69.06; 70.31; 70.59; 70.63; 74.59; 100.78 (C1); 169.36, 170.25, 170.66, 171.12 (CO, OAc).

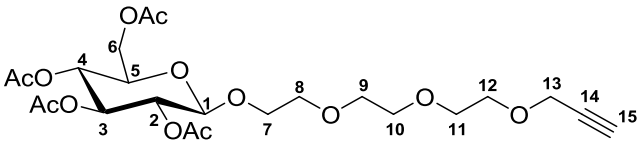

*Preparation of compound **22***

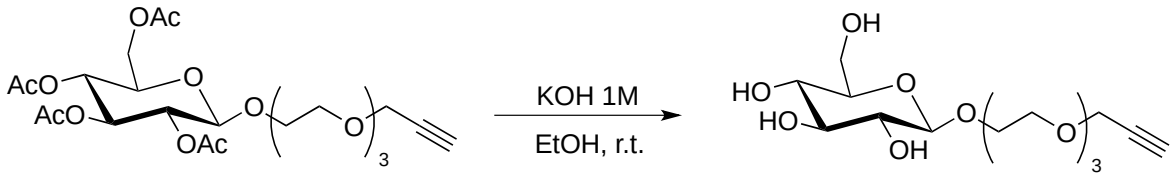

21 **22** (63%)

Compound **22** was prepared as described for the preparation of compound **7**. The product was obtained in a 63% yield.

^{1}H-NMR (δ $CDCl_3$, 300 MHz) ppm: 2.45 (t, $^{4}J_{HH}$ =2.36 Hz, H15); 3.27-3.39 (m, 3H, H2, H3, H4); 3.50-3.91 (m, 18H, 4OH, H5, H6, H7(1H), H8, H9, H10, H11, H12); 3.94-4.05 (m, 1H, H7); 4.15 (d,$^{4}J_{HH}$=2.36 Hz, H13); 4.28 (d,$^{3}J_{HH}$ =7.70 Hz, 1H, H1).

^{13}C-NMR (δ $CDCl_3$, 75 MHz) ppm: 58.33; 61.41; 68.60; 68.70; 69.01; 69.73; 70.22; 70.27; 72.52; 73.37; 74.91; 75.77; 76.38; 79.67; 103.00 (C1).

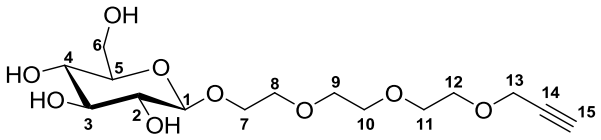

*Preparation of triazolic adduct **23***

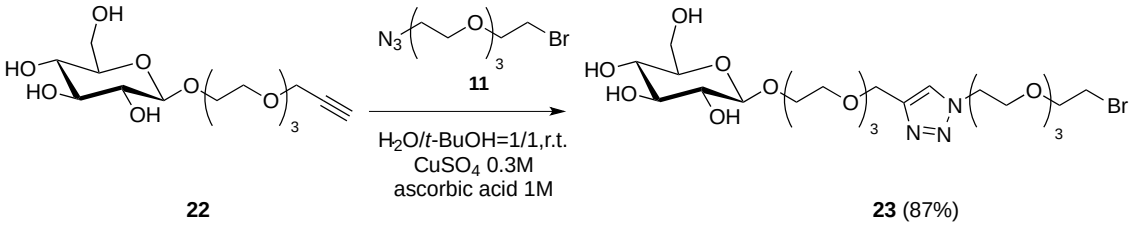

Compound **23** was prepared as described for the preparation of compound **12**. The product was obtained in a 87% yield.

^{1}H-NMR (δ CD_3OD, 300 MHz) ppm: 3.19 (t, $^{3}J_{HH}$ =7.95 Hz, 1H, H2); 3.25-3.40 (m, 3H, H3, H4, H5); 3.51 (t, $^{3}J_{HH}$ =6.53 Hz, 2H, H23); 3.57-3.76 (m, 20H, H6(1H), 7(1H), H8, H9, H10, H11, H12, H18, H19, H20, H21); 3.79 (t, $^{3}J_{HH}$ =6.53 Hz, 2H, H22); 3.82-3.85 (m, 1H, H6); 3.90 (t, $^{3}J_{HH}$ =6.35 Hz, 2H, H17); 3.96-4.04 (m, 1H, H7); 4.31 (d, $^{3}J_{HH}$ =8.02 Hz, H1); 4.59 (t, $^{3}J_{HH}$ =6.35 Hz, 2H, H16); 4.64 (s, 2H, H13); 8.15 (s, 1H, H15).

^{13}C-NMR (δ CD_3OD, 75 MHz) ppm: 30.12; 49.95; 61.29; 63.55; 68.20; 68.96; 69.35; 69.90; 69.92; 70.04; 70.11; 70.22; 73.59; 76.53, 76.60, 76.63; 102.26 (C1); 124.47 (C15); 144.16 (C14).

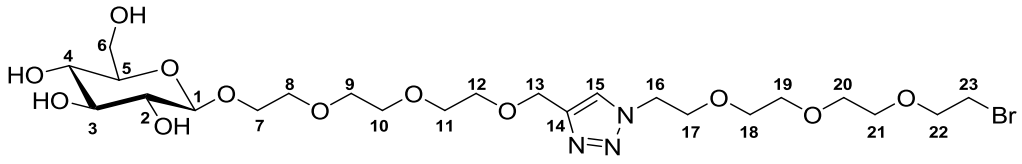

*Preparation of GA **4***

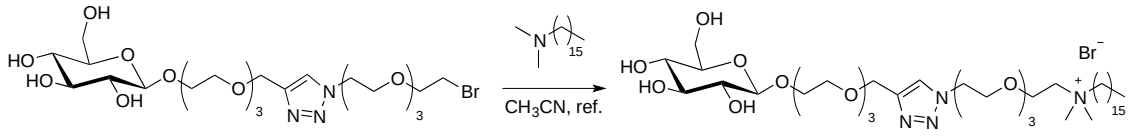

23 **4** (55%)

GA **4** was prepared with a 55% yield by alkylation of N-dimethyl-N-hexadecylamine with compound **23** according to the procedure described above for the preparation of GA**1**.

^{1}H-NMR (δ CD_3OD, 400 MHz) ppm: 0.89 (t, $^{3}J_{HH}$ =6.92 Hz, 3H, H41); 1.26-1.42 (m, 26H, H28, H29, H30, H31, H32, H33, H34, H35, H36, H37, H38, H39, H40); 1.72-1.84 (m, 2H, H27); 3.15 (s, 6H, H24, H25); 3.22 (t, $^{3}J_{HH}$ =7.88 Hz, 1H, H2); 3.26-3.42 (m, 5H, H3, H4, H5, H26); 3.52-3.78 (m, 22H, H6(1H), 7(1H), H8, H9, H10, H11, H12, H18, H19, H20, H21, H23); 3.83-3.94 (m, 5H, H6, H17, H22); 3.98-4.06 (m,1H, H7); 4.33 (d, $^{3}J_{HH}$ =7.88 Hz, 1H, H1); 4.60 (t, $^{3}J_{HH}$ =6.35 Hz, 2H, H16); 4.65 (s, 2H, H13); 8.15 (s, 1H, H15).

^{13}C-NMR (δ CD_3OD, 100 MHz) ppm: 13.05 (C41); 22.28, 22.34, 26.03, 28.88, 29.07, 29.19, 29.27, 29.35, 29.39, 31.67 (C27, C28, C29, C30, C31, C32, C33, C34, C35, C36, C37, C38, C39, C40); 50.01 (C16); 50.88 (C24, C25); 61.28 (C6); 63.01 (C23); 63.58 (C13); 64.36 (C22); 65.55 (C26); 68.21 (C7); 68.96, 69.35, 69.95, 69.98, 70.00, 70.11, 70.21, 73.65 (C5, C8, C9, C10, C11, C12, C17, C18, C19, C20, C21); 75.57 (C2); 76.63 (C3); 76.65 (C4); 102.91 (C1); 124.41 (C15); 144.10 (C14).

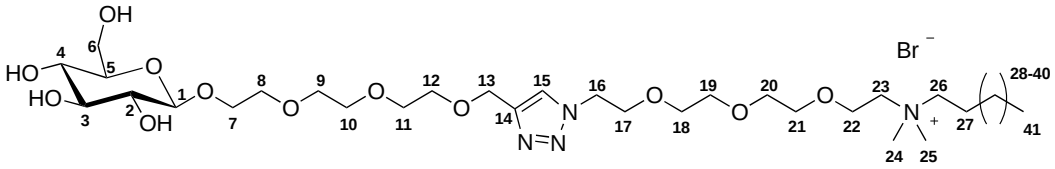

*Preparation of peracetylated lactose **18***

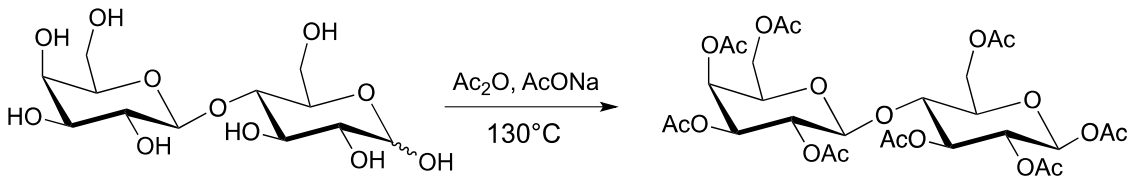

17 **18** (65%)

Compound **18** was prepared as described for the preparation of compound **14**. The product was obtained in a65% yield.

^{1}H-NMR (δ $CDCl_3$, 300 MHz) ppm: 1.94 (s, 3H, OAc); 2.01(s, 3H, OAc); 2.03 (s, 3H, OAc); 2.04 (s, 3H, OAc); 2.05 (s, 3H, OAc); 2.07 (s, 3H, OAc); 2.10 (s, 3H, OAc); 2.13 (s, 3H, OAc); 3.71-3.78 (m, 1H, H5); 3.81-3.88 (m, 2H, H4, H11); 4.03-4.15 (m, 3H, $H^{6,\ 12(1H)}$); 4.41-4.48 (m, 2H, H7, H12(1H)); 4.92 (dd, $^{3}J_1$ = 10.5 Hz, $^{3}J_2$ =3.5 Hz, 1H, H9); 5.02 (dd, $^{3}J_1$ = 9.5 Hz, $^{3}J_2$=8.3 Hz, 1H, H2); 5.08 (dd, $^{3}J_1$ = 10.5 Hz,$^{3}J_2$=7.9 Hz, 1H, H8); 5.22 (t, $^{3}J_{HH}$ = 9.5 Hz, 1H, H3); 5.32 (dd, $^{3}J_1$= 3.5 Hz, $^{3}J_2$ =1.1 Hz, 1H, H10), 5.64 (d, $^{3}J_{HH}$ = 8.3 Hz, 1H, H1).

^{13}C-NMR (δ $CDCl_3$, 75 MHz) ppm: 20.60, 20.70, 20.73, 20.84, 20.91, 20.93 (CH_3, OAc); 60.9 (C12); 61.8 (C6); 66.7 (C10); 69.0 (C8); 70.5 (C2); 70.8 (C11); 71.0 (C9); 72.7 (C3); 73.5 (C5); 75.7 (C4); 91.6 (C1); 101.0 (C7); 169.0, 169.2, 169.7, 169.8, 170.2, 170.3, 170.48, 170.51 (CO, OAc).

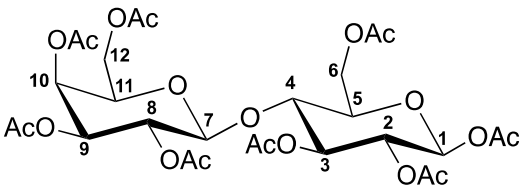

*Preparation of compound **19***

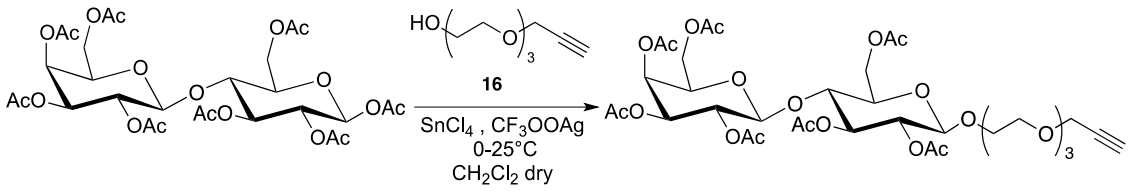

0.69 g of peracetylated lactose **18** (1.0 mmol) and 0.30 g of **16** (2.0 mmol) were dissolved in dry CH_2Cl_2. 0.33 g (1.5 mmol) of CF_3OOAg were added and the mixture was stirred at room temperature under nitrogen for 5 min. A 1M solution of $SnCl_4$ (3.0 mmol) in CH_2Cl_2 was added dropwise to the mixture upon stirring. After complete conversion of substrate, as indicated by TLC chromatography, the reaction was quenched by addition of saturated aqueous $NaHCO_3$. The mixture was then filtrate through Celite and the filtrate was extracted three times with CH_2Cl_2. The organic phase was washed with brine, dried over Na_2SO_4 and concentrated under reduced pressure. The residue was purified by silica gel column chromatography (eluent CH_2Cl_2/AcOEt=8/2) to afford 0.31 g (yield 38%) of product **19**.

^{1}H-NMR (δ $CDCl_3$, 300 MHz) ppm: 1.94 (s, 3H, OAc); 2.01(s, 3H, OAc); 2.03 (s, 3H, OAc); 2.04 (s, 3H, OAc); 2.05 (s, 3H, OAc); 2.07 (s, 3H, OAc); 2.10 (s, 3H, OAc); 2.13 (s, 3H, OAc); 2.37 (t, $^4J_{HH}$ =2.35 Hz, 1H, H21); 3.52-3.88 (m, 15H, H4, H5, H11, H13, H14, H15, H16, H17, H18); 3.90-4.10 (m, 3H, H6, H12(1H)); 4.15 (d;$^4J_{HH}$ =2.35 Hz, 2H, H19); 4.40-4.49 (m, 2H, H7, H12(1H)); 4.56 (d, $^3J_{HH}$ = 8.3 Hz, 1H, H1); 4.91 (t, $^3J_{HH}$ = 10.5 Hz,1H, H9); 5.02 (dd, $^3J_1$ = 9.5 Hz, $^3J_2$=8.3 Hz, 1H, H2); 5.08 (dd, $^3J_1$ = 10.5 Hz,$^3J_2$=7.9 Hz, 1H, H8); 5.22 (t, $^3J_{HH}$ = 9.5 Hz, 1H, H3); 5.32 (dd, $^3J_1$= 3.5, $^3J_2$ =1.1 Hz, 1H, H10).

^{13}C-NMR (δ $CDCl_3$, 75 MHz) ppm: 20.60, 20.70, 20.73, 20.84, 20.91, 20.93 (CH_3, OAc); 58.35; 61.91; 68.37; 69.01; 69.06; 70.31; 70.59; 70.63; 74.59; 77.52;100.62 (C1), 101.09 (C7); 169.09, 169.70; 169.79, 170.08, 170.17, 170.37, 170.41 (CO, OAc).

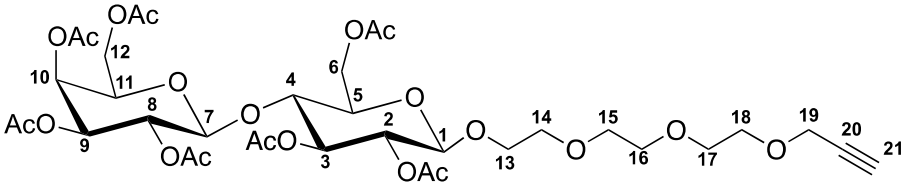

*Preparation of compound **20***

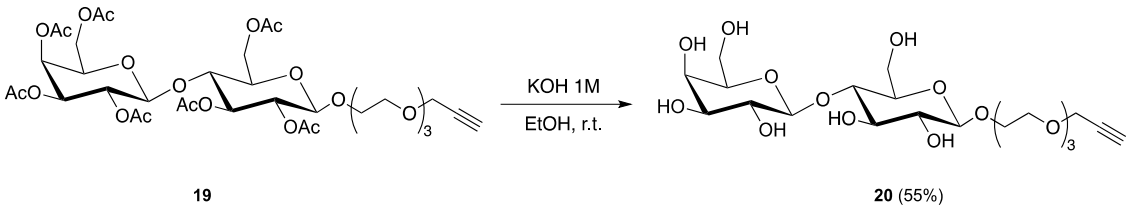

19 **20** (55%)

Compound **20** was prepared as described for the preparation of compound **7**. The product was obtained in a 55% yield.

^{1}H-NMR (δ CD_3OD, 300 MHz) ppm: 2.91 (t, $^{4}J_{HH}$ =2.35 Hz, 1H, H21); 3.30 (t, $^{3}J_{HH}$ =9.02 Hz, 1H, H2); 3.41-3.79 (m, 28H , 8OH, H2, H3, H4, H5, 6(1H), H8, H9, H11, H12, H13(1H), H14, H15, H16, H17, H18); 3.81-3.88 (m, 2H, H6(1H), H10); 3.90-4.07 (m, 1H, H13); 4.18 (d, $^{4}J_{HH}$ =2.35 Hz, 2H, H19); 4.34-4.36 (m, 2H, H1, H7).

^{13}C-NMR (δ CD_3OD, 75 MHz) ppm: 68.67; 61.41; 68.60; 68.70; 69.59; 69.73; 70.18; 70.34; 72.52; 73.33; 74.97; 75.77; 76.30; 79.67; 100.84 (C^{7}); 103.00 (C^{1}).

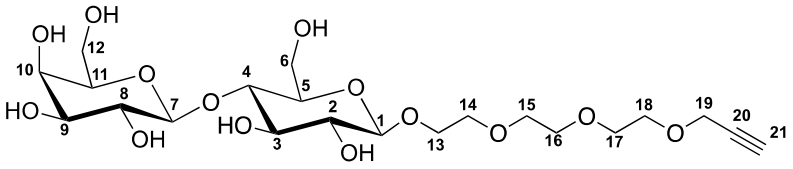

*Preparation of compound **24***

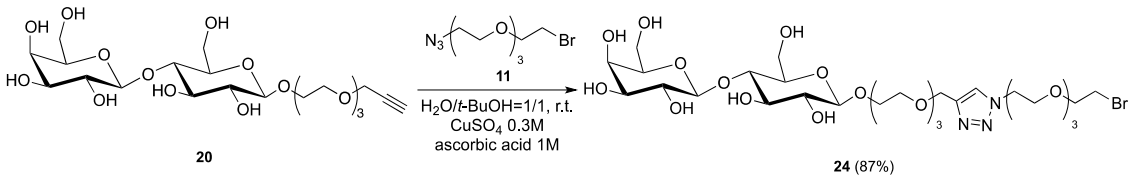

Compound **24** was prepared as described for the preparation of compound **12**. The product was obtained in a 87% yield.

^{1}H-NMR (δ CD_3OD, 300 MHz) ppm: 3.28 (t, $^{3}J_{HH}$ =8.50 Hz, 1H, H^2); 3.44 (t, $^{3}J_{HH}$ =6.53 Hz, 2H, H29); 3.30- 3.76 (m, 28H, H3-5, 6(1H), H8, H9, H11, H12, H13(1H), H14, H15, H16, H17, H18, H24, H25, H26, H27);3.79 (t, $^{3}J_{HH}$ =6.53 Hz, 2H, H28); 3.81-3.88 (m, 2H, H6(1H), H10); 3.90-4.07 (m, 1H, H13);3.90 (t, $^{3}J_{HH}$ =6.34 Hz, 2H, H23);3.96-4.04 (m, 1H, H13); 4.34-4.36 (m, 2H, H1, H7); 4.58 (t, $^{3}J_{HH}$ =6.34 Hz, 2H, H22); 4.62 (s, 2H, H19); 8.15 (s, 1H, H21).

^{13}C-NMR (δ CD_3OD, 75 MHz) ppm: 30.27; 50.10; 60.42; 61.17; 63.54; 68.15; 68.59; 61.41; 68.59; 68.70; 69.50; 69.60; 70.19; 70.40; 72.44; 73.28; 74.97; 75.75; 76.30; 79.67; 100.84 (C7); 103.00 (C1); 124.66 (C21); 144.19 (C20).

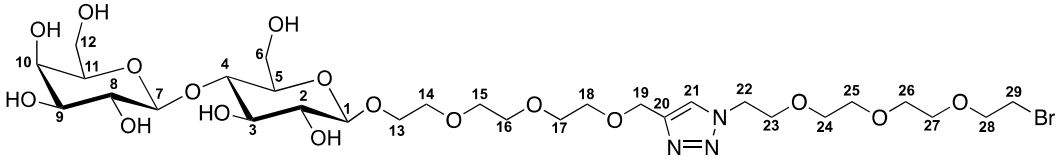

*Preparation of GA **5***

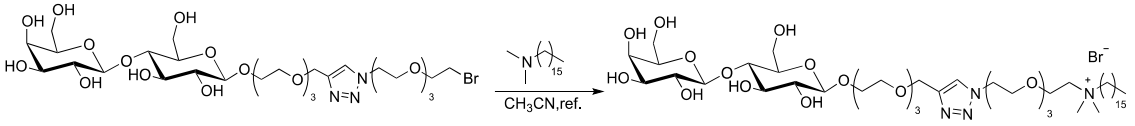

24 **5** (40%)

GA **5** was prepared with a 40% yield by alkylation of N-dimethyl-N-hexadecylamine with compound **24** according to the procedure described above for the preparation of GA**1**.

^{1}H-NMR (δ CD_3OD, 300 MHz) ppm: 0.88 (t, $^{3}J_{HH}$ =6.92 Hz, 3H, H47); 1.24-1.44 (m, 26H, H34, H35, H36, H37, H38, H39, H40, H41, H42, H43, H44, H45, H46); 1.70-1.83 (m, 2H, H33); 3.13 (s, 6H, H30, H31); 3.28 (t, $^{3}J_{HH}$ =8.50 Hz, 1H, H2); 3.30- 3.76 (m, 29H, H3-5, 6(1H), H8, H9, H11, H12, H13(1H), H14, H15, H16, H17, H18, H24, H25, H26, H27, H29); 3.81-3.88 (m, 2H, H6(1H), 10); 3.90-4.07 (m, 1H, H13); 3.96-4.04 (m, 1H, H13); 4.34-4.36 (m, 2H, H1, H7); 4.58 (t, $^{3}J_{HH}$ =6.34 Hz, 2H, H22); 4.62 (s, 2H, H19); 8.15 (s, 1H, H21).

^{13}C-NMR (δ CD_3OD, 100 MHz) ppm: 13.09 (C47); 22.32, 22.36, 26.07, 28.92, 29.10, 29.23, 29.30, 29.39, 29.43, 31.70 (C33, C34, C35, C36, C37, C38, C39, C40, C41, C42, C43, C44, C45, C46); 50.05 (C22); 50.94 (C30, C31); 60.42; 61.18; 63.58; 64.36; 65.55; 68.21; 68.96; 69.35; 69.95; 69.98; 70.00; 70.11; 70.04; 70.15; 70.21; 71.16; 73.43; 73.65; 75.57; 76.63; 76.65; 79.38; 102.51 (C7); 103.8145 (C1); 124.41 (C21); 144.10 (C20).

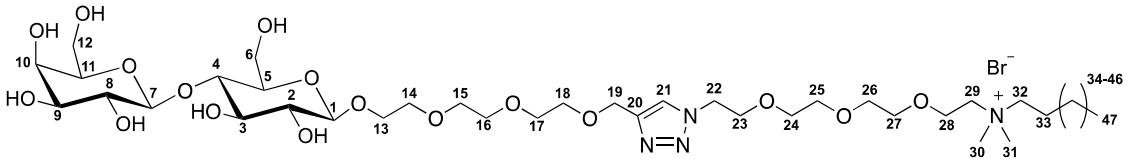

Determination of the critical micellar concentration (cmc) of amphiphile 1 and 4 by conductivity measurements

Conductivity measurements were carried out at 25 °C by adding known volumes of a GA **1** or GA **4** stock solution (5×10^{-1} M and 8×10^{-1} M, respectively) to 30 mL of deionized water. Specific conductivity, *K*, of solutions was measured after thorough mixing and temperature equilibration at each addition. Values of *K* were plotted versus concentration. The error in the conductivity measurements was within ±0.1%.

Determination of aggregates size by DLS

Aqueous solutions of GA **1** or **4** (50 mM) in PBS were characterized by DLS at a scattering angle of 173° at 25 °C. The normalized intensity autocorrelation functions were measured at an angle of 173° at 25.0±0.1 °C. The autocorrelation functions were analyzed by using the cumulant fit. The first cumulant was used to obtain the apparent diffusion coefficients *D* of the particles, further converted into apparent hydrodynamic diameters, d_h, by using the Stokes–Einstein equation $d_h = k_BT/3\pi\eta D$,where k_BT is the thermal energy and η the solvent viscosity.

Binding of 1 and 4 to fluorescent labeled ConA, FITC-ConA

The affinity between FITC-ConA and GA **1** or **4** was investigated at 25 °C by steady-state fluorescence experiments (at 525 nm; λ_{ecc}= 488 nm) according to a reported procedure[33] The fluorescence intensity of 2.5 mL of a solution containing 2.4 μg/mL of FITC-Con A and 3.2 μg/mL of glycogen in PBS was investigated as a function of the addition of small volumes of a 21.6 mM solution of amphiphile (**1** or **4**) in PBS. In a blank experiment the fluorescence intensity of 2.5 mL of a solution containing 2.4μg/mL of FITC-ConA (in the absence of glycogen) was investigated as a function of the addition of small volumes of a 21.6 mM solution of amphiphile in PBS.

33 Lis H. *et al.Chem. Rev.,* **1998**, 98, 637

Results and Discussion

In the synthetic activity of this thesis the synthetic possibility of creating a library of glycosylated amphiphiles, that could allow an extensive activity/correlation study on liposomes including them in the formulation, was explored.

Each of the glycosylated amphiphiles prepared in this work is characterized by the presence of i) a carbohydrate residue (Chart 2.1) that should attribute specificity toward lectins, a peculiar class of sugar-binding proteins[33], ii) a hydrophobic portion that should guarantee the anchorage to the lipid bilayer of a liposome, iii) an ammonium group that attributes the positive charge to the formulation, iv) a polyoxyethylenic spacer that should guarantee a good exposure of the sugar residue on the surface of liposomes.

The specificity of the carbohydrate-lectin interactions has been exploited as strategy for drug delivery where either carbohydrates or lectins have been used as homing devices to target specific cells or tissues.

In exploring the synthetic possibilities the variability of each of the portions of an ammonium salt based glycosilated amphiphile was explored, *i.e.* the sugar moiety, the hydrophilic spacer and the hydrophobic region. In fact, glucose was used for the preparation of amphiphiles **1, 2, 3** and **4** and lactose was used for amphiphile **5**. A hydrophilic spacer of different length was exploited to link the sugar residue to the ammonium group. Finally different hydrophobic portions, *i.e.* a different number of hydrocarbon tails or hydrocarbon tails of different length were used.

Amphiphiles **1-5** were synthesized according to the synthetic pathway described in Scheme 2.1 and Scheme 2.2.

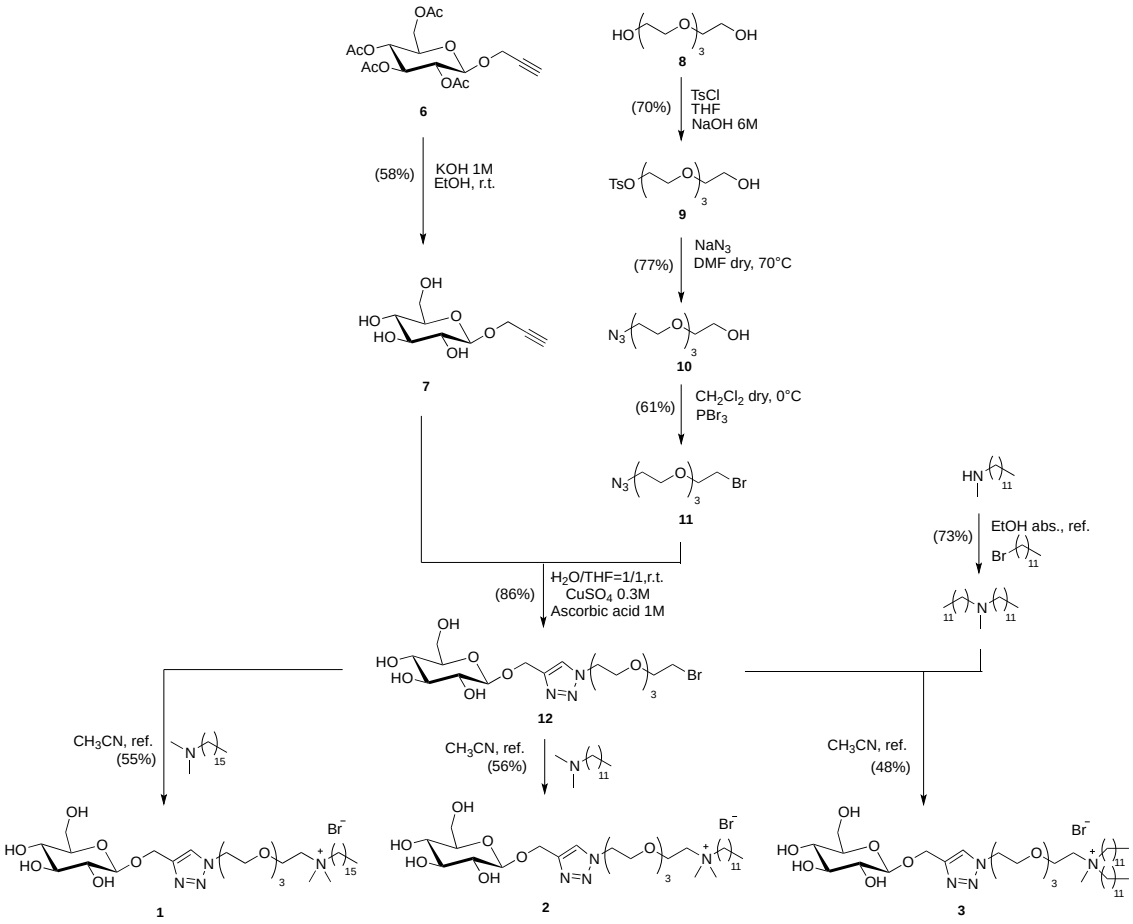

Scheme 2.1. Synthetic pattern for the preparation of GAs **1, 2** and **3**.

The key step of the convergent synthesis used for the preparation of the five amphiphiles is the Cu(I)-catalyzed "click" reaction that provides the linkage of azido-compound and the terminal alkyne with high yield and simple and mild reaction conditions[34]. The azido-compound **11** was obtained starting from tetraethylene glycol by common steps and isolated by a relatively simple procedure[16]. The alkyne **7** was obtained by the deacetylation of the commercial available tetra-*O*-Acetyl-β-D-propargylglucopyranoside. The obtainment of the click adduct **12** in high yield was confirmed by the presence of triazolic signal at 8.15 ppm in the ^{1}H NMR spectrum. Moreover, the 1,4-disubstitution of triazolic adduct was demonstrated by the presence of two correlation peaks of the triazolic proton with both adjacent methylenes at 4.59 and 4.64 ppm in the ^{1}H-^{1}H NMR NOESY spectrum. The alkylation of three tertiary amines differing for the hydrophobic tails, yielded GAs **1**, **2** and **3**. Amphiphiles **4** and **5**, characterized by a different hydrophilic spacer with respect to **1**, **2**

34 Kolb H. C. *et al.Angew. Chem.Int. Ed.*, **2001**, 40, 2004

and **3** were obtained by alkylating the same tertiary amine, N-hexadecyl-N,N-dimethylamine, with a click adduct bearing the glucose and lactose moiety, respectively.

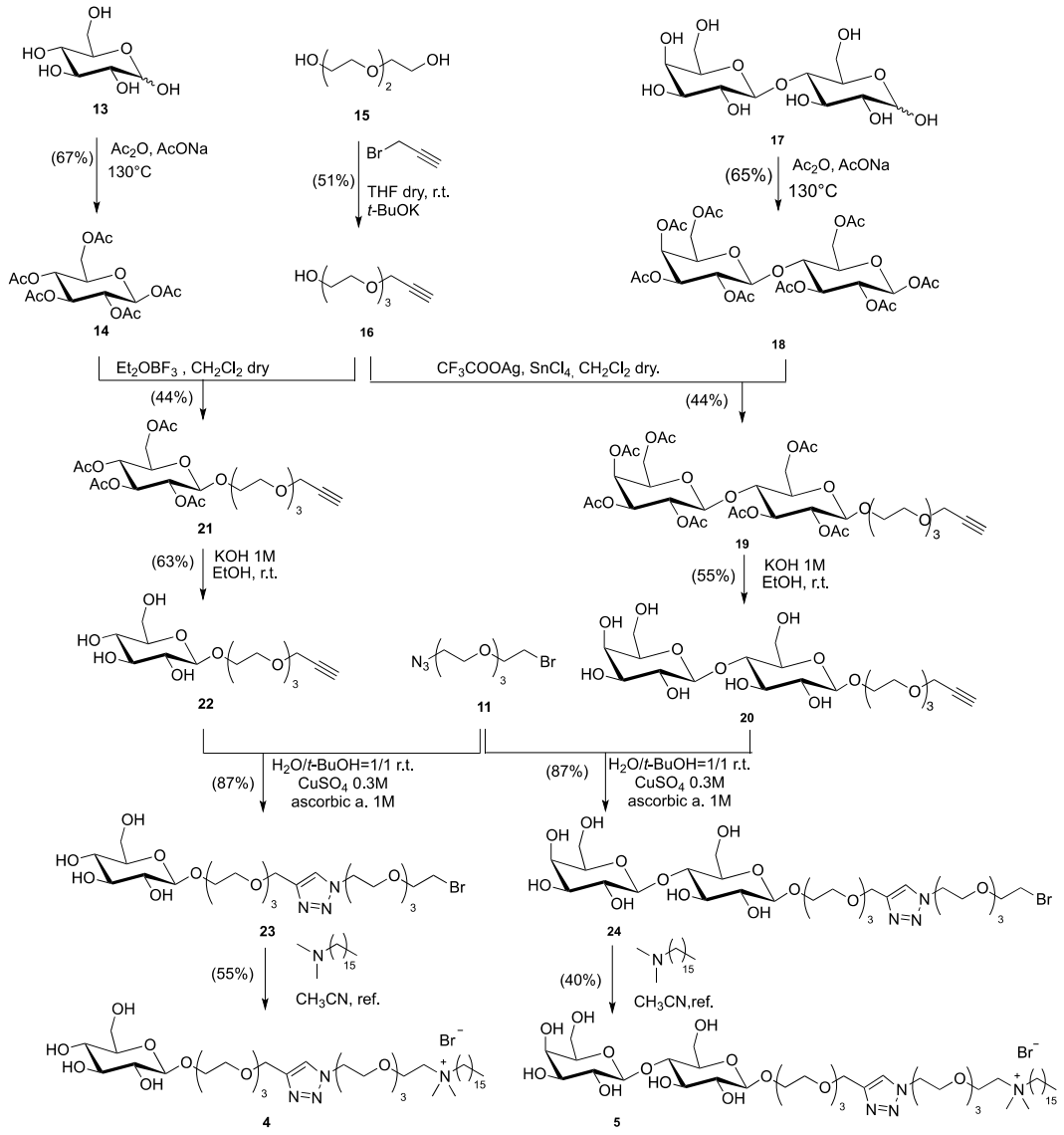

Scheme 2.2. Synthetic pattern for the preparation of GAs **4** and **5**.

In these cases, the synthetic procedures that gave the corresponding alkynes were more complex with respect to those illustrated above because they required the formation of a *O*-glycosidic bond. This aspect, that implies a higher number of synthetic steps, caused a decrease of the total yield. The alkyne **16** was obtained starting from D-glucopyranose and triethylene glycol following a reported procedure[35]. The β-*O*-glucosidic compound **21** was obtained by reacting β-peracetylatedglucopyranose **14** and compound **16** in the presence of

35 Michel O. *et al. Langmuir,* **2008,** 24,12116

$Et_2O{\cdot}BF_3$. The formation of the glycosidic bond between peracetylatedlactose **17** and **16** required a different synthetic approach because the reaction did not work in the presence of $Et_2O{\cdot}BF_3$. The obtainment of five different glycosylated amphiphiles indicated that the exploited synthetic procedure might allow the obtainment of a large library of glycosilated cationic amphiphiles. The interaction of the glycolipid included in the lipid bilayer of liposomes with the proper receptor involves a good exposure of the sugar residue on the surface of the liposomes. The introduction of two different hydrophilic spacers in the amphiphile molecules was explored to obtain GAs **1-3** characterized by the shorter spacer, and GAs **4** and **5** characterized by the longer one. GAs **1** and **4** differ only for the hydrophilic spacer, having the same sugar residue, *i.e.* glucose, and the same hydrophobic region, *i.e.* the hexadecyl tail. Therefore their aggregation properties were fully characterized in order to include them in liposome formulations and to investigate both experimentally and theoretically the binding of their formulations with Concanavalin A, Con A, a soy ben lectine specific for glucose used as a model compound in similar investigations[20].

Aggregating properties of Gas 1 and 4

Krafft point and Krafft temperature of GAs **1** and **4** were evaluated as <4 °C because their 20 mM aqueous solutions are completely transparent and stable at 4 °C. The plots of specific conductivity, *K*, versus the concentration of amphiphile **1** and **4** show two linear trends whose intersection at 1.0 X 10^{-3} M and 4.3 × 10^{-3} M, respectively defines the *cmc*s[36].

The DLS analysis of solutions of GA **1** and **4** above their *cmc* indicated the presence of micelles characterized by hydrodynamic diameter of 6.1 nm and 5.8 nm, respectively.

Binding of Gas 1 and 4 with ConA

Before investigating the binding of the liposome formulations including **1** and **4** with Con A (next chapters), the binding of pure GA **1** or **4** with Con A was investigated by florescence experiments exploiting fluorescent labeled Con A, FITC-Con A. The fluorescence of FITC-Con A is quenched upon complexation with multibranched polysaccharides of D-glucose such as glycogen, and restored by addition of monomeric D-glucose[37]. It was thus expected

36 Ananthapadmanabhan K. P. *et al. Langmuir*, **1985,** 1, 352
37 Sato K. *et al. J. Anal. Bioanal. Chem.*, **2006**, 384, 1297

that GA **1** or **4** could displace glycogen, thus dequenching the fluorescence of FITC-Con A similarly to D-glucose. Therefore, the fluorescence emission spectrum of a FITC-ConA solution quenched by glycogen was investigated upon the addition of GA **1** and **4**. The addition of small volumes of solutions of **1** and **4** restored the fluorescence of the protein as shown in Figure 2.1. The obtained results indicate that the glucose moiety of GA **1** and **4** substantially show the same capability to displace glycogen and to bind with ConA.

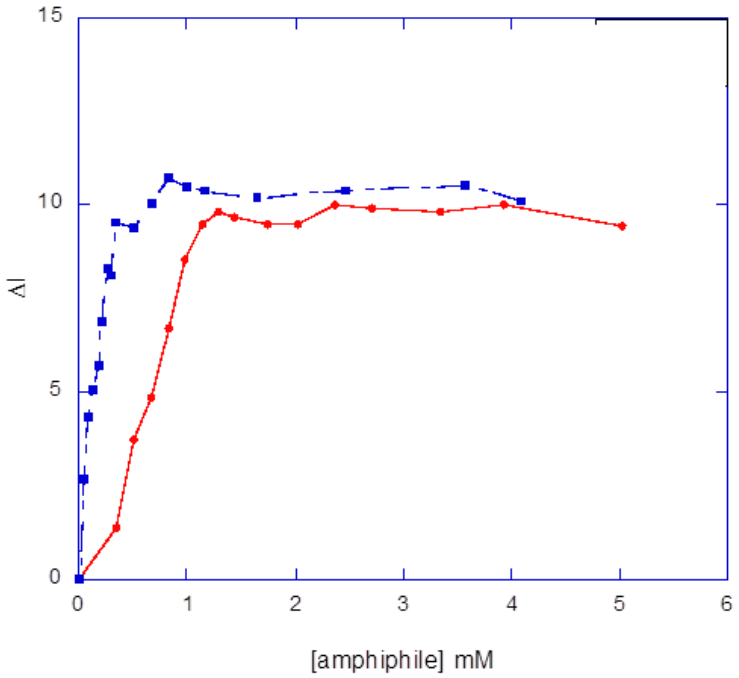

Figure 2.1. Fluorescence intensity increase observed upon the addition of GA **1** (blue squares) and GA **4** (red circles) to a solution of FITC-Con A-glycogen conjugate in PBS buffer. Initial concentration of FITC-Con A is 2.4μg/mL; initial concentration of glycogen is 3.2μg/mL.

In conclusion, the length of the polyoxyethylenic spacer has not a relevant influence on the aggregation properties of the amphiphiles and on their interaction with Con A.

Chapter 3

Inclusion of glucosylated amphiphiles 1 and 4 in liposomes formulations

This chapter deals with the physicochemical characterization of liposomes formulated with a natural phospholipid, DMPC, and glucosylated amphiphile, GA **1** or **4** at 9.5:0.5 and 9:1 molar ratio. The size and the size distribution, the main transion temperature (Tm), the surface potential and the interaction with lectins were investigated by DLS, fluorescence and UV spectroscopic measurements.

Experimental

Instrumentation

Steady-state fluorescence experiments were carried out on a Fluoromax-4 Horiba-Jobin Yvon spectrofluorimeter.

The optical density (OD) and UV measurements were carried out on Cary 300 UV–vis double beam spectrophotometer (Varian Australia PTY Ltd., Mulgrave, Vic., Australia).

DLS measurements were performed with a Malvern Nano-ZetaSizer spectrometer, equipped with a 5 mWHeNe laser (wavelength = 632.8 nm) and a digital logarithmic correlator.

Materials

2-dimyristoyl-s*n*-glycero-3-phosphocholine (DMPC) was purchased from Avanti Polar Lipids (Alabaster, AL). 4-heptadecyl-7-hydroxycoumarin (HC), 6-dodecanoyldimethylaminonaphthalene (Laurdan) Concanavalin A (ConA), from Canavalina ensiformis (Jack bean), glycogen, from bovine liver were purchased by Sigma-Aldrich.

Liposomes preparation

Aqueous dispersions of DMPC/**1(4)** liposomes were prepared according to the procedure described by Hope *et al.*[38] Lipid films were prepared on the inside wall of a round-bottom flask by evaporation of solution containing the proper amount of DMPC (dissolved in $CHCl_3$) and **1** (**4**) (dissolved in MeOH) to obtain the desired molar percentage mixture. The

38 Hope M. J. *et al.* Reduction of Liposomes Size and Preparation of Unilamellar Vesicles by Extrusion Techniques in Liposome Technology, 2nd ed.; *Gregoriadis, G. Ed. CRC Press: Boca Raton, FL,* **1992,** Vol.I, 123-139

obtained lipid films were kept overnight under reduced pressure (0.4 mbar) and PBS was added to obtain a lipid dispersion of the desired concentration. The aqueous solutions were vortex-mixed and then freeze-thawed six times from liquid nitrogen to 40 °C. Lipid dispersions were then extruded (10 times) through a 100 nm polycarbonate membrane.

Determination of aggregate size by DLS

The mean diameter and size distribution of liposomes were measured by DLS. Liposomes 1.25 mM in PBS were analyzed soon after preparation and after 48 hours. The normalized intensity autocorrelation functions were measured at an angle of 173° at 25.0±0.1 °C. The intensity size distribution of the liposomes was typically unimodal, therefore the autocorrelation function was analyzed according to the cumulant method. The autocorrelation functions were analyzed by using the cumulant fit. The first cumulants was used to obtain the apparent diffusion coefficients *D* of the particles, further converted into apparent hydrodynamic diameters, d_h, by using the Stokes–Einstein relationship $d_h = k_B T / 3\pi\eta D$, where $k_B T$ is the thermal energy and η the solvent viscosity.

Tm determination by fluorescence experiments.

The phase transition temperature, Tm, of the liposome bilayer was determined by a spectrofluorimetric method using Laurdan as a fluorescent probe highly sensitive to lipid phases. A mixed lipid film was prepared from a chloroform solution containing the proper amount of lipids (DMPC/**1** (**4**) at 95:5 molar ratio) and a volume of a Laurdan 0.4 mM chloroform stock solution to obtain a 1 μM Laurdan concentration and a 1 mM lipid concentration. Emission spectra (λ_{ecc}= 360 nm) were acquired as a function of temperature in the range 15–50 °C to determine the Tm of the formulation. Temperature was controlled by a circulating bath and the actual temperature was measured in the sample cuvette by a thermocouple. Excitation at 360 nm allows avoiding the photoselection of the probe molecules. The spectra were corrected for lamp intensity variations. The generalized polarization parameter (*GP*)[39] was calculated by equation 3.1:

$$GP = (I_B - I_R)/(I_B + I_B) \qquad \textbf{3.1}$$

39 Parasassi T. *et al. Biophys. J*., **1990,** 57, 1179

where I_B and I_R are the fluorescence emission intensities corresponding to the emission maxima characteristic of Laurdan in the pure gel and liquid-crystalline phases, *i.e.* 440 nm in the gel phase and 490 nm in the liquid crystalline phase[40]. The transition temperature for the liposome preparation corresponds to the inflection point in the GP versus temperature plot.

Tm determination by optical density (OD) measurement

Thermal phase transition of mixed liposomes was determined from the temperature-dependent changes of specific turbidity. The temperature scan, in the 20-35 °C range, was carried out at 260 nm at a 1 °C/min rate. Results were expressed in turbidity (OD) as a function of temperature. The Tm of the liposome formulation corresponds to the inflection point in the OD versus temperature plot. Measurements were made at 2.5 mM total lipid concentration in PBS.

Determination of potential surface(ψ°) of DMPC/1 (95:5) liposome

Surface potential was determined by an indirect method described in the literature that exploits the pH-sensitive fluorophore HC[41]. Liposomes were prepared as described above, in this case DMPC/**1** (**4**)**,** mixed films were prepared from a chloroform solution containing the proper amount of lipids and also a volume of a HC 10^{-4} M THF stock solution (to obtain after hydration of the lipid film a final 10^{-4} M HC concentration and a 1 mM lipid concentration).

Fluorescence measurements of 5 mM liposome suspension of DMPC/**1**/HC (95/5/0.3) in PBS were performed by scanning the excitation wavelength between 300 and 400 nm, at an emission wavelength of 450 nm, varying the pH between 2 and 12 by addition of concentrated sodium hydroxide or hydrochloric acid. The dissociation degree of HC incorporated into liposomes was monitored by the ratio of the excitation fluorescence intensities at 380 nm and 330 nm (pH independent isosbestic point). pKa of HC in the liposome bilayer and consequently, the surface potential (ψ°) was obtained by the plot of I_{380}/I_{330} ratio as a function of pH.

40 Parasassi T. *et al*. *J. Fluoresc*., **1998,** 8(4), 365
41 Zuidan, N. J. *et al. Biochim. Biophys. Acta,***1997**, *1329*, 211

Agglutination detection by optical density measurement.

The agglutination of functionalized liposomes in the presence of ConA was determined from the time-dependent changes of specific turbidity of a 1 mL sample of 0.8 mM DMPC/GA (95:5) liposomes in PBS in a 1 cm quartz cell upon addition of Con A (0.33 mg/mL final concentration) in PBS. Scan was carried out at 525 nm immediately after mixing and every minute till 5 hours.

Agglutination detection by DLS measurement.

The agglutination of functionalized liposomes in the presence of ConA was determined from the time-dependent changes of size distribution in a 1 mL sample of 0.8 mM DMPC/**1** or DMPC/**4** (95:5) liposomes in PBS upon addition of Con A (0.33 mg/mL final concentration) in PBS. Scan was carried out immediately after mixing and agglutination has been followed for 5 hours.

Results and discussion

Liposomes size and stability

Liposome size can vary from very small to large vesicles and size is a critical parameter in determining liposome circulation half-life because it affects clearance by the reticuloendothelial systems (RES). In fact, small liposomes are opsonized less rapidly and to a lower extent compared to large liposomes.

The size of DMPC/**1 (4)** liposomes (at 1.25 mM concentration) was determined by DLS measurements. The results obtained by DLS analysis are reported in Table 3.1. Soon after extrusion and after 24 hours the presence of a stable monomodal distribution (confirmed by the low value of polydispersity index, PDI) of liposomes characterized by a hydrodynamic diameter in agreement with extrusion protocol were observed only for the 95:5 formulation, whereas a polydistribution was found for the 90:10 formulations. The intensity of light scattering is directly proportional to the sixth power of the particle radius and to the square of the mass of the aggregates, therefore though a peak corresponding to small aggregates can show a low intensity, this population could also be the major one, or very abundant. In the case of 9:1 DMPC/**1** (**4**) liposomes the presence of a second population of small aggregates, whose abundance significantly increases after 24 hours, indicates that also a relatively low amount (10%) of glucosylated amphiphile **1** or **4** strongly destabilizes the

lipid bilayer due probably to a detergent effect. Thus, only the 95/5 DMPC/**1**(**4**) formulations were selected for further investigations.

Table 3.1. Hydrodynamic diameter of the DMPC/GA liposomes obtained from dynamic light scattering measurements at 25°C.

Formulations	**Size, nm t 0 (Peak area Intensity,%)**	**PDI t 0**	**STDV, nm t 0**	**Size, nm t 24 h (Peak area Intensity, %)**	**PDI t 24 h**	**STDV t 24 h**
DMPC/**1** 95/5	95	0.173	±23	106	0.164	±20
DMPC/**1** 90/10	245, 48 (90, 10)	0,364	±30	230,50	0,370	±25
DMPC/**4** 95/5	110	0.05	±15	115	0.07	±13
DMPC/**4** 90/10	135, 24* (95, 5)	0.26	±20	166, 30* (77, 33)	0.33	±18
1	6	0.06	±2	10	0.05	±2
4	6	0.002	±3	8	0.007	±2

Main transition temperature (Tm)

Lipids are characterized at a certain temperature, Tm, by a phase transition which involves substantial changes in the organization and motion of the fatty acyl chains within the bilayer. Below the Tm lipids are in a rigid, well-ordered arrangement ("solid" gel-like phase); above the Tm are in a liquid-crystalline ("fluid") phase (Figure 3.1)[42].

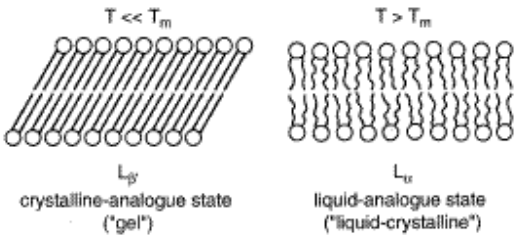

Figure 3.1. Schematic representation of the lipid arrangement in a planar bilayer below and above the main lamellar chain-melting phase transition temperature, *i.e.* the Tm.

42 Walde P. *et al. Biomol. Bioeng.*, **2001** 18(172), 143

When a membrane is heated through the Tm the surface area increases and the thickness of the lipid bilayer decreases as the membrane goes through a phase transition. The mobility of the lipid chains increases dramatically. This is the reason why mechanical treatments of lipid vesicles have to be carried out above Tm, in the fluid state of the membranes.

Below the Tm, the saturated hydrophobic chains exist predominately in a rigid, extended all trans conformation, similar to their crystalline state. As a result, the surface area per lipid is minimal and the bilayer thickness is maximal. Above the Tm, the chains are rather disordered with a number of gauche conformations in the hydrocarbon chains, that make the lipid bilayer fluid (mechanically treatable) and characterized by increased lateral and rotational lipid diffusion rather similar to a liquid; as a result, the surface area per lipid increases and the bilayer thickness decreases by 10 to 15%. Tm value depends to some extent on the curvature of the bilayer and on the experimental conditions, in particular if the amphiphiles have polar head groups that can undergo protonation/deprotonation.

The Tm of the 95:5 DMPC/**1** and DMPC/**4** liposome formulations were measured by both fluorescence and turbdimetric measurements. It is known that the fluorescence properties of a particular membrane probe, *i.e* Laurdan, included in a lipid bilayer, can give information on the Tm of the lipid bilayer[43]. In a lipid membrane Laurdan does not have specific affinity towards any phospholipid head group and distributes equally, at the level of glycerol backbone, between the gel and the liquid-crystalline phases, however, it displays a phase-dependent emission spectral shift, from 440 nm in the gel to 490 nm in the liquid-crystalline phase, due to the solvent dipolar relaxation phenomenon[39]. The red shift depends on the water concentration and mobility close to the Laurdan naphthalene moiety, and is observed only in the liquid crystalline phase, because water mobility is significantly slower in the tightly packed gel phase, and the dipoles cannot reorient during the Laurdan excited state[40]. Thus, the value of *GP* (Experimental part) is related to water penetration and to the phase state of the lipid membrane.

The turbidimetric method of analysis of liposome suspensions is based on measuring temperature-dependent sample turbidity, determined as optical density (OD) at 260 nm, where the absorption of the sample is negligible; hence, the light attenuation by the particle suspension is only due to scattering, and variations in phase transition depend on the geometric and physical parameters of liposomes, such as dimensions and refractive indexes of the assemblies.

---

43 Aleandri S. *et al. Soft Matter*, **2012**, 8, 5904

The results obtained by fluorescence and turbidity measurements are reported in Table 3.2. The values obtained by the two techniques are in optimal agreement and are very close to each other and to the Tm of DMPC, indicating that the presence of 5% of both **1** or **4** does not induce any significant change in the organization of the lipid bilayer of DMPC. This result is not surprising because the two GA bear the same alkyl chain and the main transition, as explained above, occurs in the hydrophobic region of the lipid bilayer.

Table 3.2. Tm values of DMPC/**1**(**4**) measured by both fluorescence and turbdimetric measurements. Uncertainty in determination is 0.5 °C.

	T_m (°C) Fluorescence	T_m (°C) OD
DMPC	24.2	24.1
DMPC/**1** 95/5	24.5	24.2
DMPC/**4** 95/5	24.5	24.3

Potential Surface (ψ°)

The potential at the interface between the lipid bilayer and adjacent electrolyte solution is defined as the surface potential, ψ_0; this potential is due to the fixed charges within or attached to the membrane phase (with the Stern layer). The measurement of surface potential can be made through the determination of a so-called potential-determining ion. The extent of the association of a potential determining ion depends on its concentration in the bulk because its electrochemical potential must be the same in both phases (*i.e.* at the surface and in the bulk). In proteins, biological materials and metal oxides, H_3O^+ is frequently a potential-determining ion because of the pH dependence on the degree of dissociation of acid or basic groups. It seems reasonable to consider that potential-determining ions completely leave the solution phase and become desolvated and in tight chemical association with the membrane surface. The surface potentials are not usually readily measurable with electrodes due to the thickness of the membrane phase. Here we obtained surface potential by the use of the lipophilic, pH-sensitive fluorophore HC, following a procedure described in the literature[41].

Its fluorophore is the hydroxycoumarin moiety, which is a weak acid. At pH < pK_a the maximal fluorescence intensity is found at an excitation wavelength of ~ 320 nm, and at pH > pKa the excitation maximum is shifted to the wavelength of ~ 380 nm. The fluorescence intensity at the excitation wavelength of 330 nm is the pH-independent isosbestic point, which reflects the actual level of the fluorophore present in the lipid assembly. In Figure 3.3a excitation fluorescence spectra of HC included in DMPC liposomes at low and high pH value are reported; in Figure 3.3b excitation fluorescence spectra registered in the titration of HC included in DMPC liposomes are reported. Therefore, the dissociation degree of HC incorporated into the mixed DMPA/GA liposomes can be monitored by the ratio of the excitation fluorescence intensities at 380 and 330 nm (380 nm/330 nm) as a function of the pH (see figure 3.2).

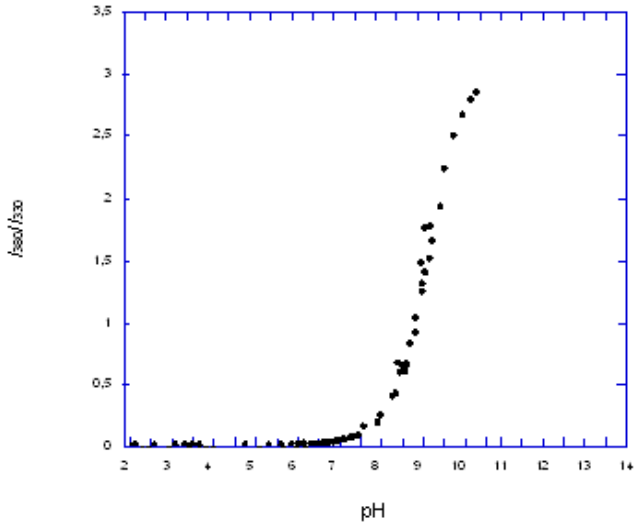

Figure 3.2. Excitation fluorescence intensities at 380 and 330 nm (I_{380} /I_{330}) as a function of the pH for the 95:5 DMPC/**1**.

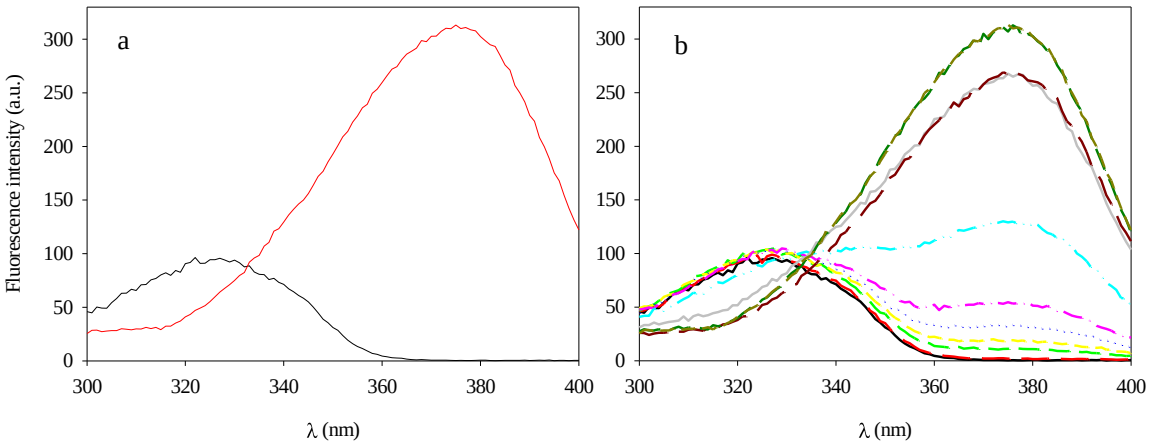

Figure 3.3. a) Excitation fluorescence spectra of HC included in DMPC liposomes at low pH value (black trace) and high pH value (red trace); b) Excitation fluorescence spectra registered in the titration of HC included in DMPC liposomes

Proton binding to a molecule which is present at the water/lipid interface, such as HC, can be described by[44]

$$pK_a = pK_H + \Delta pK_{pol} + \Delta pK_{e1} \qquad \textbf{3.2}$$

where pK_H is the proton association constant, ΔpK_{pol} is the shift in pK_a due to a change in surface polarity (dielectric constant), and ΔpK_{e1} is the shift in pK_a due to a change in surface potential. We assume that DMPC liposomes are neutral throughout the pH range used in this study. Therefore, ΔpK_{el} of HC in charged liposomal membranes can be estimated by taking the pK_a of HC in DMPC liposomes as a neutral reference, assuming that there is no change in surface polarity (see equation 3.2). The value of ΔpK_{el} is then used to calculate the electrical surface potential at the location of the chromophore in the charged membranes, ψ_0^{HC} (V), by conversion and rearrangement of Boltzmann equation:

$$\psi_0^{HC} = - \Delta pK_{el}\, kTln10/e = - (pK_a^{charged} - pK_a^{neutral})K_B Tln10/e \qquad \textbf{3.3}$$

where K_B is the Boltzmann constant, T is the absolute temperature, *e* is the electron charge and $pK_a^{charged} - pK_a^{neutral}$ are the pK_a in charged bilayers and in neutral DMPC bilayers respectively.

95:5 DMPC/**1** and DMPC/**4** formulations were characterized, as expected, by a positive value of potential surface ψ° (23±6 mV and 24±3 mV, respectively), due to the exposure of ammonium groups on vesicles surface. Also in this case, the obtained values are very similar to each other and this could have been expected considering that the two molecules feature the same polar headgroup that is probably located in the same region of the bilayer.

Interaction of amphiphile 1 and 4 with Con A (agglutination assay)

In order to evaluate the interaction of the sugar residues on the surface of liposomes with Con A and to investigate possible differences due to the different length of hydrophilic spacer turbidity and DLS measurements were performed. In fact, the interaction of Con A with sugar decorated liposomes results in aggregation of vesicles, known as agglutination,

44 Tatulian A.S. *et al. Phospholipids Handbook*, **1993**, 551

due to the presence of multiple binding sites for carbohydrates on the protein (multivalent binding), and agglutination can be monitored by turbidity and DLS.

OD measurements.

In the case of 95:5 DMPC/**4** liposomes changes of OD were observed upon the addition of Con A, and vesicle precipitation occurred in ~100 minutes. This result clearly indicates that agglutination took place (Figure 3.4, red line). On the other hand, when the same experiment was carried out on 95:5 DMPC/**1** liposomes an increase of the OD value was observed, however precipitation did not occur (Figure 3.4, blue line). This results suggests that also in this case agglutination occurs, but the phenomenon is slower than in the case of DMPC/**4** liposomes. In the case of DMPC liposomes, *i.e.* devoid of GA, the addition of Con A also induced agglutination, as reported in the literature[45] however OD changes were not detected for at least 4 hours and precipitation was observed only after 24 hours. In the absence of Con A, neither OD changes nor precipitation were observed. Thus, the presence of 5% of the amphiphile **1** or **4** strongly affects the kinetic of the interaction of liposomes with Con A, further the efficacy of interaction with Con A depends on the length of the hydrophilic spacer, being more efficient in the case of GA **4**. This suggests that in the case of DMPC/**4** vesicles the sugar moiety is more exposed to the bulk and, as a consequence, more accessible to the lectin.

DLS measurements

The results obtained by DLS measurements are reported in Figure 3.5. In the presence of DMPC/**4** liposomes agglutination and precipitation occured, in good agreement with the results obtained by turbidity measurements. On the other hand, when the same experiment was carried out on DMPC/**1** liposomes neither agglutination or precipitation was observed. However this apparent discrepancy with the results obtained by turbidity measurements could be due to the low concentration conditions. Therefore DLS results are in good agreement with OD measurements.

45 Engel A. *et al. Journal of Pharmaceutical Sciences*, **2003**, 92, 2229

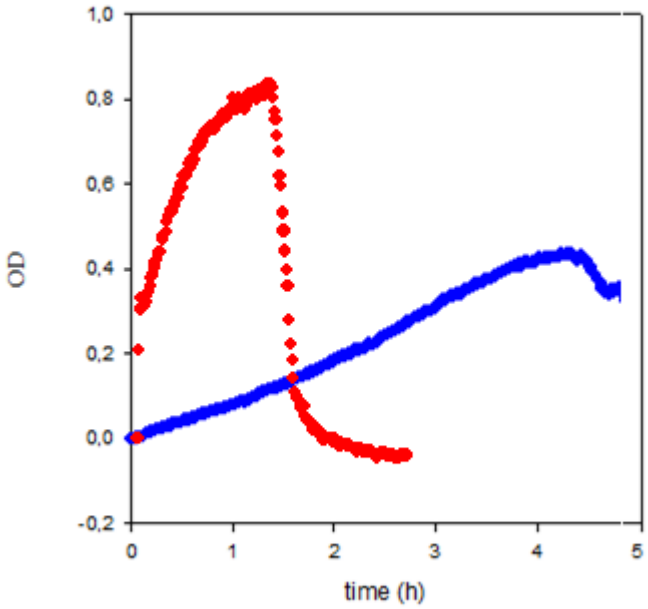

Figure 3.4. Turbidity increase observed upon the addition of Con A to a suspension of 95:5 DMPC/GA vesicles in PBS (GA **4** red line; GA **1** blue line). Con A concentration is 0.33 mg/mL; total lipids concentration is 0.8 mM.

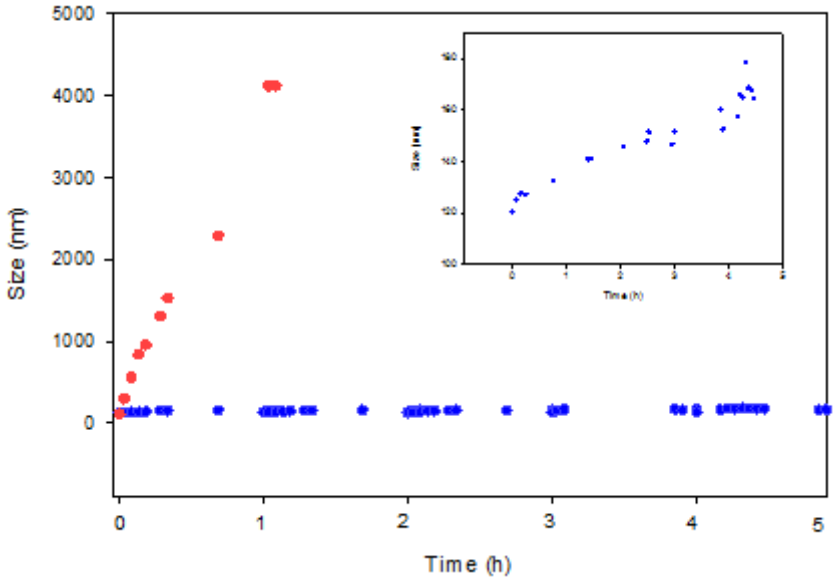

Figure 3.5. Size changes increase observed upon the addition of Con A to suspensions of 95:5 DMPC/GA vesicles (GA **4** red circles; GA **1** blue circles, plotted in a different scale in the upper right).in PBS. Con A concentration is 0.33 mg/mL; total lipids concentration is 0.8 mM.

Summarizing, the presence of 5% of the GA in liposomes does not alter the physicochemical properties of the lipid bilayer of DMPC liposomes, whereas when the its percentage increases it has a strong perturbing effect. DMPC/**4** liposomes were shown to interact with con A also in the dilute conditions of DLS experiments, thus demonstrating a better efficacy of interaction with respect to DMPC/**1** liposomes. It is clear that the length of the polyoxyethylenic spacer has a fundamental role on the exposure of the sugar moiety on the surface of liposomes and hence on the binding of glycosylated liposomes to lectins.

Chapter 4

Investigation of the interaction of Concanavalin A with glycosylated liposomes by molecular dynamics simulation.

This chapter reports on the theoretical investigation of the interaction of ConA with lipid bilayers composed of DMPC and GA **1** or **4** by molecular dynamics calculations. Molecular dynamics is a branch of computational chemistry that allows studying, through simulations, the time evolution of molecular system models. These are based on a simplified description of atomic interactions, obtained through the use of a set of functions of potential energy, defined as force field, parameterized by experimental data or obtained from results of quantomechanical calculations. Forces acting on the particles that compose the system derive from molecular potential functions, and by applying the principles of classical mechanics it is possible to obtain the evolution of the system as a function of time, named trajectory. The trajectories obtained are used to calculate the structural and thermodynamic properties of the studied system on the basis of the *ergodic hypothesis* that establishes the equivalence of the time average, for long periods of simulation, with statistical average of the microstates that characterize the system.

The first molecular dynamics simulation was reported by Alder and Wainwright[46] who studied the dynamics of an assembly of hard spheres to simulate a crystal/liquid system. With the advent of faster computers and of high-level programming languages, it was possible to simulate much more complex molecular systems such as liquid water[47], alkanes[48] and small proteins[49]. Moreover, molecular dynamics has been used successfully to simulate molecular aggregates of amphiphilic molecules such as micelles and lipid membranes, thus obtaining information on some biological phenomena[50]. The first molecular dynamics simulation of a lipid bilayer, performed by van der Ploeg and Berendsen[51] in 1982, involved a system of 32 dodecanoate molecules arranged in a bilayer. With the increase of computational power, it has been possible to simulate systems with a higher extent of complexity. Several studies concerned peptides at the membrane/water

46 Alder, B. J. *et al. J. Chem. Phys.,* **1957**, 27, 1208
47 Rahman, A. *et al. J. Chem. Phys.*, **1971**, 55, 3336
48 Ryckaert, J. *et al. Chem. Phys. Lett.*, **1975**, 30, 123
49 McCammon, J. *et al. Nature*, **1977**, 267, 585
50 Lookman T. *et al. Biochemistry*, 21, **1982**,5593
51 van der Ploeg, P. *et al. J. Chem. Phys.*, **1982**, 76, 3271

interface[52], the formation of pores and peptides channels in lipid bilayers[53], the interaction of proteins[54], medicinal plant extracts and drugs[55] with lipid membranes. At present, the accuracy of these techniques gives the possibility of analyzing and studying the binding of a protein with a ligand also considering the role of the solvent. An example is the paper by Kadirvelraj *et al*.[32] that reports on the role of water molecules in the binding of Con A with a trimannoside saccharide ligand. It was shown that along all the simulation a number of water molecules remained in the lectin binding site with an active role in the binding.

Recently it has been possible to simulate very complex systems involving a very large number of atoms by the coarse-grain method. In this method groups of atoms are assembled into beads to reduce the number of degrees of freedom, thus reducing the complexity and length of simulation. Though the obtained description is not atomistic, however this method gives valuable information on very complex systems such as liquid crystals[56] and cell membranes[57]. Another valuable methodology that allows simulating very complex and large systems is the metadynamics. Metadynamics is a powerful algorithm that can be used both for reconstructing the free energy and for accelerating the sampling of rare events in systems described by complex Hamiltonians, at the classical or at the quantum level. In the algorithm the normal evolution of the system is based on a history-dependent potential constructed as a sum of Gaussians centered along the trajectory followed by a suitably chosen set of collective variables. The sum of Gaussians is exploited for reconstructing iteratively an estimation of the free energy and forcing the system to escape from local minima[58].

In this work the simulation of the membrane/protein systems was carried out at the atomistic level on a preassembled lipid bilayer embedded in water as requested for such a system. In fact, the molecular dynamic simulation of such a complex system, involving a large number of lipid and water molecules, requires a preassembled lipid bilayer because, due to computational times and costs, it is not possible to start from a random configuration.

---

52 Bernèche, S. *et al. Biophys. J.*, **1998**, 75, 1603
53 Tieleman, D. P. *et al. Biophys. J.*, **1998**, 74, 2786
54 Lumb C. N. *et al. Biophysical Journal*, **2013**,104, 613
55 Telenius J. *et al. FEBS Journal* **2013,** 280, 2785
56 Wang Y. *et al. Acc. Chem. Res.*, **2007**, 40(11), 1193
57 SanSom M.S.P. *et al. J. Chem. Phys.*, **2004**, 121, 11942
58 Laio A. *et al. Rep. Prog. Phys.*, **2008**, 71, 126601

Further, before the molecular dynamics investigation of the two DMPC/GA systems it was necessary to analyze, through a docking procedure, the binding of the saccharidic residues with the protein. In fact, the docking procedure allows a quite accurate prediction of the binding modes of a small molecule (ligand) with a large protein. Molecular dynamic simulation and docking procedure both required an accurate choice of force fields.
The report on the simulation carried out on our lipid/protein systems will be preceded by a brief description of the basic principles underlying the adopted methodology to facilitate the reading to people who are not acquainted with theoretical chemistry.

Docking: basic principles

The molecular modeling prediction by the docking method involves a protocol that consists of two fundamental steps, i) a search strategy and ii) a scoring function.
The search strategy makes use of a search algorithm and can generate a number of configurations that include the experimentally determined binding mode and all the possible binding modes of the ligand with the receptor. All six degrees of translational and rotational freedom of the ligand are explored along with the internal conformational degrees of freedom of both the ligand and the protein. Therefore, to reduce the complexity and size of calculation, it is necessary to apply constraints, restraints and approximations as, for example, that of treating the ligand and target as rigid bodies with the exploration of the only six degrees of translational and rotational freedom or, that of considering only the conformational space of the ligand by assuming a rigid receptor throughout the docking protocol.
The scoring function makes use of the searching algorithm and allows distinguishing the experimental binding modes from all other explored modes. At present, it is possible to use the scoring function by two different approaches. In the first approach the full scoring function is used to set a protein ligand conformation, then the whole system is modified by the search algorithm, and finally the same scoring function is applied again to set the new structure. The alternative approach consists in using a two stage scoring function in which, first, a reduced function is used to direct the search strategy and then a more rigorous scoring function is used to rank the resulting structures. Currently there are different methods for docking studies, the principal techniques are: molecular dynamics, Monte

Carlo methods, genetic algorithms, fragment-based methods, distance geometry methods, *tabu* searches and systematic searches[59].

- Molecular dynamics (MD). The employment of standard MD to find the global minimum energy of a docked complex involves the calculation of solutions to Newton's equations of motion. The main problem linked to this method is that often an MD trajectory will become trapped in a local minimum and will not be able to step over high energy conformational barriers and so the quality of the results is strictly dependent on the starting conformation of the system.

- Monte Carlo (MC) methods are among the most established and widely used stochastic optimization techniques. The advantages of the MC technique are that i) a simple energy function can be used which does not require derivative information and ii) energy barriers can simply be stepped over. The standard MC method involves applying random Cartesian moves to the system and accepting or rejecting the move based on a Boltzmann probability.

- Genetic algorithms. The essence of a genetic algorithm is the evolution of a population of possible solutions via genetic operators (mutations, crossovers and migrations) to a final population, optimizing a predefined fitness function. For this reason the genetic algorithm methods require the generation of an initial population whereas conventional MC and MD require a single starting structure in their standard implementation. AutoDock4[60] is a program that uses a genetic algorithm as a global optimizer combined with energy minimization as a local search method. In AutoDock4, used in this work, the fundamental point is that the ligand is flexible and the receptor is rigid and represented as a grid. The genetic algorithm uses two point crossover and mutation operators. For each new population a user determined fraction undergoes a local search procedure using a random mutation operator where the step size is adjusted to give an appropriate acceptance ratio. The fitness function involves five terms i) a Lennard-Jones 12-6 dispersion/repulsion term; ii) a directional 12-10 hydrogen bond term; iii) a coulombic electrostatic potential; iv) a term proportional to the number of sp3 bonds in the ligand to consider unfavourable entropy of ligand binding due to the restriction of

59 Taylor R.D. *et al. Journal of Computer-Aided Molecular Design*, **2002**, 16, 151
60 Morris G.M. *et al. J. Comput. Chem.*, **2009**, 16, 2785

conformational degrees of freedom; and v) a desolvation term. This scoring function is based loosely on the AMBER force field from which protein and ligand parameters are taken. Judson *et al.*[61] were among the first to report the application of a genetic algorithm to the docking method. The method was tested by docking a protected tripeptide, Cbz-Gly-[P(O)OH]-Leu-Leu, into thermolysin and it produced conformations which were close to the experimental binding mode. In the last ten years the application of this method to protein/ligand was used also to carbohydrates-protein studies. An example concerns the work by Agostino *et al.*[62] who investigated the application of molecular docking to carbohydrate–lectin recognition processes. Specifically they considered 15 different combinations of lectins (galectins, DC-SIGN, langerin, and SP-D) and ligands (single or polycarbohydrates based on mannose, glucose, galactose and fucose) whose crystal structures (as protein/ligand complexes) were available in high quality. Their results demonstrated that docking algorithms can identify the correct binding modes.

- Fragment-based methods. The logic of fragment based docking methods can be described in sequence as i) dividing the ligand into separate portions or fragments, ii) docking the fragments, iii) linking of fragments. These methods require subjective decisions on the importance of the various functional groups in the ligand, which can result in the omission of possible solutions, due to assumptions made about the potential energy landscape. Furthermore, a judicious choice of base fragment is essential for these methods, and can significantly affect the quality of the results.

- Distance geometry methods determine the binding modes between protein and ligand considering only hydrogen bonding. This method samples the conformational space identifying possible binding modes that are then used to direct an embedding algorithm.

- Tabu searches. PRO_LEADS is a docking algorithm that may be described as a stochastic evolution of the system using a tabu search with a generalized scoring function, ChemScore. An initial random ligand conformation is generated (referred to as the *current solution)* and then scored. Random moves are then applied to the ligand to generate a population of solutions (typically 100 solutions). These solutions are then

61 Judson R. S. *et al. Mol. Struct.: Theochem.*, **1994**, 308, 191
62 Agostino M. *et al. Frontiers in Immunology*, **2011**, 2,1

scored and ranked in ascending order. The highest rank solution is then accepted as the new *current solution* (assuming it is the lowest energy so far). A new random population is then generated from this new *current solution,* and the process is repeated for a user-defined number of iterations. However, to ensure diversity of the *current solution* a tabu list is used. This list stores the orientations of the last 25 *current solutions.* If the lowest energy solution from the ranked population is the lowest energy so far, it is always accepted as the new *current solution.*

- Systematic searches. EUDOC is a systematic search of rigid body rotations and translations of a rigid ligand within a rigid active site. It is based on a previous program, SYSDOC, that uses the fast affine transformation to perform the systematic search. The intermolecular energy is calculated by the AMBER-AA force field with a distance dependent dielectric.
- Multiple method algorithms. Multiple method algorithms involve the combination of different docking techniques into a single strategy. In this method, that increase the effectiveness of a docking protocol, a two steps strategy is adopted in which an initial computationally inexpensive method is used, followed by a time consuming yet more accurate method to generate a final docking solution.

Molecular Dynamic Simulation: basic principles

Molecular dynamics, as all computational techniques, is subject to assumptions and approximations that reduce the accuracy of simulation, thus it is necessary to know and to evaluate the limits of the used computational technique in order to avoid overestimation of the model and hence of the obtained results. The key issues to be considered in molecular dynamics simulation are i) the space phase size accessible to the system and ii) the accuracy of the molecular model used in the simulation of the system. An actually achievable efficient sampling of space phases in short periods of simulation can be obtained by introducing approximations that reduces the degrees of freedom of the system. Concerning the accuracy of the force field, it is possible to assume that the motion of atoms can be sufficiently described by the laws of classic mechanics, if we exclude chemical reactions, systems at low temperature or the motion of hydrogen atoms.

The force field[63]

A molecular dynamic simulation involves the integration of Newton's motion equations that, for a system of interacting particles, is described by equation 4.1.

$$m_i \frac{\partial^2 \boldsymbol{r}_i}{\partial t^2} = \boldsymbol{F}_i \qquad \textbf{4.1}$$

where $\boldsymbol{r}_i$ is the position of the particle *i*, and $\boldsymbol{F}_i$ is the force acting on it, that for a conservative system is equal to the derivative of the potential energy with respect to the position (equation 4.2)

$$\boldsymbol{F}_i = -\frac{\partial V(\boldsymbol{r}_i)}{\partial \boldsymbol{r}_i} \qquad \textbf{4.2}$$

The function $V(\boldsymbol{r}_i)$ represents the force field which the system particles are subjected to, and which all motions depend on. An example of a potential function used in many programs of molecular dynamics simulations of protein/lipid bilayer systems is reported as equation 4.3.

$$V(\boldsymbol{r}_1, \boldsymbol{r}_2, .. \boldsymbol{r}_n) = \sum_{bond} \frac{k_b}{2}(b - b_0)^2 + \sum_{ang.} \frac{k_\vartheta}{2}(\vartheta - \vartheta_0)^2 + \sum_{\text{imp.dihed.}} \frac{k_\xi}{2}(\xi - \xi_0)^2 + \sum_{\text{prop.dihed}} \frac{k_\phi}{2}(\phi - \phi_0)^2$$
$$+ \sum_{i,j} \left[\left(\frac{C_{ij}^{12}}{r_{ij}^{12}} - \frac{C_{ij}^{6}}{r_{ij}^{6}} \right) + \frac{q_i q_j}{4\pi\varepsilon r_{ij}} \right] \qquad \textbf{4.3}$$

The first term of equation 4.3 refers to the bond deformation energy and involves a harmonic potential, in which b_0 represents the bond length that corresponds to a minimum of energy, and k_b is the force constant. The second term is related to bond angle deformation energy, it also involves a harmonic function where ϑ_0 is the angle corresponding to the minimum energy value, and k_ϑ is the force constant. The third and the fourth terms of the equation refer to the dihedral angles (improper and proper). The improper dihedral angles are introduced to correct the artifacts resulting from the deformation of planar geometries. In most molecular dynamic programs the hydrogen atoms are "fused" to the carbon atom to which they are linked. In other words, the carbon

63 Mackerell A. D. *et al. J. Comput. Chem.*, **2004**, 25, 1584

atom does not keep its characteristics and is replaced by a pseudo atom (*united atoms*) that takes into account the incorporation of hydrogen atoms.

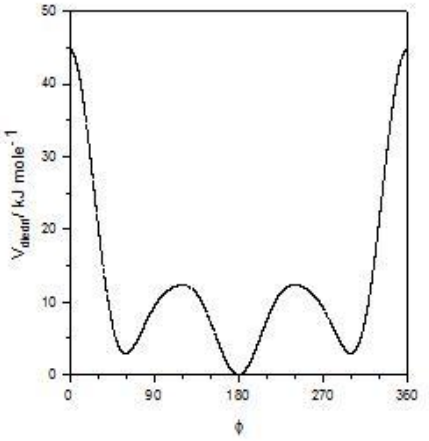

Figure 4.1. Ryckaert-Bellemans potential energy graphic for dihedral angles in alkyl chain.

The use of these pseudo atoms has the advantage, compared to the explicit treatment, to reduce computation time (motions of stretching of the hydrogen atoms are eliminated and thus it is possible to use a longer time step of integration; further, the choice of pseudo atoms also reduces the interactions between non-related atoms). The disadvantage of this approximation concerns the cases of chiral carbon atoms linked to a hydrogen atom because the inversion of configuration could occur during the simulation. Different types of functions are used to describe the torsional energy of proper dihedral angles; the function reported in equation 4.3 is one of the most commonly used. In the simulation of alkanes or of molecules with long alkyl chains (for example in micellar systems or lipid bilayers) the function of Ryckaert-Bellemans (equation 4.4**,** where $\varphi=\phi-180°$) is frequently used.[5] This function allows obtaining a distribution of *trans/gauche* conformations of alkyl chains in optimal agreement with experimental data. Figure 4.1 describes the Ryckaert-Bellemans function versus the dihedral angle.

$$V_{diedri}(\phi_{ijkl}) = \sum_{n}^{5} C_n \cos(\varphi)^n \qquad \textbf{4.4}$$

The last term of the equation 4.3 takes into account two-body interactions between not covalently bound atoms, *i.e.* van der Waals interactions and Coulombic interaction between *i* and *j* atoms having respectively q_i and q_j charges. The van der Waals interactions can be expressed by using different kinds of functions and equation 4.3 uses the function of Lennard-Jones. In the case of atoms separated by three covalent bonds the parameters of Lennard-Jones are suitably reduced to avoid the strong repulsions due to short distances. Others functions of force field involve mixed terms for the description of the coupled motions such as the deformation of the bond length and bond angle. The parameterization of the force fields, namely the definition of force constants and equilibrium values for the various terms, can be obtained by two different approaches. The first approach obtains the parameters from *ab initio* calculations performed on small molecules characterized by structural similarities with the simulated molecular system. Alternatively, the parameters can be obtained by an empirical approach, such as the parameterization of the force field based on the use of experimental data from X-ray crystal structures, spectroscopic analysis results, energy of vaporization, solvation free energies and NMR data. In molecular dynamics simulations a large portion of the computing time is employed to calculate the non-bonding interactions between atoms. Actually, while for the binding interactions the calculation time is proportional to the number of N atoms of the system, the calculation time for the non-bonding interactions is proportional to N^2. Therefore, the simulation time and the size of the system will be strongly influenced by the non-bonding interaction calculation speed. The simplest method to make quick calculation of non-bonding interactions, is applying the cutoff method to non-bonding interactions. This consists in calculating the interactions between atoms that are not covalently linked only for those that are located inside a sphere of a cutoff radius (R_c). The introduction of a cutoff radius is useful for short-range interactions, those whose magnitude decreases rapidly as a function of the increase of distance between the interacting groups or interacting atoms (such as van der Waals interactions). Electrostatic interactions are treated in molecular mechanics by pairwise calculation using the Coulomb law. However, also in this case with the increasing size of the involved systems, and especially with the inclusion of explicit water molecules, the calculation of all possible interactions would take more than 90% of computational time and would make simulations unfeasible. One possibility to overcome this problem, as seen above for short-range interactions, is truncating the forces at a certain distance (cutoff). However in this case the cutoff introduces significant nonphysical effects

especially at and also beyond the cutoff distance. Several methods of avoiding these artifacts have been developed. A method that is used for uncharged molecular systems though composed by atoms with partial charges, involves the transformation of the electrostatic interactions into dipolar interactions using the concept of charge groups. Neighboring atoms in the molecule are grouped in such a way that the group has zero net charge, so that for long distances the sum of the contributions of monopole (r^{-1}) between the various pairs of atoms is zero, and the only contribution is the multipole interaction (r^{-n}, $n \geq 3$). For example in the GROMOS[64] force field the asparagine aminoacid is splitted into three different charge groups (Figure 4.2). One group is formed by the amide nitrogen and its hydrogen proton, another group is formed by the carbon atom and the carbonilic oxygen, finally the last group is formed by the lateral residue.

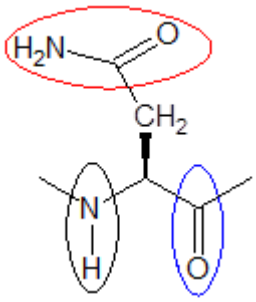

Figure 4.2. Charge groups used in GROMOS for asparagine aminoacid.

A different method involves the introduction of the particle mesh Ewald technique[65], which is able to run stable simulations also on highly charged systems as for example nucleic acids. Force fields commonly used in molecular dynamics simulations of biomolecular systems such as proteins, carbohydrates and nucleic acids, are AMBER[66], CHARMM[67], GROMOS[68] and OPLS[69].

64 Biomolecular Simulation: The GROMOS96 Manual and User Guide Vdf Hochshulverlag AG an der ETH Zürich, Zürich **1996**
65 Essmann U. *et al. J. Chem. Phys.*, **1995**, 103, 8577
66 Cornell W. D. *et al. J. Am. Chem. Soc.*, **1995**, 117, 5179
67 MacKerell A. D. *et al. J. Phys. Chem. B*, **1998**, 102, 3586
68 Scott W. R. P. *et al. J. Phys. Chem. A*, **1999**, 103, 3596
69 Jorgensen W. L. *et al. J. Am. Chem. Soc.*, **1996**, 118, 11225

All of these force fields started out as *united-atom* approaches and recently AMBER, CHARMM and OPLS (OPLS-AA) have moved to an *all-atom* (AA) description. Only GROMOS keeps the *united-atoms* approach.

At present, two force fields are commonly used in the simulation of lipids and phosholipids : one is part of CHARMM force field and the other one, introduced by Berger[70], combines the GROMOS87 bonding parameters (bonds, angles, dihedral angles) with the Ryckaert-Bellemans potential for the hydrocarbon chains and the OPLS[71] (*united-atoms)* parameters for the Lennard-Jones interactions. Both of these force fields reproduce reasonably well the available experimental data of the structure and dynamics of lipid bilayers[72], however the Berger force field has the advantage of a low computational cost due to the use of *united-atoms* scheme.

The presence in a system of different types of complex systems such for example a protein and a lipid bilayer imposes a particular attention to select the appropriate force fields to describes correctly the properties of each component of the system and the reciprocal interactions.

An obvious solution to simulate a multicomponent biomolecular system is to use a force field containing the parameters for describing all the molecules or biomolecules of the system.

Currently CHARMM is the only force field that offers the possibility of simulating all types of biomolecules (proteins, nucleic acids, sugars and lipids) but has two main limitations: a) it is an *all-atoms* force field, b) in the simulation of lipid bilayers it is necessary to use a high value of surface tension (or to use a fixed area) to obtain reasonable areas per lipids[73].

The alternative approach of combining two force fields to describes the different parts of the system requires considerable care. Some studies used the combination of *all-atoms* OPLS force field for the protein and of the Berger force field (derived from OPLS) for the lipid bilayer to simulate membrane proteins[74], ion channels[75] and membranes composed of glycolipids and phospholipids[76]. The reason for this choice is that the Berger force field,

---

70 Berger O. *et al. Biophys. J.,* **1997**, 72, 2002
71 Jorgensen W. L. *et al. J. Am. Chem. Soc.*, **1988**, 110, 1657
72 Tieleman D. P. *et al. Condens. Matter*, **2006**, 18, S1221
73 Sonne J. *et al. Biophys. J.*, **2007**, 92, 4157
74 Bjelkmar P. *et al*. *PloS Computational Biology*, **2009**, 5, 1000289
75 Chakrabarti N. *et al.Biophysical Journal*, **2010**, 98, 784
76 Kapla, J. *et al. J. Phys. Chem. B,* **2012**, 116, 244

derived from OPLS, reproduces the properties of a lipid bilayer with a low computational cost and allows a consistent treatment of the van der Waals interactions if combined with the OPLS-AA force field.

Boundary conditions

The simulation of a real molecular system by a model that considers only a limited number of molecules involves the correct treatment of boundary effects for obtaining the macroscopic properties of the system. If we consider a solute embedded in a box of water molecules of appropriate size, the water molecules on the edge of the box will suffer the result of different forces compared with the molecules inside the box. In a model system, where the size of the system is reduced with respect to the real system this effect becomes relevant. In order to minimize the effects at the edges of a finite system, it is possible to use periodic conditions. Therefore, the simulated system (solute and solvent) is placed in a cubic box or any geometric shape that is able to fill the entire space (hexagonal prism, truncated octahedron, elongated dodecahedron), the box is then surrounded by identical images of the box itself obtained by translation, along the axis x, y, z, of a quantity equal to the length of the box side. The two-dimensional case of this operation is shown in Figure 4.3. The interactions considered in the simulation are those of the particles of the central box with all the first neighboring particles. In the case of the black atom *i* in the central box we will consider the interactions with the atoms located within the circle defined by the cutoff radius (R_c) (approximation of the Minimum Image). In order to avoid artifacts in the simulation the cutoff radius must not be larger then the half of the box side ($l/2>R_c$), sothat the *i* atom will interact with the *j* atom and not with its periodic image *j'*.

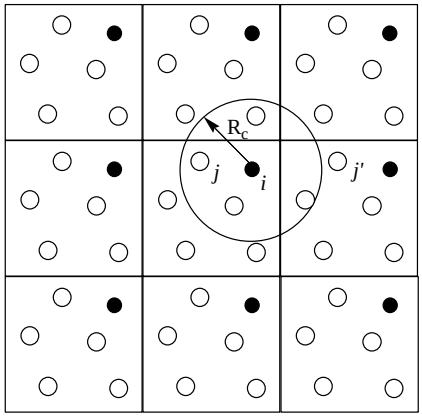

Figure 4.3. Representation of a two-dimensional cubic box. The circle around the black dot represents the *minimum image* in which the black particle interacts with only the particles that are located within the circle of radius Rc. From: van Gustern *et al. Angew. Chem. Int. Ed. Engl,* **1990**,29, 992

The choice of the box geometry (cubic, rectangular, truncated octahedron etc) is related to the molecule geometry; for example, in the case of a globular protein a truncated octahedral box can be chosen because this can be better approximated to a spherical geometry compared to a cubic geometry; in this way it is possible to reduce the number of solvent molecules involved in the simulation and consequently the simulation time.

Integration of Newton's equation of motion

Molecular dynamics simulates the time evolution of a finite system of particles through the integration of Newton's equations of motion. The integration of these second order differential equations is made by numerical methods since there is no analytical solution. The algorithms used to integrate the Newton's equations differ according to i) their calculation accuracy (order of the algorithm), ii) size of computer memory and iii) the type of representation.

The algorithms use a Taylor expansion for the quantities related to the position and velocity of each particle that composes the system. In these algorithms developments up to third order are typically used because those of the second order provide inaccurate results and those of higher order require large computational resources and long calculation times.

The Verlet algorithm is the most frequently used: the position and the acceleration of a particle at time t+Δt are calculated from the positions and accelerations at time t-Δt and tby equations 4.5 and 4.6.

$$\boldsymbol{r}_i(\mathrm{t}+\Delta\mathrm{t}) = \boldsymbol{r}_i(\mathrm{t}) + \boldsymbol{v}_i \cdot \Delta\mathrm{t} + \frac{1}{2}\boldsymbol{a}_i \cdot (\Delta\mathrm{t})^2 + \ldots \qquad \textbf{4.5}$$

$$\boldsymbol{r}_i(\mathrm{t}-\Delta\mathrm{t}) = \boldsymbol{r}_i(\mathrm{t}) - \boldsymbol{v}_i \cdot \Delta\mathrm{t} + \frac{1}{2}\boldsymbol{a}_i \cdot (\Delta\mathrm{t})^2 - \ldots \qquad \textbf{4.6}$$

The sum of equation 4.5 and 4.6 equation gives equation 4.7.

$$\boldsymbol{r}_{\mathrm{i}}(\mathrm{t}+\Delta\mathrm{t}) = 2\cdot\boldsymbol{r}_i(\mathrm{t}) - \boldsymbol{r}_i(\mathrm{t}-\Delta\mathrm{t}) + \boldsymbol{a}_i \cdot (\Delta\mathrm{t})^2 = 2\cdot\boldsymbol{r}_i(\mathrm{t}) - \boldsymbol{r}_i(\mathrm{t}-\Delta\mathrm{t}) + \frac{\boldsymbol{F}_i(\mathrm{t})}{\mathrm{m}_i}\cdot(\Delta\mathrm{t})^2 \qquad \textbf{4.7}$$

In equation 4.7, Fi (t) is the force acting on the particle *i* at time t. The terms higher than the fourth order are neglected in the series expansion. The velocities do not explicitly appear in the algorithm of Verlet, in fact they are calculated from the position of the particles at time t+Δt and t-Δt (equation 4.8).

$$\boldsymbol{v}_i = \frac{\partial \boldsymbol{r}_i(\mathrm{t})}{\partial \mathrm{t}} = \frac{1}{2\cdot\Delta\mathrm{t}}\left[\boldsymbol{r}_i(\mathrm{t}+\Delta\mathrm{t}) - \boldsymbol{r}_i(\mathrm{t}-\Delta\mathrm{t})\right] \qquad \textbf{4.8}$$

The magnitude of the error on the velocity is Δt^3.

The choice of integration algorithm is done on the basis of different considerations; i) the algorithm should involve only an evaluation of the interactions between the components of the system for each integration step, ii) the choice of the order of the algorithm depends on the type of model chosen.iii) the form of the algorithm, iv) computing resources and memory. In integrating the equations of motion a fundamental parameter is the step of integration (*time-step*), which is chosen at least an order of magnitude lower compared to the fastest motion of atoms in the simulated system. This fact represents a limit, especially if in the system there are high frequency motions, which are usually negligible and of little interest (such as the vibrations of bonds involving hydrogen atoms) with respect to the motion of the entire system. A solution to this limitation can be "freezing" such high-frequency vibrational motions by using proper constraints on bond lengths that are maintained to their equilibrium value in the course of the simulation. In this way it is possible to use longer integration time steps that allow carrying out longer simulations of the system, thus allowing the study of motions such as the folding of proteins that occur on time scales of tenths of nanoseconds.

Control of the temperature and pressure in molecular dynamics simulations

In the integration of the equations of motion, the energy of the system is conserved and the system finds itself in adiabatic conditions. If the simulation is also carried out at constant volume the simulated system will generate a microcanonical ensemble with constant number of particles, volume and energy (N, V, E). The microcanonical ensemble is not suitable to reproduce the experimental data since these are usually obtained at constant pressure and temperature One of the methods for controlling the temperature in a molecular dynamics simulation is the weak coupling with a thermal bath[77], this method was used in the simulations performed for this thesis. One of the merits of this method is its simplicity. The algorithm simulates the coupling of the system with an external thermal bath at the temperature T_0. The bath acts as a source of thermal energy and the temperature is maintained constant to the reference value (T_0) through a rescale of the velocities of the atoms. The deviation of the system temperature from T_0 is corrected according to equation 4.9.

77 Berendsen H. J. C. *et al. J. Chem. Phys.*, **1984**, 81, 3684

$$\frac{dT(t)}{dt} = \frac{1}{\tau}\left[T_0 - T(t)\right] \qquad \textbf{4.9}$$

The result is an exponential decay of the system temperature to the reference temperature with a time constant τ. The time constant τ represents the magnitude of the coupling between the heat bath and the system; if τ is large the coupling will be weak and the temperature will reach slowly the reference value. If τ is small the coupling will be strong with a fast decay of the temperature to T_0.

The change of temperature between subsequent steps is given by equation 4.10.

$$\Delta T = \frac{\delta t}{\tau}\left[T_0 - T(t)\right] \qquad \textbf{4.10}$$

and the scaling factor for the velocities is given by equation 4.11.

$$\lambda = \left[1 + \frac{\delta t}{\tau}\left(\frac{T_0}{T(t)} - 1\right)\right]^{1/2} \qquad \textbf{4.11}$$

The value that is usually chosen for the coupling constant with the thermal bath is a few hundred fs when the time period of integration is 1 fs. The control of pressure is obtained by using a method similar to that of weak coupling with a thermal bath used for the control of temperature. The equations are modified so that the net result of the system relaxation is a first order pressure to a predetermined value P_0 (equation 4.12).

$$\frac{dP(t)}{dt} = \frac{P_0 - P(t)}{\tau_p} \qquad \textbf{4.12}$$

To keep the system pressure to the reference value P_0, the volume of the box that encloses the investigated system is scaled by a μ factor which is equivalent to scaling the atomic coordinates $\boldsymbol{r}_i$ by a $\mu^{1/3}$ factor. The μ factor is given by equation 4.13:

$$\mu = \left[1 - \kappa \frac{\delta t}{\tau_p} \left(P_0 - P(t) \right) \right] \qquad \textbf{4.13}$$

And the new position of each atom will be given by equation 4.14:

$$\boldsymbol{r}_i^{'} = \mu^{1/3} \boldsymbol{r}_i \qquad \textbf{4.14}$$

The value of the coupling constant, τ_p , should be small enough (this is equivalent to a strong coupling) to obtain the equilibrium value of the pressure, and at the same time large enough (weak coupling) to avoid perturbation of the system properties.

Methods

Force Field

The approach of combining two force fields to describes the different parts of the system composed of ConA and a lipid bilayer of DMPC and GA **1** or **4** was used in this work. In particular the combination of OPLS- AA force field for the protein and of the Berger force field (derived from OPLS) were used.

The GAs **1** and **4** were considered as built by four molecular portions as shown in Figure 4.4 for the GA **1**.

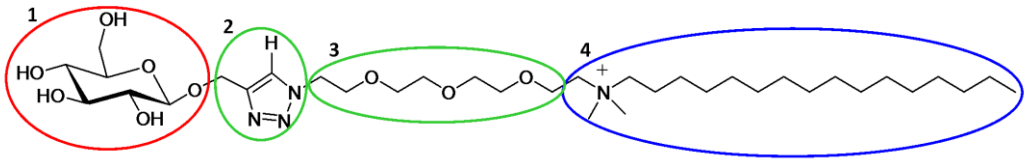

Figure 4.4. Structure of GA **1** sezioned in four portions for parametrization by force fields.

The glucose residue that interact with the binding site of the ConA was described with the OPLS-AA force filed for carbohydrates[78], the trioxyethylenic residue was described with the OPLS[79] *united-atom* force field and the region of the ammonuim group and alkyl chain was described with the Berger force field. In the case of the triazole moiety, absent as a residue in the standard force fields, the Berger nonbonding parameters were used whereas the bonding parameters and the partial atomic charges were obtained by *ab initio* calculations as described below.

Force Field Parameters for the triazole moiety

The force field parameters for the triazole moiety were calculated by using the 1-ethyl-4-(methoxymethyl)-1*H*-1,2,3-triazole and 1-(2-methoxyethyl)-4-(methoxymethyl)-1*H*-1,2,3-triazole as models to reproduce the neighbour groups linked to triazole ring in GAs **1** and **4**. The quantum mechanical calculations were performed by using GAUSSIAN03[80] program package whereas the molecular mechanics calculations were performed by using GROMACS[81] simulation package. The partial atomic charges of the triazole were evaluated using the *RESP*[82,83] fit method of the electrostatic potential obtained from the HF/6-31G(d) wave function using the Merz-Singh-Kollman scheme[84,85]. The electrostatic potential was calculated on the B3LYP/6-31 G(d,p) optimized geometry of the 1-ethyl-4-(methoxymethyl)-1*H*-1,2,3-triazole by using a high point density around the molecule (17 points/Å^2 and 10 layers around the van der Waals molecular surface). The *RESP* fit of the

78 Damm W. *et al. J. Comp. Chem.*, **1997**, *18*, 1955
79 Hezaveh S. *et al. J. Chem. Phys.*, **2011**, *135*, 164501
80 Frisch M. J. *et al. Gaussian 03, Revision C.02*. Gaussian, Inc.: Wallingford CT, **2004**
81 Hess B. *et al. J. Chem. Theory Comp.*, **2008**, *4*, *435*
82 Bayly, C. I. *et al. J. Phys. Chem.*, **1993**, *97*, 10269
83 Cornell W. D. *et al. J. Am. Chem. Soc.*, **1993**, *115*, 9620
84 Singh, U. C. *et al. J. Comp. Chem.*, **1984**, *5*, 129
85 Besler B. H. *et al. J. Comp. Chem.*, **1990**, *11*, 431

electrostatic potential was performed by using the *antechamber* tool of AMBER software package[86]. In order to extract the *RESP* atomic charges for the triazole ring, the atomic charges of the methoxymethyl and ethyl fragments were constrained at the value reported in the OPLS force field for carbohydrates[78] and dimethoxyethane[79] respectively. Figure 4.5 shows the partial atomic charges obtained from the RESP fit.

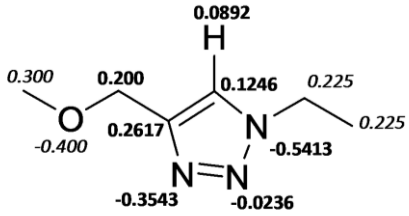

Figure 4.5. Partial atomic charges obtained from the *RESP* fit of electrostatic potential of 1-ethyl-4-(methoxymethyl)-1*H*-1,2,3-triazole. The atomic charges constrained to the value reported in the OPLS force field are reported in italics.

The bonding parameters of triazole moiety were obtained by the GROMOS96 force field[87]. The torsional parameters for the dihedral angles *C-O-C-C*, *O-C-C-C* and *N-C-C-O* between the triazole ring and the methoxymethyl and methoxyethyl groups were obtained by *Density Functional Theroy (DFT)* calculations. All of these dihedral angles were described by using the Ryckaert-Bellemans potential. The C_n parameter of the Ryckaert-Bellemans potential, reported in Table 4.1, were obtained by fitting the torsional profile calculated at the B3LYP/6-31 G(d,p) level of theory.

Table 4.1. Force Field parameters for the torsional angle obtained by the Ryckaert-Bellemans equation $V(f)=\Sigma[C_n(\cos(\varphi)^n]$

Torsional Angle	***C_n (n=0, 1,2..5)***
C-O-C-C	3.9130, 25.6431, 11.5944, -38.8938, -7.1775, 11.0126
O-C-C-C	-4.3735, -4.2109, 2.4316, 2.7585, 1.3785, 0.887
N-C-C-O	2.1255, 26.3373, -0.6412, -33.3946, 2.3117, 3.3173

86 Case D.A. *et al.* **2006**, AMBER 9, University of California, San Francisco.
87 Parameters obtained from the Automated Topology Builder (ATB) and Repository version 1.2 web site (http://compbio.biosci.uq.edu.au/atb/) relative to Alanine-Triazole-Propionic acid.

Figure 4.6 shows the torsional profiles of the potential energy obtained by quantum mechanical calculations and by molecular mechanics calculation using the parametrized dihedral angles.

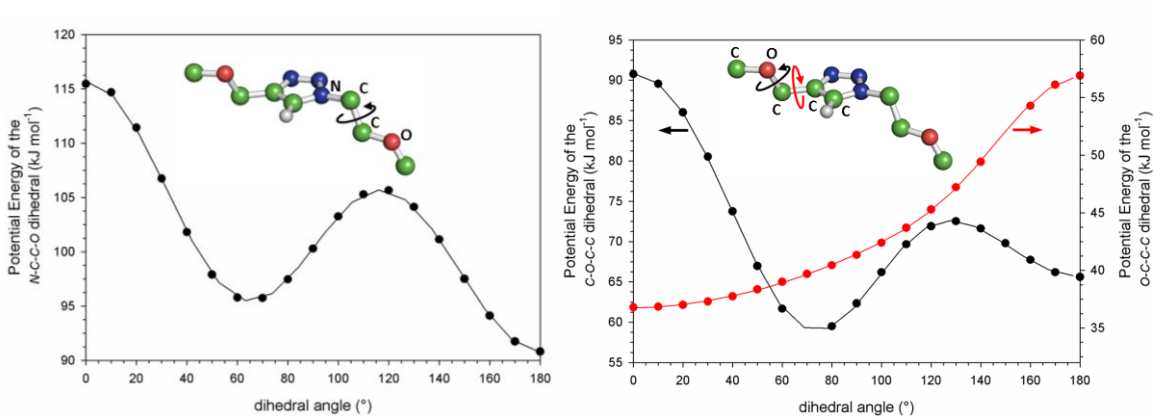

Figure 4.6.: Torsional energy profiles for the dihedral *C-O-C-C*, *O-C-C-C* and *N-C-C-O* of 1-(2-methoxyethyl)-4-(methoxymethyl)-1*H*-1,2,3-triazole. The points represent the values obtained by DFT calculations whereas the lines represent the values obtained by molecular mechanics calculation using the parametrized dihedral angle.

*Topology of GAs **1** and **4***

The topologies of GAs **1** and **4**, that contains all the bonding and non-bonding parameters to described the molecules, were created according to the GROMACS rules[88] combining the OPLS and the Berger force fields.

The half-e double-pairlist method[85] was used to ensure proper scaling of the 1-4 interactions, between atoms separated by three bonds, when the Berger and OPLS-AA force fields are combined in the GROMACS package.

In the topology of GA **1** and **4** the 1-4 nonbonding interactions, relative to glycosydic bond, were scaled using two different procedures. In GA **1**, characterized by the presence of a single methylene between the glucose residue and the triazole ring (Figure 4.7), the 1-4 interaction for C8-C1, C7-OR and C7-C2 were scaled according to the OPLS-AA model, whereas a scaling based on the half-e double-pairlist method was applied to O1H-C9 and O1H-N13.

88 van der Spoel, D. *et al. Gromacs User Manual version 4.5.4*, **2010**

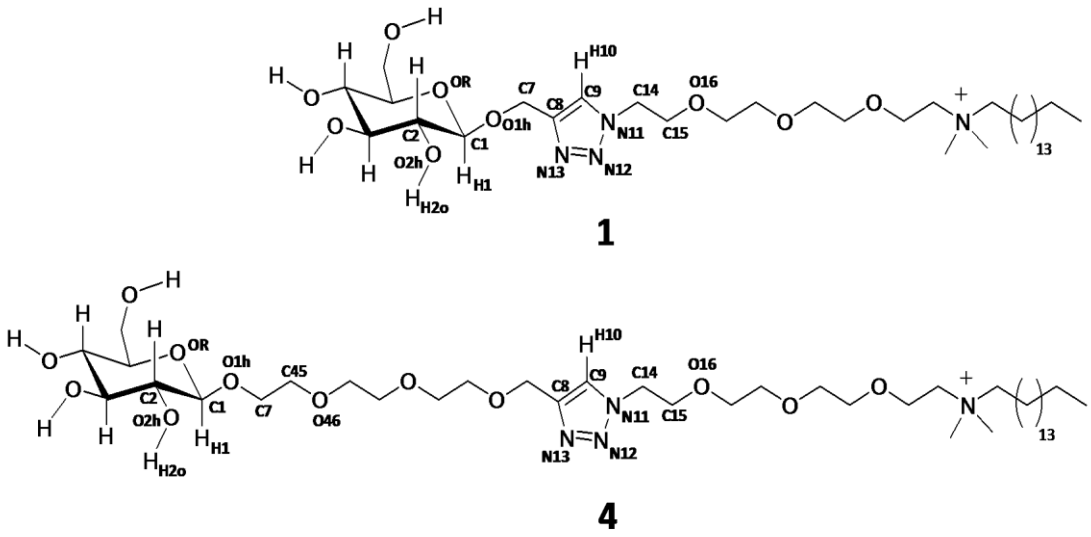

Figure 4.7. Structure of GAs **1** and **4.** The atoms of the glycosydic link and the triazole ring are labelled according to the symbols used in the molecular topologies.

In GA **4** the 1-4 interaction for C45-C1, C7-OR and C7-C2 were scaled according to the OPLS-AA model, whereas a scaling based on the half-e double-pairlist method was applied to O1h-O46.

Docking

The structures of GAs **1** and **4** optimized by the parameterization described above were docked to the structure of Con A elucidated by X-rays (PDB code 3D4K[32]) by Autodock (v.4.2). Though Con A is a tetrameric protein, in the computational study only Chain A of ConA, that contains 237 aminoacidic residue and Mn 238 and Ca 239 ions that are structurally significant, was considered in order to reduce the size of the system. Water molecules were excluded from the protein for the docking study. A Lamarckian genetic search algorithm was used to identify low energy binding sites and orientations of the glycolipids. Pre-calculated atom affinities, electrostatics and solubilities were computed on a grid box by Autogrid (v.4.2). The box was centered at the center of the putative binding cavity, its dimensions were 12.6 nm x 12.6 nm x 12.6 nm. A point grid with a 0.0475 nm spacing nm was used. Point grid Gasteiger atom charges were assigned to the protein and ligand atoms using AutoDockTools. 100 randomly seeded runs were performed for 10 runs, with an intial population of 150 individuals, and 25 milion maximum number of evaluations. Binding modes were ranked by an empirical force-field based scoring function

implemented in Autodock. The Rate of Gene mutation and Crossover of the Genetic Algorithm was set to 0.02 and 0.8 respectively. 1000 total simualtions were performed

Molecular Dynamic Simulations

System Build up

The initial 95:5 and 90:10 DMPC/GA(**1** or **4**) systems were built by replacing the proper number of DMPC molecules with the same number of glycolipid molecules in a DMPC bilayer using Web Lab package. The initial DMPC/GA/Con A configurations in this study were built by superimposition of the GA/Con A structures, selected from the preliminary docking study, on the DMPC/GA bilayer by using the Membrane package of VMD (Visual molecular dynamics)[89]. From this procedure two structures were selected for each GA: structures A and B for GA **1** and C and D for the GA **4**. This operation was done by superimposing only the sugar residue of the glycolipid in the system from the docking procedure to sugar residues in the DMPC/GA bilayer to find the optimal matching. The system was subsequently solvated with SPC (Simple Point Charge) water molecules[90]. The tree negative charges of the protein were neutralized with Na^+ ions and the positive charges of the glycolipid with Br^- ions. The initial DMPC/Con A system (*i.e*. in the absence of glycolipid) was assembled by placing the protein in the same position of the A DMPC/**1**/Con A system. The box dimension for each system was 6.5 x 6.5 x 14 nm.

Molecular Simulations

All MD simulations were carried out with GROMACS v.4.6.1.

Titratable residues of proteins were modelled according to their protonation state in water at pH = 7.

The Mn^{2+} [91]and Ca^{2+} [92] ions, included in the protein structure, and Na^+ [92] and Br^- [93] ions were treated by using the OPLS-AA parameters.

Lennard-Jones and electrostatic interactions were calculated using a cut-off of 1.2 nm and the long-range electrostatic interactions were evaluated by using the particle mesh Ewald method (PME)[94].

89 Humphrey W. *et al. J. Mol. Graph.*, **1996.** 14, 27
90 Berendsen H. J. C. *et al.*, Interaction models for water in relation to protein hydration. In: Intermolecular Forces. Pullman B, ed. Dordrecht, The Netherlands: D. Reidel Publishing Company. **1981**, 331
91 Ghitti M. *et al. Angew. Chem. Int. Ed.*, **2012**, 51, 7702
92 Aqvist J. *et al J. Phys. Chem.*, **1990**, 94, 8021
93 Lybrand T.P. *et al.J. Am. Chem., Soc.*, **1985**, 107, 7793
94 Essman U. *et al. J. Chem. Phys.*, **1995**, *103*, 8577

All bonds were constrained using the LINCS[95] algorithm whereas the geometry of water molecules was fixed by the SETTLE[96] algorithm. The simulations were carried out with a time step of 2 fs. The temperature of protein, lipids, water and ions was kept constant separately at 323 K using the Berendsen thermostat[97] with a time constant of 0.1 ps. The pressure was controlled using the Berendsen barostat[97] (P = 1 bar, τ_p = 1.0 ps). Pressure coupling was applied semiisotropically: the z and the x-y (isotropic) box dimensions were allowed to vary independently. Periodic boundary conditions were applied in the three dimensions. The systems were energy minimized and run for 10 ps at constant volume with a weak positional restraints on heavy atoms of protein and lipids, followed by 10 ps at constant pressure. Finally the systems were equilibrated with 10 ns of unrestrained MD in the NPT ensemble. Production runs were performed without restraints; 50 ns simulations were performed in the case of the DMPC/**1** and DMPC/**4** systems and 70 ns simulations were performed in the case of the DMPC/**1**/ConA, DMPC/**4**/ConA and DMPC/ConA systems Details on the simulated systems are summarized in Table 4.2.

Table 4.2. Features of the simulated lipid bilayer systems and corresponding simulation times.

System composition	DMPC molecules	Glycolipid molecules	Con A	Water molecules	Time of simulation (ns)
DMPC/**1** 95:5	116	6	-	13728	60
DMPC/**1** 90:10	116	12	-	13574	60
DMPC/**4** 95:5	116	6	-	13939	60
DMPC/**4** 90:10	116	12	-	13682	60
DMPC/Con A	116	-	1	13587	80
DMPC/**1**/Con A A	116	6	1	13587	80
DMPC/**1**/Con A B	116	6	1	13230	80
DMPC/**4**/Con A C	116	6	1	13055	80
DMPC/**4**/Con A D	116	6	1	13092	80

95 Hess B. *et al. J. Comp. Chem.*, **1997**, *18*, 1463
96 Miyamoto S. *et al. J. Comp. Chem.*, **1992**, *13*, 952
97 Berendsen, H. J. C. *et al. J. Chem. Phys.*, **1984**, *81*, 3684

Results and discussion

Docking

In this docking study the interaction of a single molecule of GA (**1** or **4**) with the Con A, was simulated. The goal of the docking study was to identifying the binding site of the GA with the protein. The hydrophobic chain of GA was not considered to reduce the computational cost, and the docking was centered on the protein. 10 runs of docking were performed and, as known, from each run 100 configurations were obtained (total 1000). The obtained 1000 configurations were first visualized all together as shown in Figure 4.8 to have an idea of the regions of interaction, then only the structures characterized by the lowest energy (Figure 4.9) were considered. The results confirmed that the binding site is close to Ca^{2+} and Mn^{2+} ions, as reported in the literature[32].

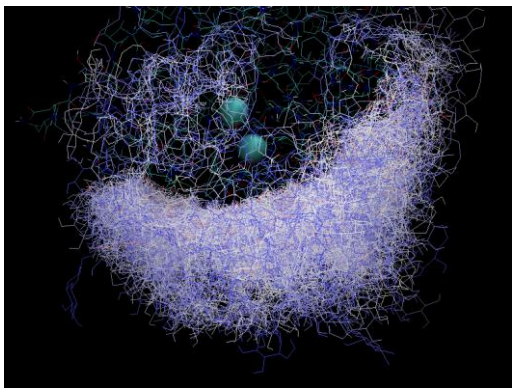

Figure 4.8. Visualization of the 1000 results of the docking procedure on Con A/**4** system.

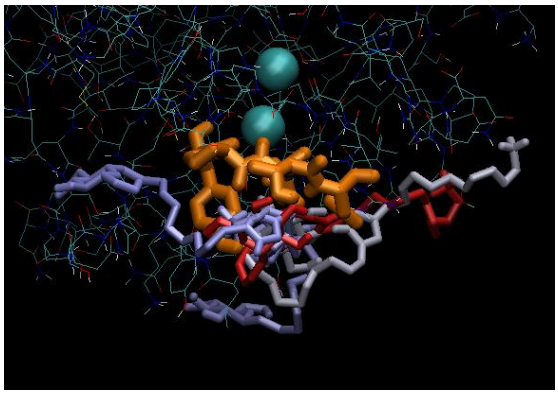

Figure 4.9. Visualization of the lowest energy configurations obtained by the docking of Con A/**4** system. Ca^{2+} and Mn^{2+} ions inthe binding site of protein are represented as green balls.

Molecular Dynamics simulations

Simulation of the DMPC/1 and DMPC/4 systems

The aim of these simulations was to investigate the influence of the different hydrophilic spacer on the exposure of the sugar residue of the GA embedded in a DMPC bilayer to the bulk. The build up of the DMPC/GA systems was done by the WebLab program with the inclusion of the 6 GA molecule in a DMPC bilayer. The systems were simulated for 60 ns and some relevant distances informative on the exposure of the sugar residue into the bulk analyzed from the trajectories by the VMD program.

In particular, the distances between the quaternary nitrogen (N25) and the closer nitrogen of the triazolic ring (N11) in the case of both GAs and the distances between N25 and glucosidic oxygen (O1H) and N11 and O1H in the case of the GA **4** (Figure 4.10) were analyzed. The results relative to the O1H–N11 for both 95:5 and 90:10 DMPC/**4** systems are reported in Figure 4.11.

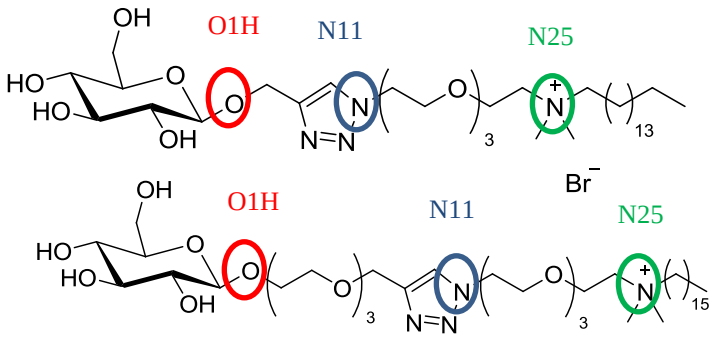

Figure 4.10. Visualization of the GA atoms considered in the distance analysis.

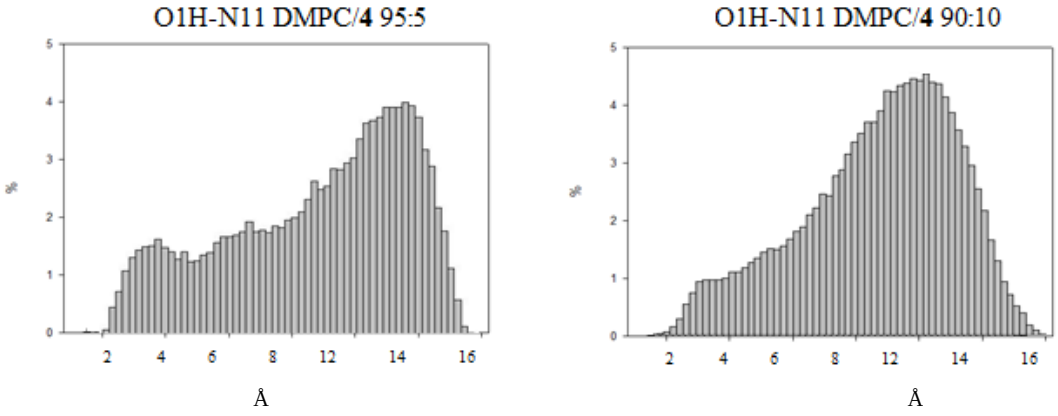

Figure 4.11. Analysis of O1H-N11 distances for the 95:5 and 90:10 DMPC/**4** systems. Histograms report the probability distribution of distances calculated over the trajectory.

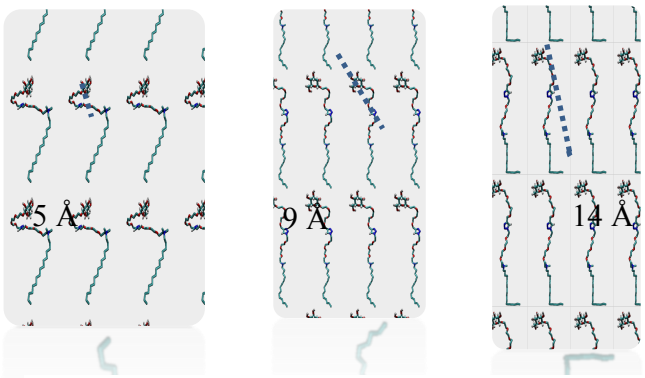

Figure 4.12. Three different configurations of the GA **4** embedded in the DMPC bilayer. For each configuration the O1H-N11 distance is indicated.

Histograms in Figure 4.11 report the probability distribution of distances calculated over the trajectory. Samples of the possible configurations characterized by certain distances are reported in Figure 4.12. Large distribution of distances were observed for both systems with a peak at 14 Å, thus suggesting that this segment of the GA is elongated, as shown in Figure 4.13 for the 14 Å value. Note that the other two values correspond to folded configurations of the polyoxaethilenic segment.The results relative to the O1H–N25 distances, for the 95:5 and 90:10 DMPC/**4** systems are reported in Figure 4.13, and samples of the possible configurations characterized by certain O1H-N25 distances are reported in Figure 4.14. Also in this case large distributions were observed with a peak at 8 Å in the case of the 95:5 system and 12 Å in the case of the 90:10 system. As suggested by Figure 4.14 a value ~12 Å for the O1H-N25 distance involves a folded hydrophilic spacer.

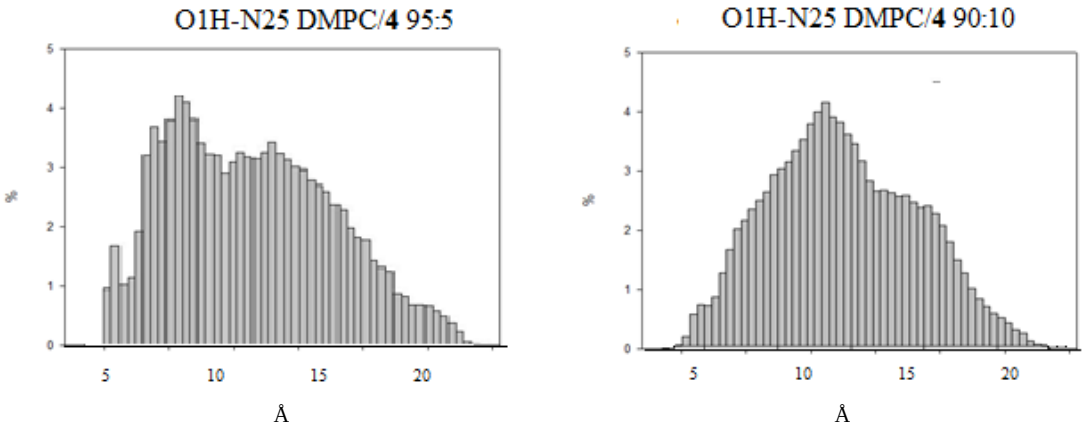

Figure 4.13. Analysis of O1H-N25 distances for the 95:5 and 90:10 DMPC/**4** systems. Histograms report the probability distribution of distances calculated over the trajectory.

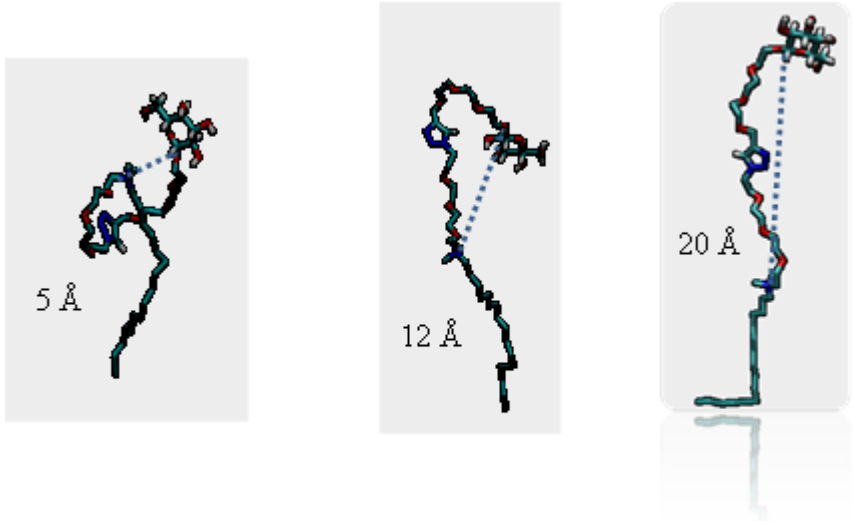

Figure 4.14. Three different configurations of the GA **4** embedded in the DMPC bilayer. For each configuration the O1H-N25 distance is indicated.

The results relative to the N25-N11 distance, for the 95:5 and 90:10 DMPC/**4** and DMPC/**1** systems are reported in Figure 4.16. All the probability distributions observed in Figure 4.15 are very large with two peaks for shorts and long distances in each of the reported histograms. The large distribution and the presence of two peaks both indicate a high variability of the N25-N11 distance and a high mobility of the first portion of the hydrophilic spacer (*i.e.* the portion close to the lipid/water interface). Figure 4.16 shows samples of GA **4** featuring the N25-N11 distances corresponding to the probability distribution peak in the histograms in Figure 4.15.

Even if the DMPC/**1** (**4**) 90:10 analysis didn't put in evidence a destabilization of these systems, in analogy with the experimental part there were considered only the DMPC/**1** (**4**) 95:5 fort the interaction with the ConA.

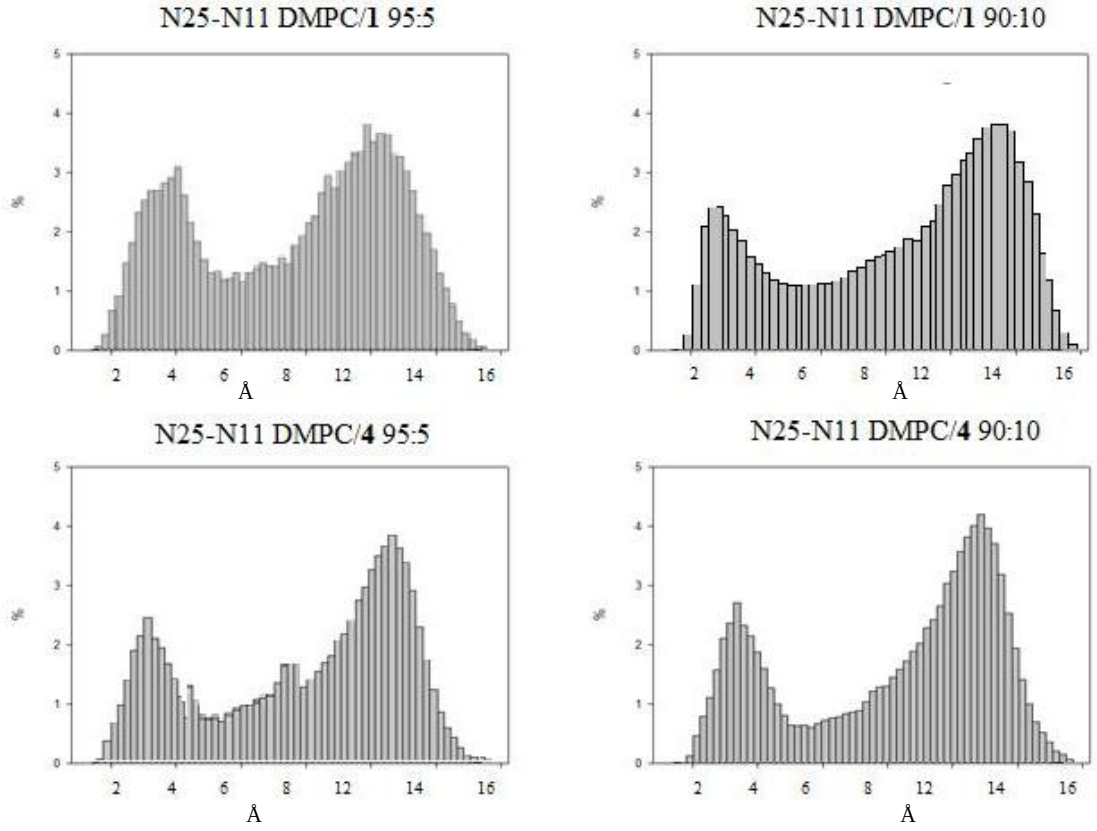

Figure 4.15. Analysis of N25-N11 distances for the 95:5 and 90:10 DMPC/**1** and DMPC/**4** systems. Histograms report the probability distribution of distances calculated over the trajectory.

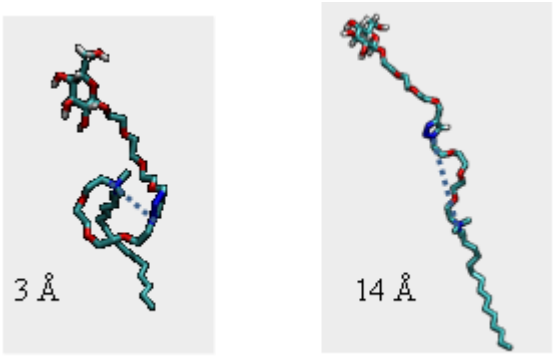

Figure **4.16.** Two different configurations of the GA **4** embedded in the DMPC bilayer. For each configuration the N25-N11 distance is indicated.

Simulations of the DMPC/GA/ConA systems

The simulations of the selected A, B, C and D DMPC/GA/ConA systems were aimed at investigating the interactions of ConA with DMPC bilayers characterized by the presence of the different GA **1** or **4** and comparing them with the system in the absence of GA, *i.e.* DMPC/ConA system. The five lipid/ConA systems were built up and simulated for 80 ns and the parameters that characterize the five lipid/protein systems were analyzed over the trajectories. In particular the following parameters were investigated after a qualitative analysis of the evolution of the binding site and of aminoacidic residues involved in the binding:

- The Area/lipid parameter
- The root mean square deviation (RMSD) of the protein that evaluates the position of its atoms with respect to starting coordinates.
- The distance between the protein and the lipid bilayer
- The number of H-bond between the protein and DMPC molecules
- The number of H-bond between the protein and glycolipid molecules.

Assembling of lipid/ConA systems

The five lipid/ConA systems were assembled as explained in the experimental part, by matching the sugar residue of GA in the lowest energy structures obtained by docking with the sugar residues of GAs in the corresponding minimized 95:5 system. The best matching was made visually by VMD by selecting only the DMPC/**1**/ConA and DMPC/**4**/ConA configurations that did not shows contacts or overlaps of ConA with DMPC/**1** and DMPC/**4** systems. Figure 4.17 shows two explicative examples, that is a configuration with a high DMPC/ConA overlapping, (left) that was not suitable as a starting configuration for the simulation and a configuration where the protein is close to the lipid bilayer without touching it (right) that was suitable for simulation. Figure 4.18 reports the four initial configurations selected for the DMPC/**1**/ConA system, *i.e.* configurations A and B and for the DMPC/**4**/ConA system, *i.e.* configurations C and D. The reference DMPC/ConA system was built by removing the 6 GA molecules from system A.

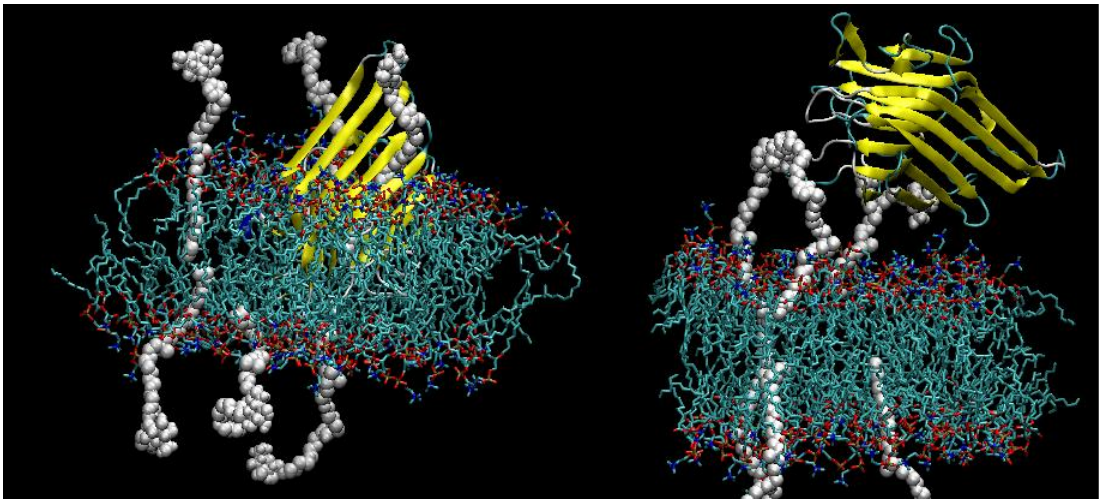

Figure 4.17. Two configurations of the DMPC/**4**/ConA system. The left panel shows a configuration characterized by high extent of overlapping between Con A and DMPC (not suitable as a starting configuration for simulation). Right panel shows a configuration where the protein is close to the lipid bilayer without ConA-DMPC overlappings (suitable as a starting configuration for simulation). DMPC is drawn in green, red and blue, GA is drawn in white.

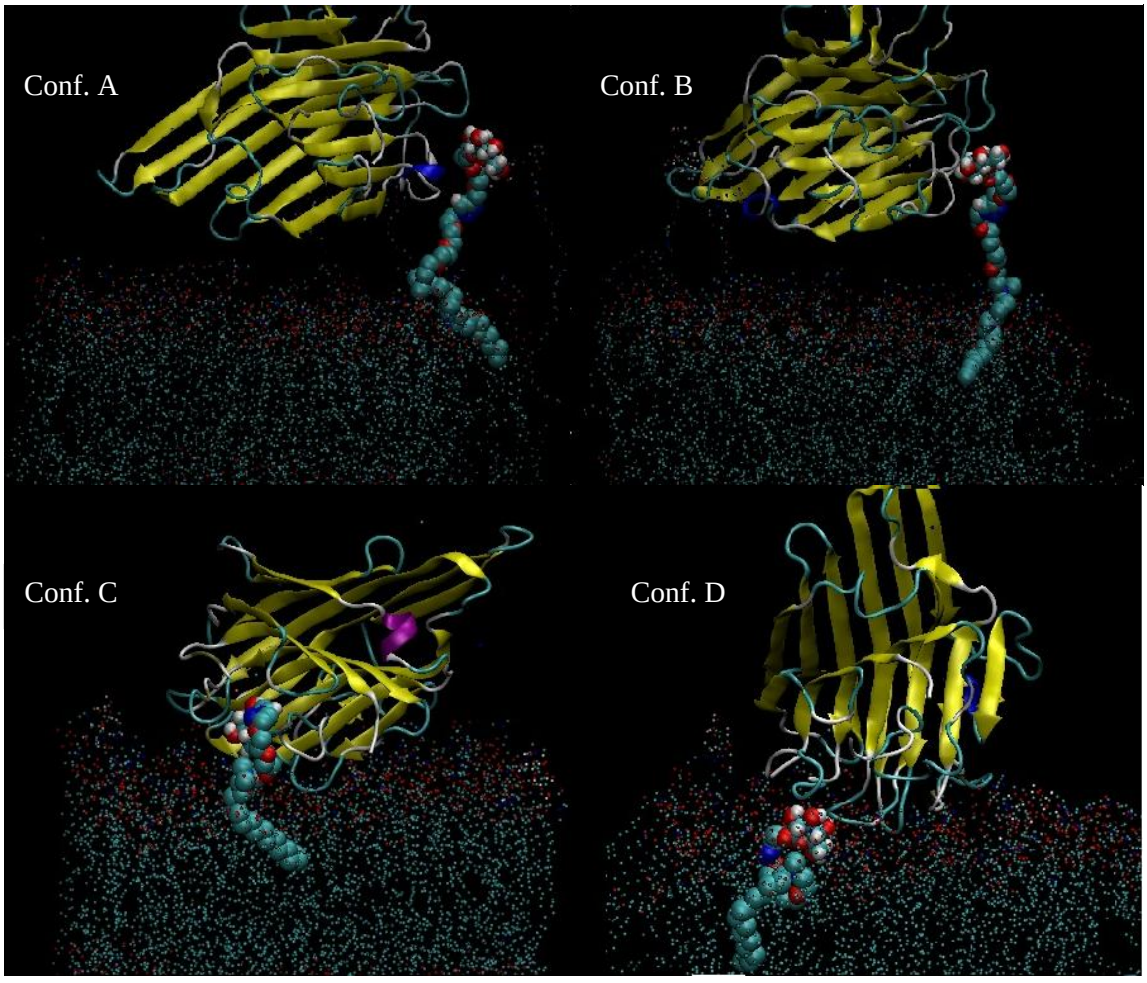

Figure 4.18. Starting configurations of DMPC/**1**/Con A (A and B), and DMPC/**4**/Con A (C and D).

Qualitative analysis of the evolution of the binding site and of aminoacid residues of Con A involved in the binding with GA

The aim of this qualitative analysis was having an overview of the position of the protein and the GAs, during the simulation, and to identify the aminoacid residues and the regions of GA involved in the Con A-GA binding. Figures 4.19-4.22 show the evolution of the binding site during the simulation for the A, B, C, D systems, snapshots of the systems at t=0 and at certain interesting times during the trajectory are reported. For each snapshot the aminoacid residues involved in the interaction with the GA were identified considering a cut off of 0.35 nm, the same used in the H-bonds analysis reported in one of the next sessions.

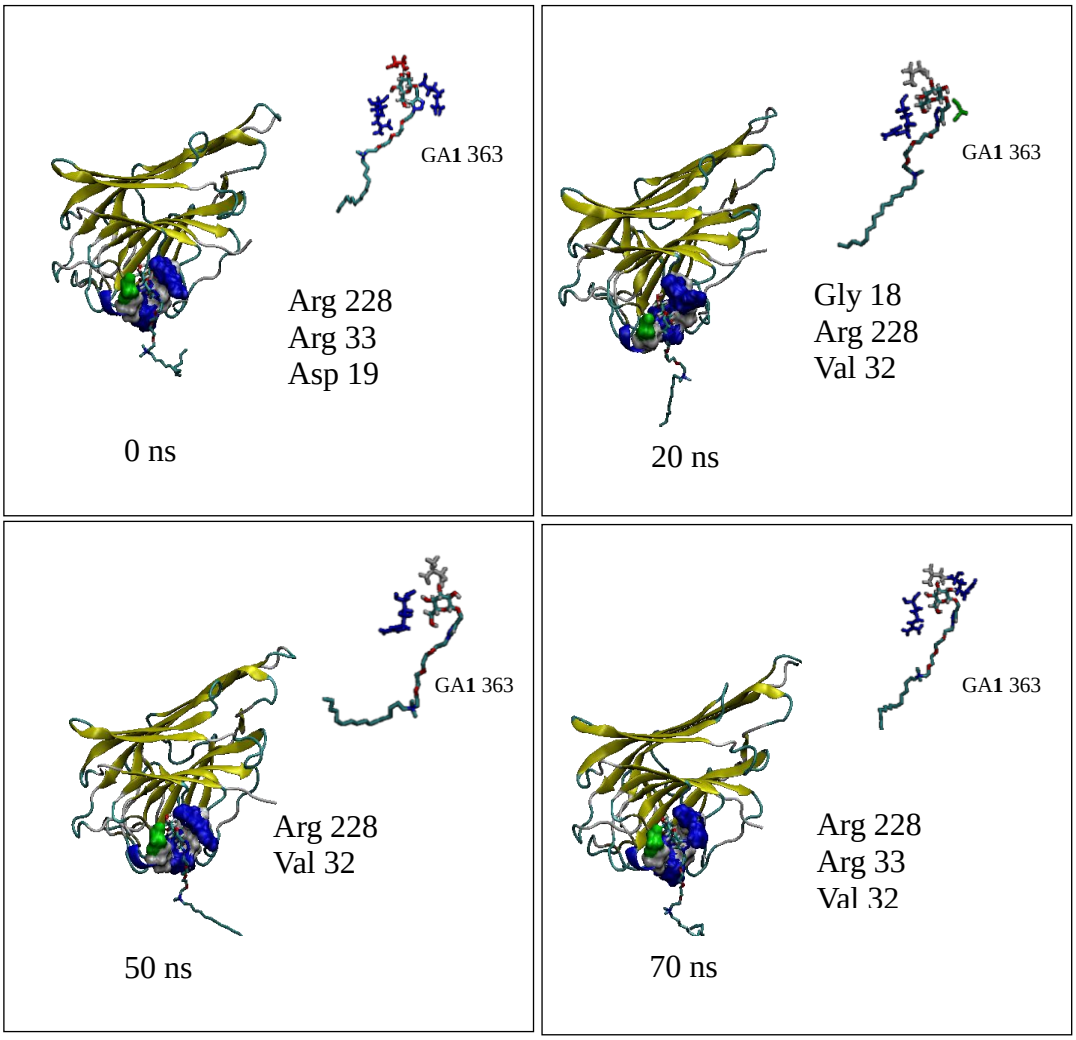

Figure 4.19. Evolution of the binding site during the simulation of the A system and aminoacid residues involved in the binding with GA.

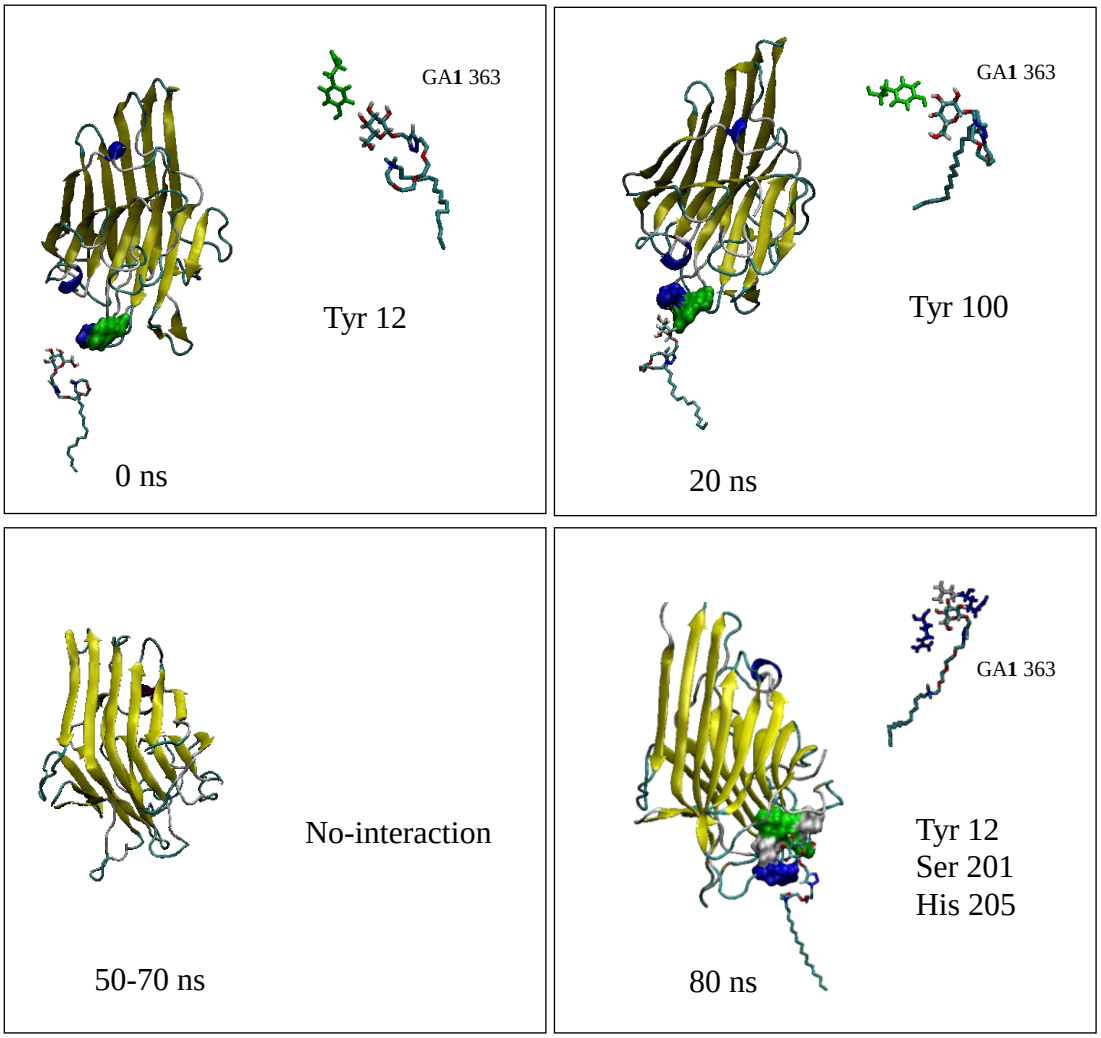

Figure 4.20. Evolution of the binding site during the simulation of B system and aminoacid residues involved in the binding with GA.

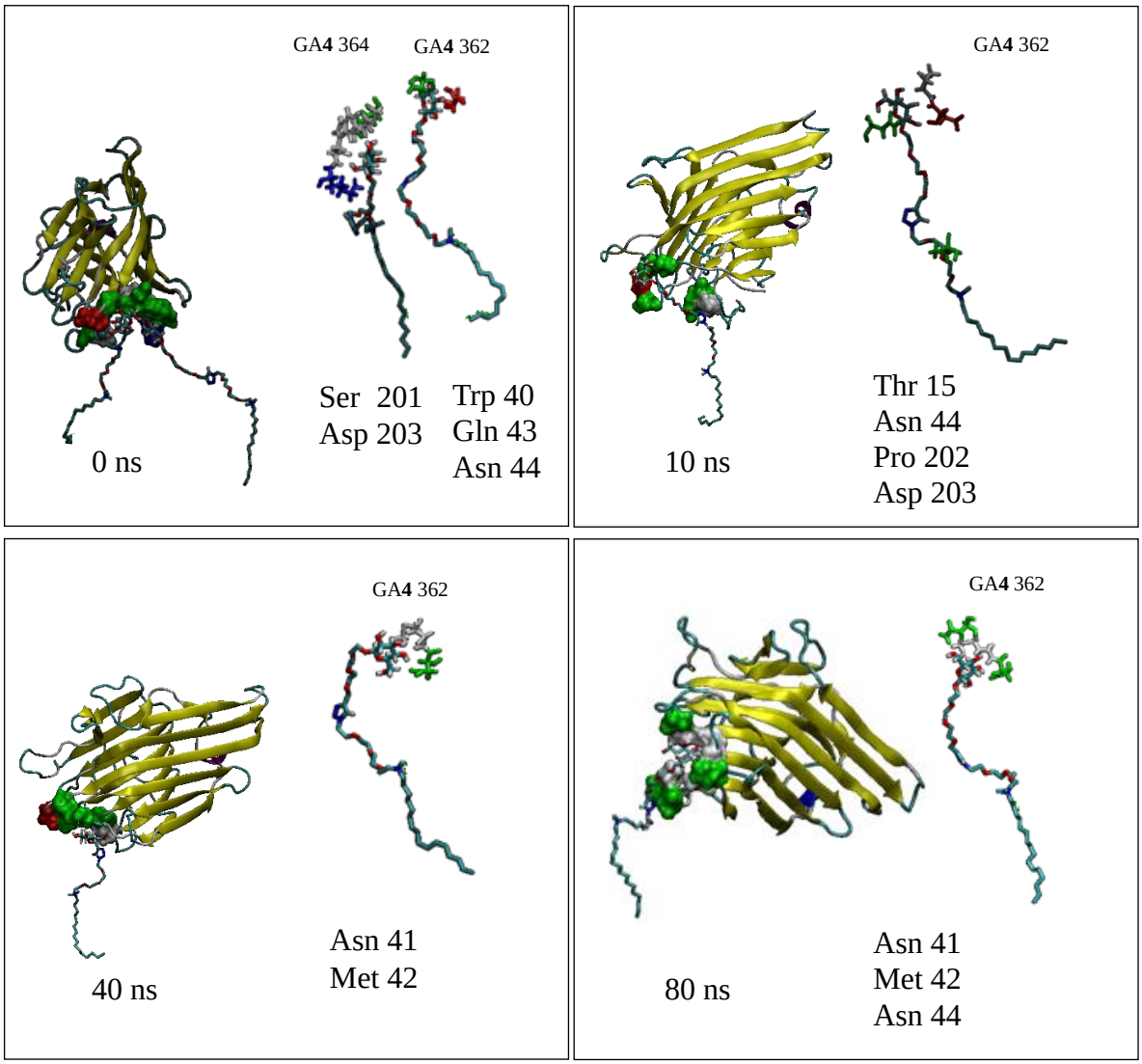

Figure 4.21. Evolution of the binding site during the simulation of C system and aminoacid residues involved in the binding with GAs.

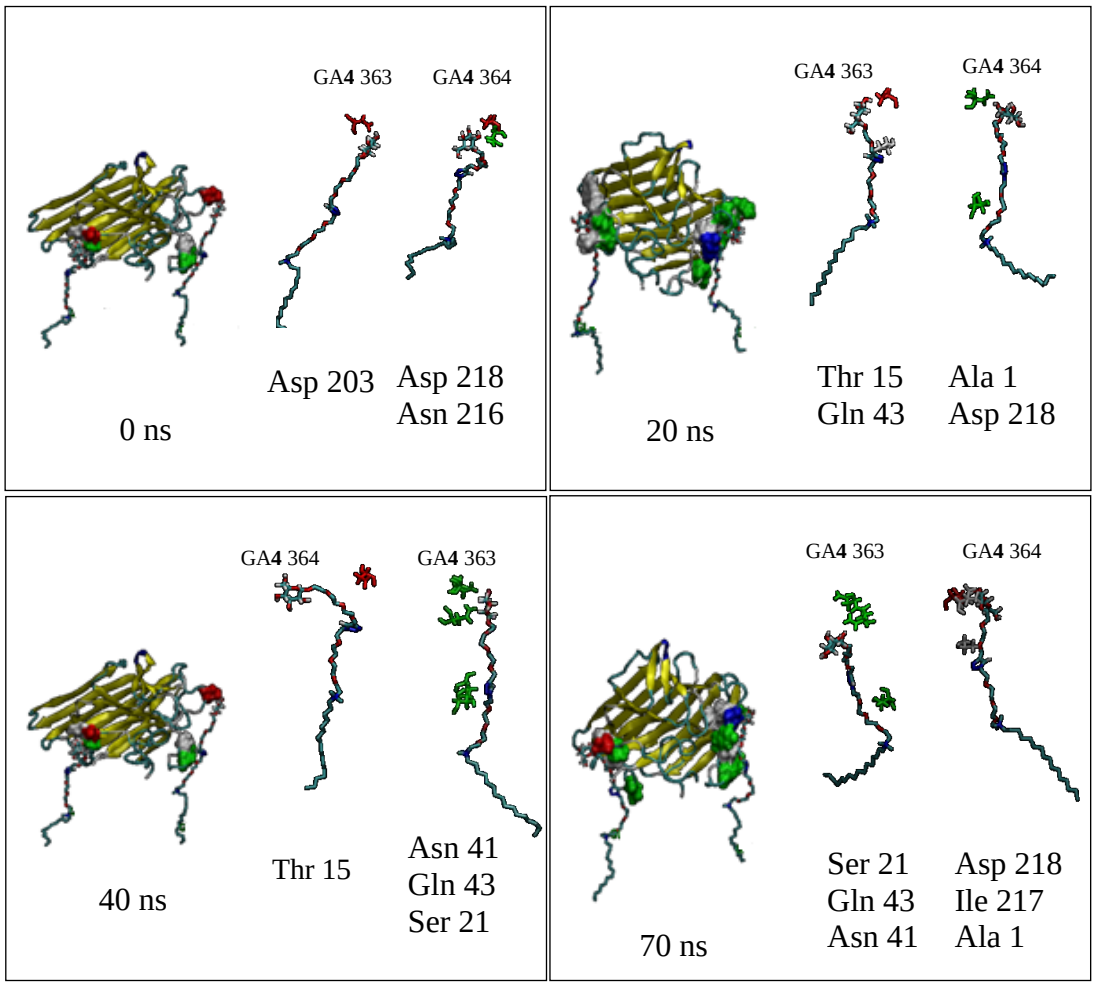

Figure 4.22. Evolution of the binding site during the simulation of D system and aminoacidic residues involved in the binding with GAs.

It can be observed that:

- In the four cases the aminoacidic residues involved in the binding with the sugar residue are in general the same as those given by the X-ray analysis[32], *i.e.* Arg 228 in A system, (Figure 4.19), Tyr 100 in B system (Figure 4.19), Asp 218 in D system (Figure 4.2), or in any case very close to them such as Ser 201 or Thr 15 in C system (Figure 4.20).

- The binding site does not change over the simulation, in fact the aminoacids involved in the binding are the same or located in the binding site as demonstrated by the residue numbering.

- In the case of both the DMPC/1/ConA system (A and B) only one GA is involved in binding with ConA. In the case of the C system the starting configuration that involves two GAs in the binding with the protein changes during the simulation into configurations

involving only one GA in the binding. On the other hand two GAs are constantly involved during the simulation of the D system in the binding with the protein.

The A/lipid parameter

The A/lipid parameter, (equation 4.15) where A is the area of the face box, and lipid is the number of DMPC of one of the two considered layers, *i.e.* 58 for these systems, simulates the headgroup lipid area. This is a parameter that can be obtained also experimentally and the comparison of the experimental and theoretical value of the A/lipid ratio allows estimating tha reliability of the model used in simulation. In this work the headgroup area was not measured experimentally however it was analyzed over the trajectory.

$$A/Lipid = xy/58 \qquad \textbf{4.15}$$

Figures 4.23-4.25 show how the A/Lipid parameter changes over the trajectory in the DMPC/ConA (Figure 4.23), in the A and B systems (Figure 4.24) and in the C and D systems (Figure 4.25). The analysis indicates that in the the DMPC/ConA and in the two DMPC/**1**/ConA systems the A/Lipid parameter does not change during the trajectory thus indicating a good reliability of the model. On the other hand, in both the DMPC/**4**/ConA systems the A/Lipid parameter fluctuates periodically during the trajectory. The variability of the A/lipid parameter implies that there is a fluctuation on the z axis so that the system reacts by changing xy to keep the volume constant. The variability observed is unusual because the headgroup surface should not change over the trajectory, moreover the model used, with the exception of GA molecules. is the same of that used for the A and B systems. The periodic fluctuation observed in the cases of C and D systems has probably to be ascribed to artifacts due to the use of the Berendsen barostat. The Berendsen thermostat and barostat do not strictly provide a correct NPT ensemble, but is very useful, because efficient and rapid, to obtain structural an dynamic properties of the system. The version of GROMACS 4.6.1 contains an implementation of this barostat that can give artefacts. In the development of the work it will be necessary to change barostat and use, for example, the Parinello-Rahman barostat[98] which yelds a correct NPT ensemble.

[98] Parinello M. J. *et al. Appl. Phys*., **1981**, 52, 7182

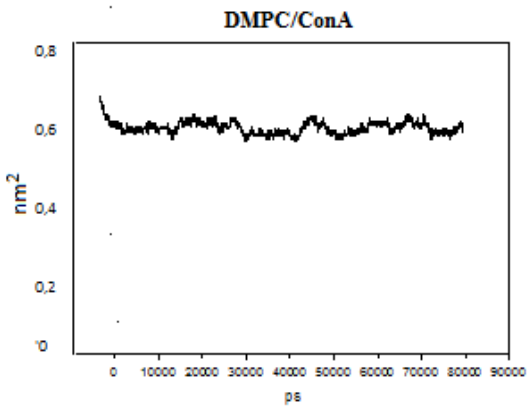

Figure 4.23. Plots of A/Lipid parameter versus the time of the simulation (ps) for the DMPC/ConA system.

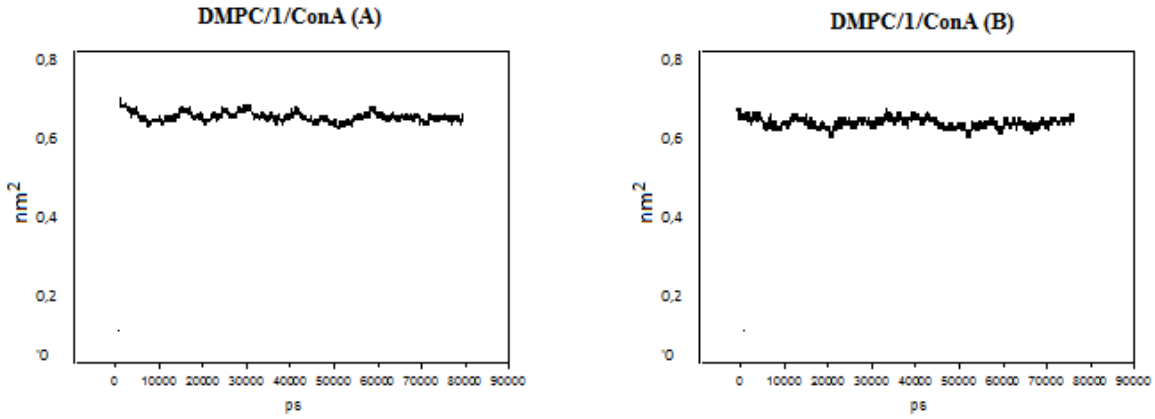

Figure 4.24. Plots of A/Lipid parameter versus the time of the simulation (ps) for the A and B systems.

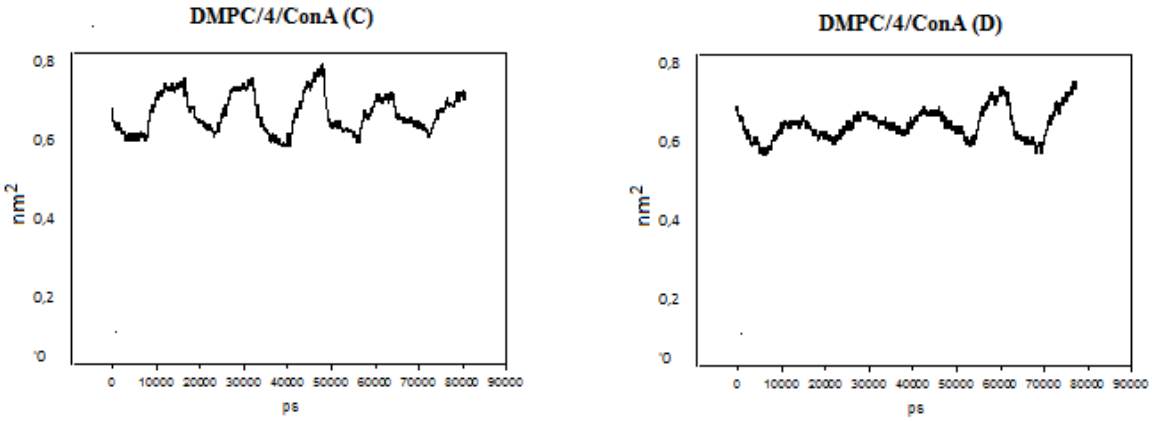

Figure 4.25. Plots of A/Lipid parameter versus the time of the simulation (ps) for the C and D systems.

RMSD parameter of ConA

The root mean square deviation (RMSD) of certain atoms in a system with respect to a reference structure can be calculated with the program g_rms by least-square fitting the structure to the reference structure at time 0 (t_2=0) and subsequently calculating the RMSD (equation 4.16)[99],

$$RMSD(t_1, t_2)=[\, M^{-1} \sum_{i=1}^{N} m_i \, \|r_i(t_1)-r_i(t_2)\|^2 \,]^{1/2} \qquad \textbf{4.16}$$

where $M=\sum_{i=1}^{N} m_i$ is the total mass of the system and $r_i(t)$ is the position of atom i at time t. In this case RMSD evaluates the position of the atoms of the protein with respect to the starting configuration that corresponds to its structure obtained by X-ray, (PDB 3D4K[32]).

The computation of RMSD is a way to check when the system reaches the equilibrium. Figures 4.26-4.28 report the RMSD for the DMPC/ConA and A, B, C, D systems during the trajectory. The RMSD analysis indicates that the protein reaches a good conformational stability after 10 ns of simulation. Therefore 70000 ps (70 ns) were considered as effective time of production for all the simulated systems in all the analysis.

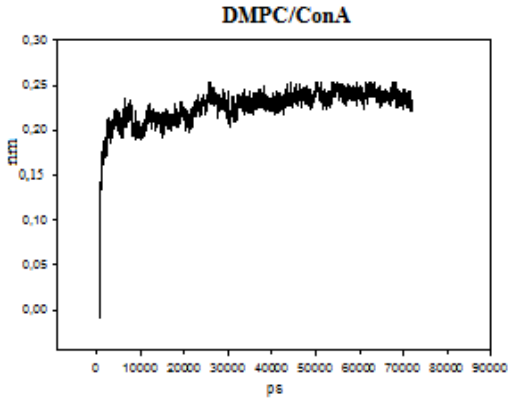

Figure 4.26. Plot of RMSD of DMPC/ConA systems versus time of simulation (ps).

[99] User gromacs manual version 4.0 from www.gromacs.org

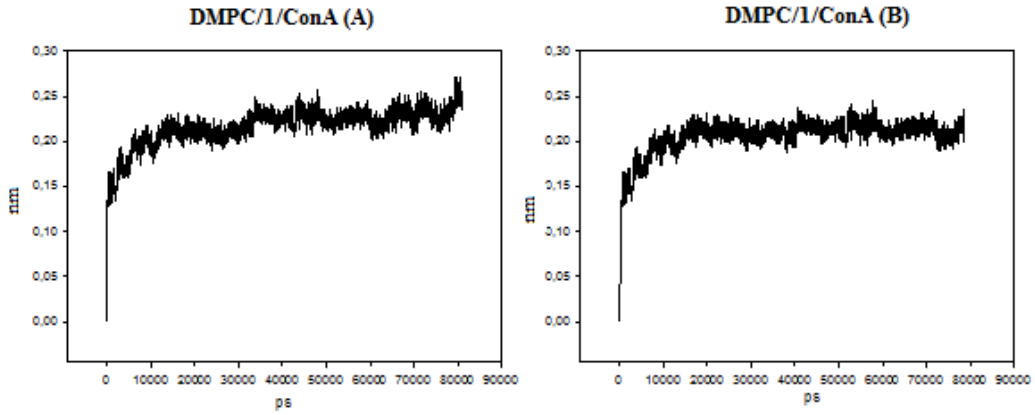

Figure **4.27.** Plot of RMSD of A and B systems versus time of simulation (ps).

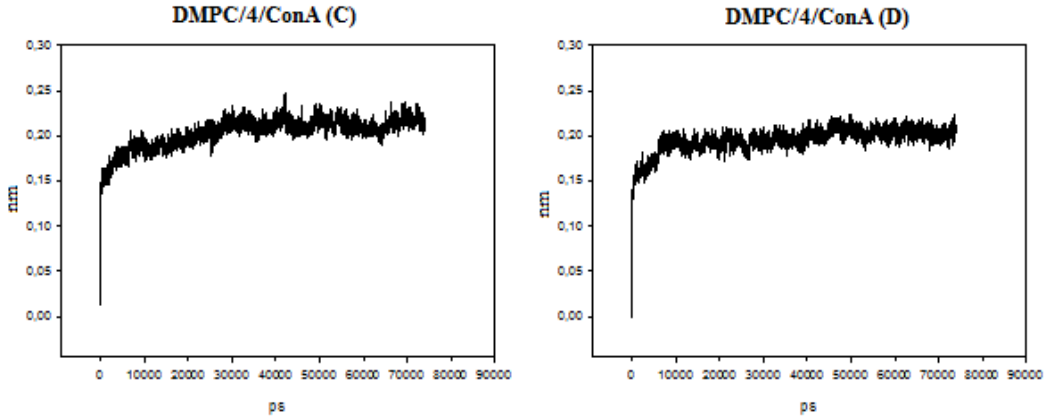

Figure **4.28.** Plot of RMSD of C and D systems versus time of simulation (ps).

Protein-lipid bilayer distance

In order to study the distance and orientation of the protein with respect to the lipid bilayer the distance between the mass center of the protein and the DMPC bilayer was analyzed. This analysis can give an idea of the interactions of the protein with the lipid bilayer, these can be stronger or weaker with respect to the initial configuration. This analysis was carried out by using the g_dist program (*i.e.* GROMACS). Figures 4.29-4.31 show the plots of the protein-lipid bilayer distance versus the time of simulation. According to the RMSD of the protein, only the production time will be considered (*i.e.* since time=10ns). In the case of DMPC/**1**/ConA systems, the distance of the protein from the lipid bilayer increases (from ~2.7 to ~3 nm) in system A and remains constant (at ~3 nm) in system B; note that in the DMPC/ConA system (Figure 4.29) the distance does not vary (~2.7 nm). On the other hand, the presence of GA **4** has an attractive effect toward the protein during the simulation in both the C and D investigated systems (from ~3 to ~2.7 nm). In the case of the DMPC/**4**/ConA system in the starting configuration the protein is set at a larger distance due to the longer hydrophilic spacer however during the simulation the folding of the spacer induce a descrease of the ConA-lipid bilayer distance to the same value (~2.7) observed in the DMPC/ConA system.

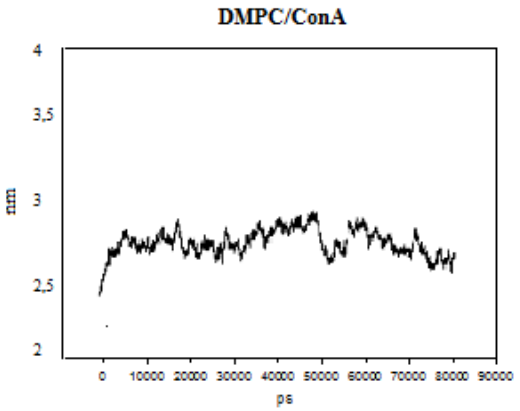

Figure 4.29. Variations of the protein – DMPC lipid bilayer distance in the DMPC/ConA system.

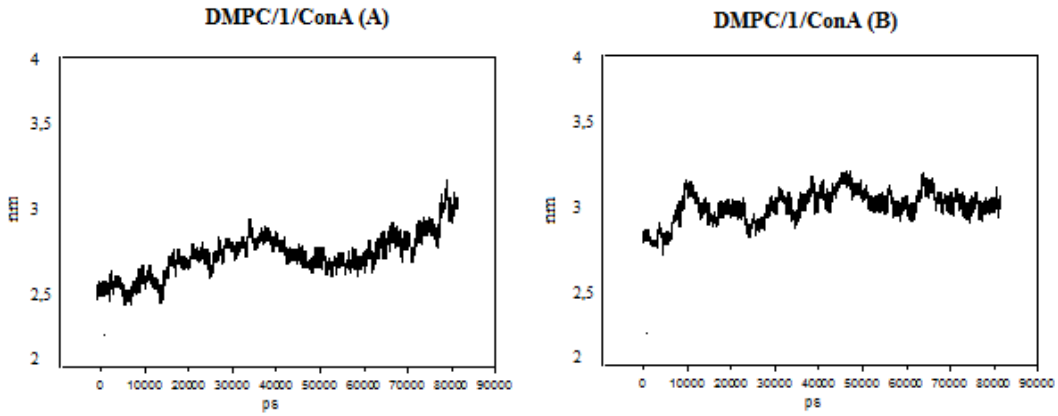

Figure 4.30. Variations of the protein –DMPC lipid bilayer distance in the A and B systems.

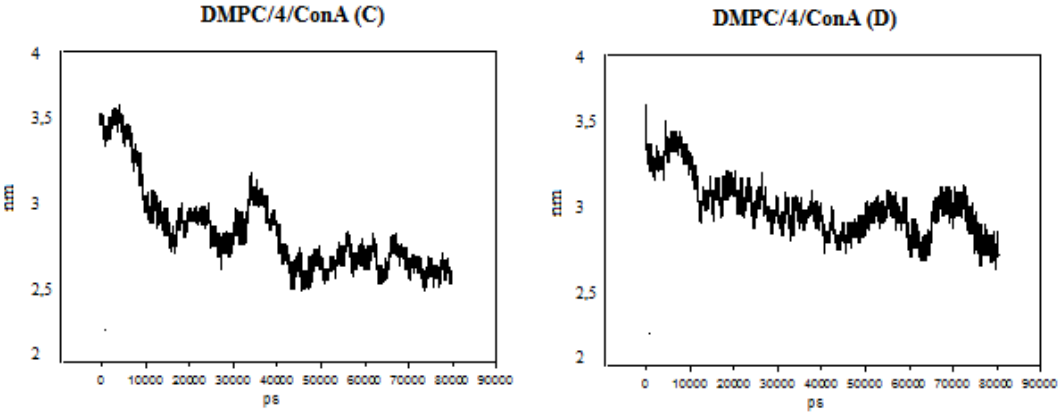

Figure 4.31 Variations of the protein –DMPC lipid bilayer distance in the C and D systems.

Number of protein-DMPC H-bonds

The interaction between ConA and the lipid bilayers can be mediated by the hydrophobic interaction, dipolar interactions and H-bonds depending on the position of the protein with respect to the lipid bilayer. This analysis was carried out by using the g_hbond program (*i.e.* GROMACS) with a cutoff of 0.35 nm. If the protein interacts with the surface of the lipid bilayers H-bonds between the phosphate group and carbonyl groups of DMPC and some aminoacidic residues of the protein might have a very relevant role in the attraction and stabilization of the protein. Figures 4.32-4.34 report the variation of the number of H-bonds between the protein and DMPC molecules during the simulation. The number of H-bonds in the DMPC/ConA system was ~ 6 in the initial configuration and was maintained as such during the simulation. The presence of GA **1** involved a number of 6-9 H-bonds though in a part of the trajectory of the B configuration the number decreased. On the other hand, the presence of the GA **4** in the DMPC bilayer involves a higher number of H-bonds, *i.e.* 9-12. This result can be due to the different orientation of the protein with respect to the lipid bilayer mediated by the GAs. In the case of the DMPC/**4**/ConA systems theGA **4** molecules induce a higher extent of contact surface, as indicated by the larger number of protein-DMPC H-bonds.

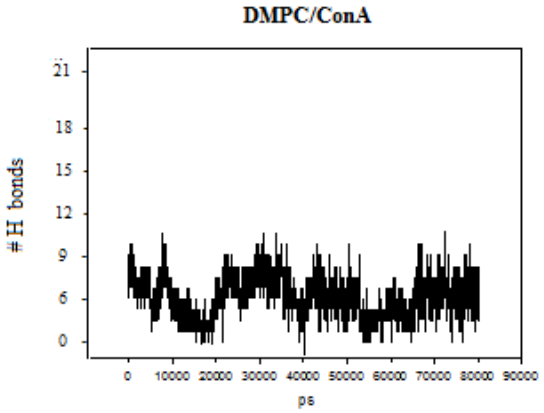

Figure 4.32. Plots of the number of DMPC-ConA H-bonds versus the time of the simulation (ps) for the DMPC/Con A system.

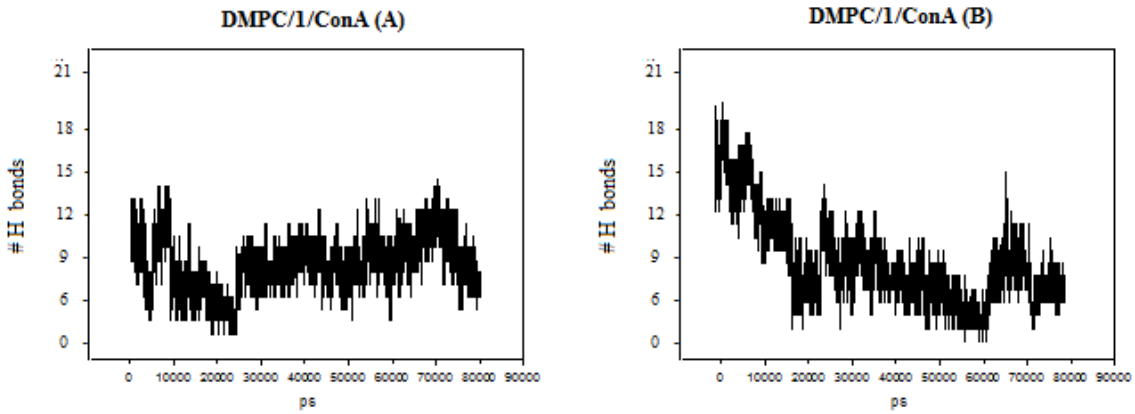

Figure 4.33. Plots of the number of DMPC-ConA H-bonds versus the time of the simulation (ps) for the A and B systems

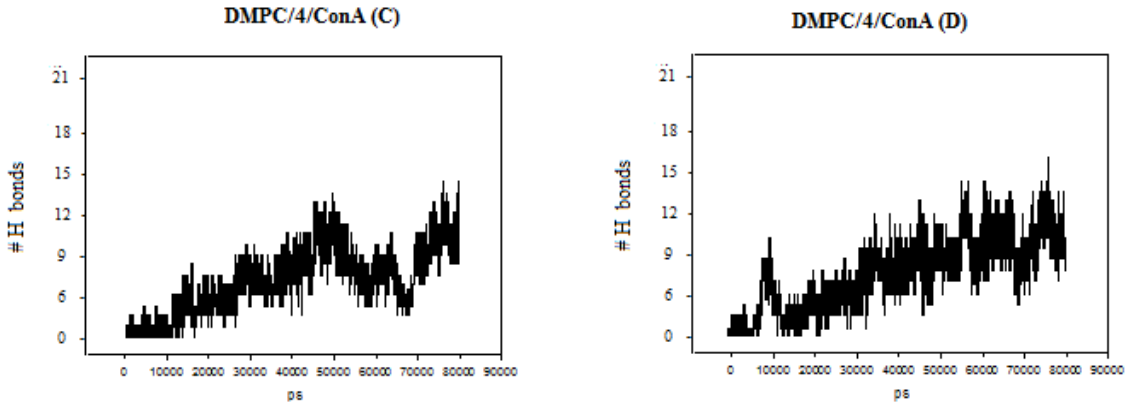

Figure 4.34. Plots of the number of DMPC-ConA H-bonds versus the time of the simulation (ps) for the C and D systems.

Number of protein/glycolipid H-bonds

The analysis of the number of H-bonds occurring between the protein and glycolipid **1** and **4** is reported in the plots shown in Figures 4.35 and 4.36. In the case of DMPC/**1**/ConA systems the initial configuration influences the number of H-bonds of the protein with GA **1** occurring during the simulation. In the first configuration (A) the number of H-bonds set to 2 in the initial configuration remains constant for all the trajectory, this is in agreement with what observed in the qualitative analysis where the GA is in contact with the same number of aminoacids during the simulation. On the other hand in the second configuration (B) the minor number of H-bond, *i.e.* 1, of the initial configuration involves in some phases of the evolution the complete loss of H-bonds, as also described in the qualitative analysis. In the case of the DMPC/**4**/ConA systems in the C configuration the number of H-bonds

varies between 0 and 4 during the trajectory whereas in the D configuration it varies between 0 and 7. The larger number of interactions depends on two main factors, as also shown in the qualitative analysis: first the presence of a longer hydrophilic spacer increases the probability of contacts; second the involvement of two GA in the binding (system D).

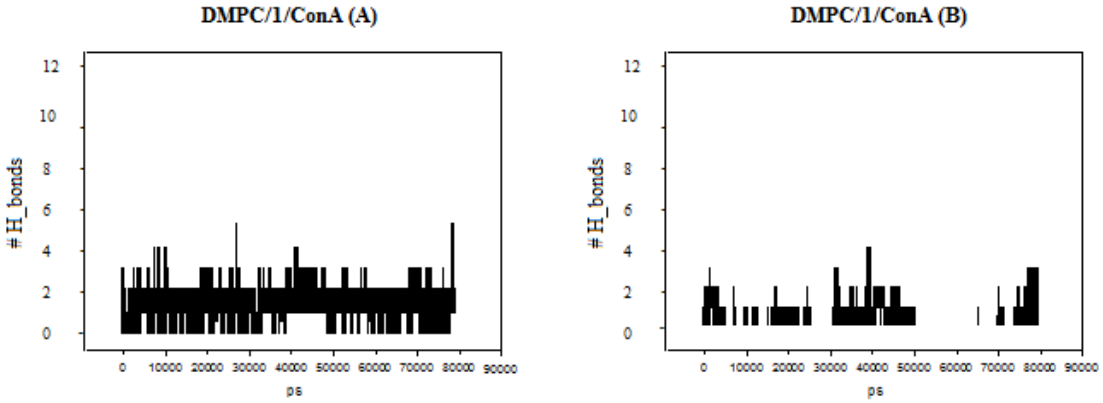

Figure 4.35. Plots of the number of glycolipid - ConA H-bonds versus the time of the simulation (ps) for the A and B systems.

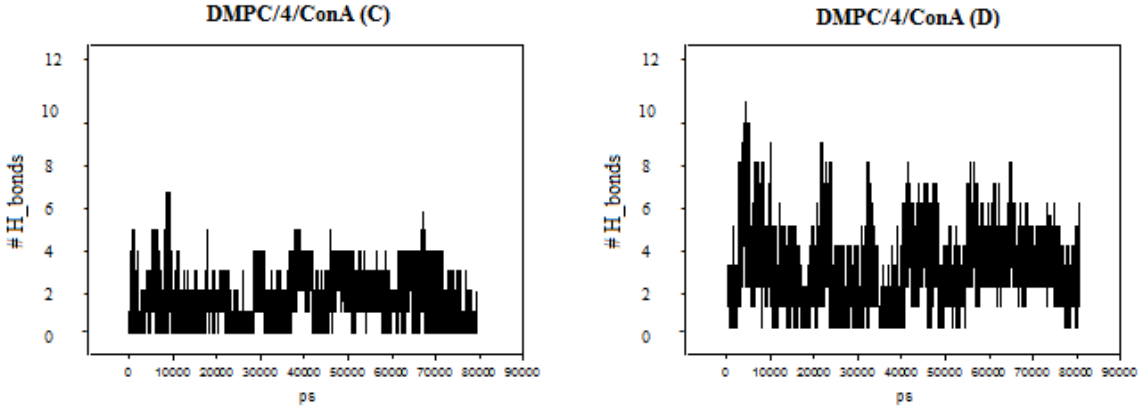

Figure 4.36. Plots of the number of glycolipid - ConA H-bonds versus the time of the simulation (ps) for the C and D systems.

Conclusions

In this work the molecular dynamic was used to study the interaction of two different GA **1** and **4** embedded in DMPC bilayer with the Con A. In Table 4.3 the relevant results obtained by the analysis of the molecular dynamic simulation trajectories relative to the simulated systems are summarized.

Table 4.3. Summary of relevant results obtained by the analysis of the molecular dynamic imulation trajectories relative to the simulated systems

	Simulated systems				
Investigated parameters	**DMPC/Con A**	**A**	**B**	**C**	**D**
H-bonds DMPC-Con A	6	7	7	10	10
H-bonds GA-ConA	-	2	1-2	3-4	5-7
Distance (nm) DMPC-ConA	~2.7	~3	~3	~2.5	~2.7

It is clear that the presence and the type of GA influences the interactions of ConA with the DMPC bilayer. In particular the major length of the hydrophilic spacer in GA **4** mediates a higher number of hydrogen bonds thus contributing to a better binding with the protein.

Concluding remarks

In this thesis the synthetic possibility of creating a library of glycosylated amphiphiles was explored. It was shown that the adopted synthetic procedures allow modulating fairly easily the hydrophobic region, the sugar residue and the hydrophilic spacer of an ammonium salt scaffold. In view of the inclusion of the glycolipids in lectin targeting liposomes, it was considered that the length of the hydrophilic spacer might be a crucial parameter for controlling both the exposure of the sugar moiety on the surface of liposomes and its mobility for the interactions with the lectins. Therefore GA **1** and GA **4** characterized by the same hydrophobic region and the same sugar residue (glucose) but by a different hydrophilic spacer were compared for what concern their interaction with concanavalin A (ConA), a glucose specific plant lectin.

The interaction of lipid bilayers composed of a natural phospholipid (DMPC) and GA **1** or GA **4** with the protein were investigated by both an experimental and a theoretical approach.

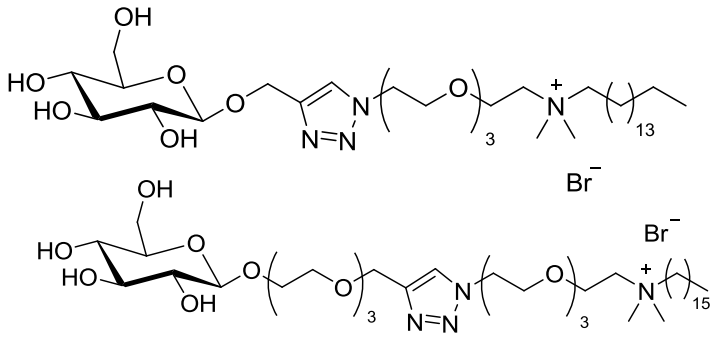

The experimental investigation showed that the displacement of glycogen from the binding sites of the protein occurred in the presence of a lower concentration of GA**1** with respect to Ga**4** thus indicating a better capability of the glucose moiety of GA**1** to interact with the binding sites of the protein. At the monomeric level this is probably due to a coiled conformation of GA**4** that might hinder a good exposure of the sugar moiety with respect to GA**1**. However, when included in lipid bilayers the behavior of the two glycosylated amphiphiles is different. Infact the results of agglutination experiments showed that GA **4** containing liposomes interact with the lectin better than GA **1** containing liposomes. The turbidity experiments showed that the addition of ConA to suspensions of DMPC/**1** and DMPC/**4** liposomes induced a modest increase and a relevant increase of optical density,

respectively as shown in Figure 1 (circle symbols). Further, in the case of DMPC/**4** liposome precipitation was observed at ~ 100 minutes. The DLS experiments reported in Figure 1 (triangle symbols), confirmed the turbidity experiment results showing a relevant increase of the size of liposomes upon addition of ConA only in the case of DMPC/**4** liposomes. Agglutination occurs according to a mechanism analogous to that described in Figure 2, and can be ascribed to the multivalent nature of the sugar-lectin interaction.

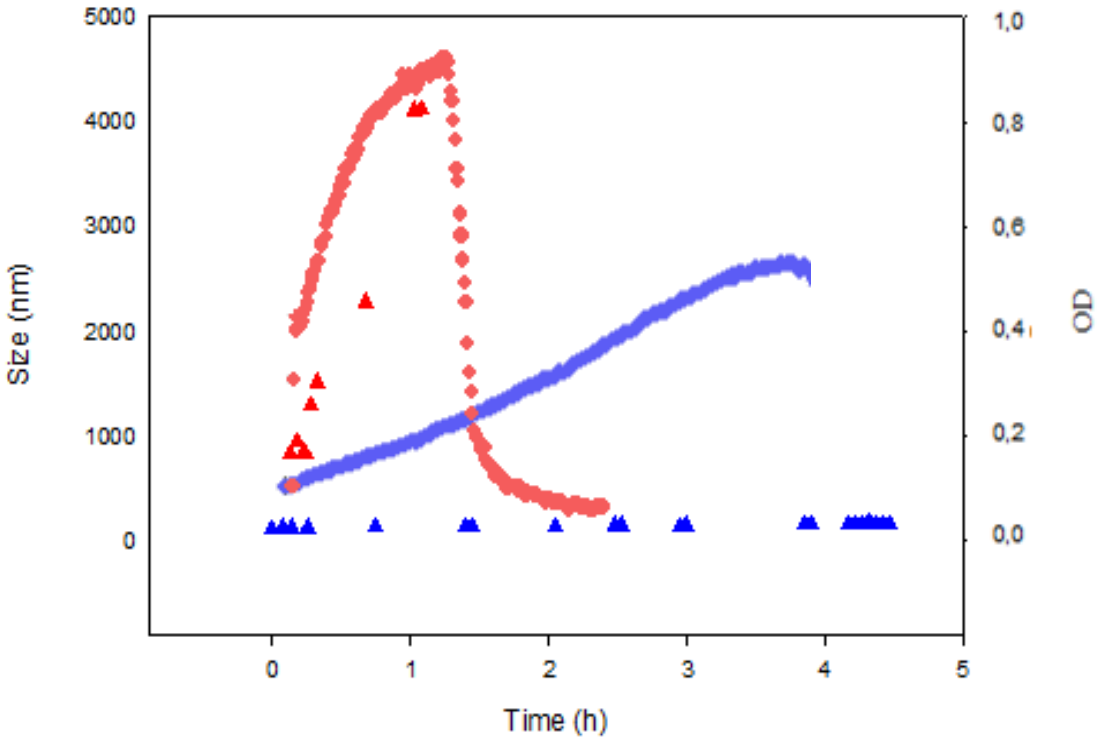

Figure 1. Turbidity increase (GA **4** red circles; GA **1** blue circles) and size changes (GA **4** red triangles; GA **1** blue triangles) observed upon the addition of Con A to a suspension of 95:5 DMPC/GA vesicles in PBS. Con A concentration is 0.33 mg/mL; total lipids concentration is 0.8 mM.

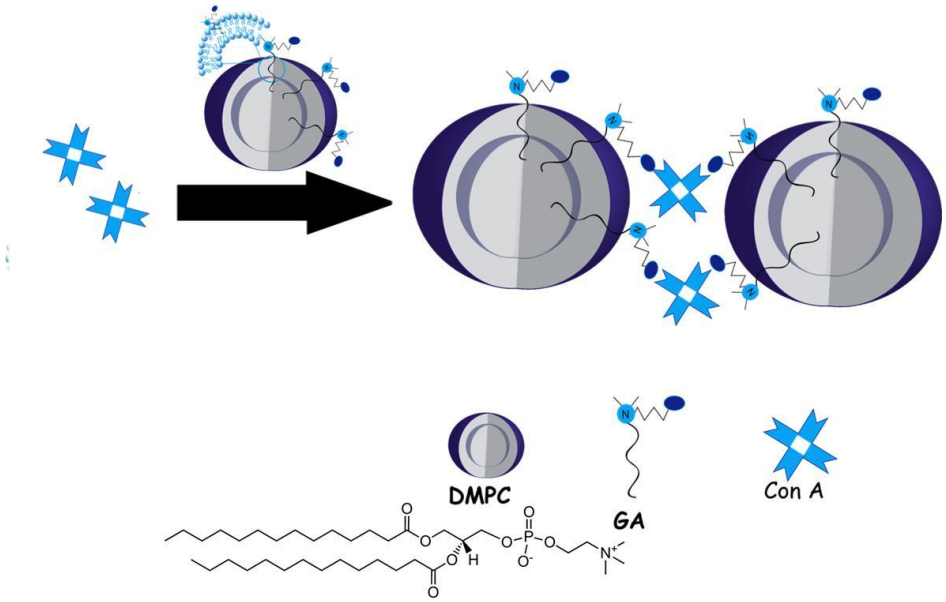

Figure 2. Schematic representation of agglutination.

The experimental results were nicely confirmed by the molecular dynamics simulations that gave an atomistic description of the interactions involved in the binding of DMPC/GA bilayers with ConA. The results of simulation analysis showed that the DMPC/**4** bilayer interacts at a larger extent with the protein as demonstrated by the higher number of H-bond of the lipid bilayer with ConA. The higher number of H-bonds implies a larger surface of contact between the lectin and the lipid bilayer. The involvement of a higher extent of protein-lipid bilayer interaction is mediated by the interaction of ConA with two molecules of GA **4** instead of the single GA **1** molecule involved in the interaction of ConA with the DMPC/**1** bilayer, Figure 3, and by a larger number of H-bond between GA **4** and the aminoacids of the binding site due to the longer hydrophilic spacer. Therefore both the experimental and theoretical approaches allowed us to identify which is the better hydrophilic spacer for the interaction of glycosylated liposomes with ConA among the two explored.

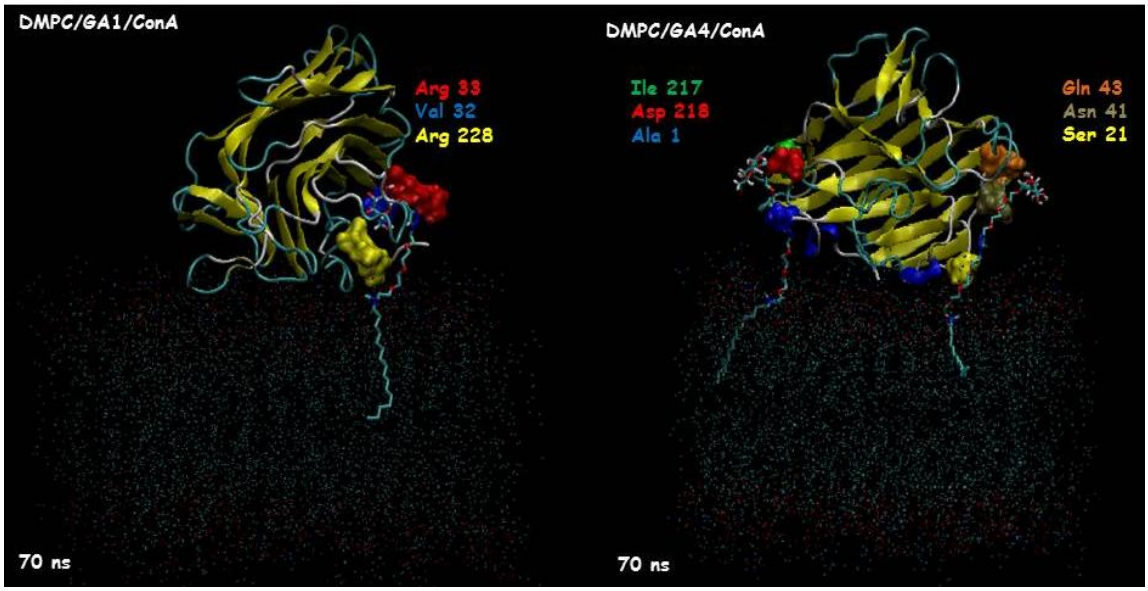

Figure 3. Representative images of the binding between GA**1**(left) and GA**4** (right) the lectin during the simulation.

Future developments

Other experiments are scheduled to confirm and clarify the results obtained in this work of thesis. X-ray measuraments on the explored formulations in the presence and in the absence of ConA will give further insights on the interactions involved. Further the other structural parameters of GA should be investigated to elucidate the influence of the hydrophobic anchor on the stability of the formulations and on their physicochemical features. For what concerns the sugar moiety, glucose has been investigated as a model for two main reasons: i) the easiness of the synthetic procedures involving glucose and ii) the easy availability of ConA that is a glucose specific lectin. However, human lectins are specific for galactose therefore in the future the sugar residues of choice will be galactose and lactose, and the biological evaluation will be carried out on liposomes functionalized with these sugars. However some cell lines express glucose receptors and a preliminary evaluation on cells will be carried out also exploiting DMPC/**1** and DMPC/**4** liposomes.